RT 186: Product Assurance for Electronics in Harsh Environments

Pradeep Lall
John and Anne MacFarlane Endowed Professor
Director, NSF-CAVE3 Electronics Research Center
Technical Council and Governing Council of NextFlex

Auburn University
Auburn, AL 36849
(O) 334-844-3424
Email: lall@auburn.edu

cave³
NSF Center for Advanced Vehicle and Extreme Environment Electronics

AUBURN UNIVERSITY

REPORT DOCUMENTATION PAGE			*Form Approved* *OMB No. 0704-0188*

1. REPORT DATE *(DD-MM-YYYY)*	2. REPORT TYPE	3. DATES COVERED *(From - To)*
09-30-2018	Presentation	08-16-2017 - 09-30-2018

4. TITLE AND SUBTITLE RT 186: Product Assurance for Electronics in Harsh Environments	5a. CONTRACT NUMBER HQ0034-13-D-0004
	5b. GRANT NUMBER
	5c. PROGRAM ELEMENT NUMBER
6. AUTHOR(S) Pradeep Lall	5d. PROJECT NUMBER
	5e. TASK NUMBER HQ003417F0387
	5f. WORK UNIT NUMBER
7. PERFORMING ORGANIZATION NAME(S) AND ADDRESS(ES) Auburn University Auburn, AL 36849	8. PERFORMING ORGANIZATION REPORT NUMBER
9. SPONSORING/MONITORING AGENCY NAME(S) AND ADDRESS(ES) US Army Aviation and Missile RDEC 5400 Fowler Road, Redstone Arsenal, AL 35898 Office of the DASD (Systems Engineering) 3040 Defense Pentagon, Room 3C167, Washington, DC 20301-3040	10. SPONSOR/MONITOR'S ACRONYM(S)
	11. SPONSOR/MONITOR'S REPORT NUMBER(S)

12. DISTRIBUTION/AVAILABILITY STATEMENT

Approved for public release

13. SUPPLEMENTARY NOTES

14. ABSTRACT

15. SUBJECT TERMS

16. SECURITY CLASSIFICATION OF:			17. LIMITATION OF ABSTRACT	18. NUMBER OF PAGES	19a. NAME OF RESPONSIBLE PERSON
a. REPORT	b. ABSTRACT	c. THIS PAGE			19b. TELEPHONE NUMBER *(Include area code)*

Effect of Green EMCs on Fatigue Reliability of Molded Cu-WB Systems

S. Deshpande, P. Lall

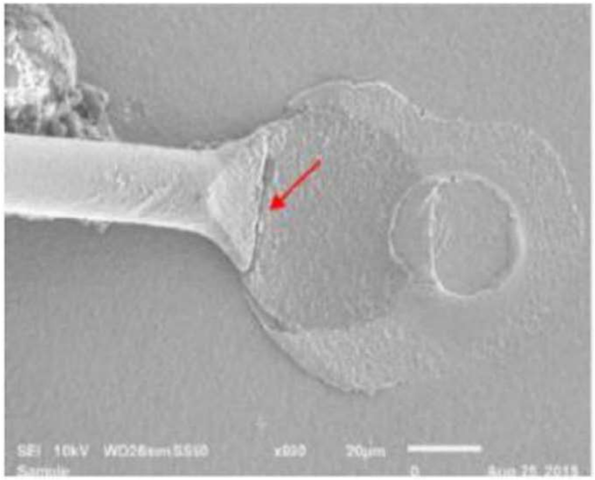

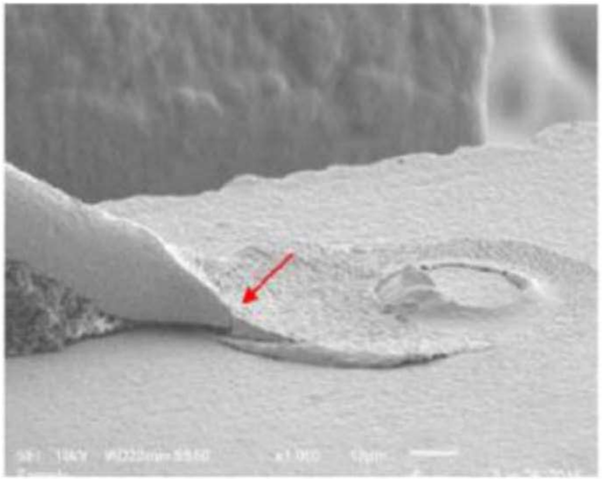

Objectives

- Study effect of thermal cyclic loading (AEC-Q100 standard for grade-0 package) on the reliability of Cu wirebond QFN packages molded with automotive grade green epoxy mold compounds (EMC).
- Develop model for finite element analysis by extracting data from 3D model generated using X-ray Micro-CT system.
- Study effect of different properties (E, CTE) of EMCs on the reliability of wirebonded packages using FEA.

Motivation – Prior CAVE Data

- Migration of Au to Cu wirebonding is recent change in packaging field; driven by cost, mechanical and electrical advantages.

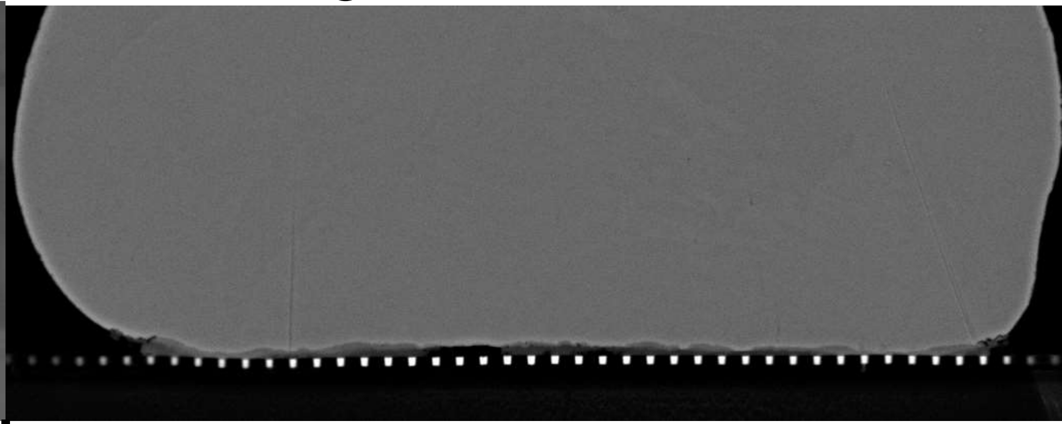

- ❑ Package molded with traditional EMC (High contamination)
- ❑ 175°C, HTSL, 1500 Hours of Aging
- ❑ Complete cracking at WB interface due to corrosion related mechanisms

- ❑ Package molded with **green EMC** (very low contamination)
- ❑ 175°C, HTSL, 1500 Hours of Aging
- ❑ Very small peripheral cracking at WB interface

cave³
NSF Center for Advanced Vehicle and Extreme Environment Electronics

AUBURN UNIVERSITY

Motivation

- Cu is more reactive than Au hence susceptible to environmental conditions such as humidity, ionic contamination, pH value, bond metallurgies etc.

- Prior CAVE data has shown that green EMC have better HTSL, HTOL, HAST reliability for Cu wirebonded packages compared with traditional EMCs.

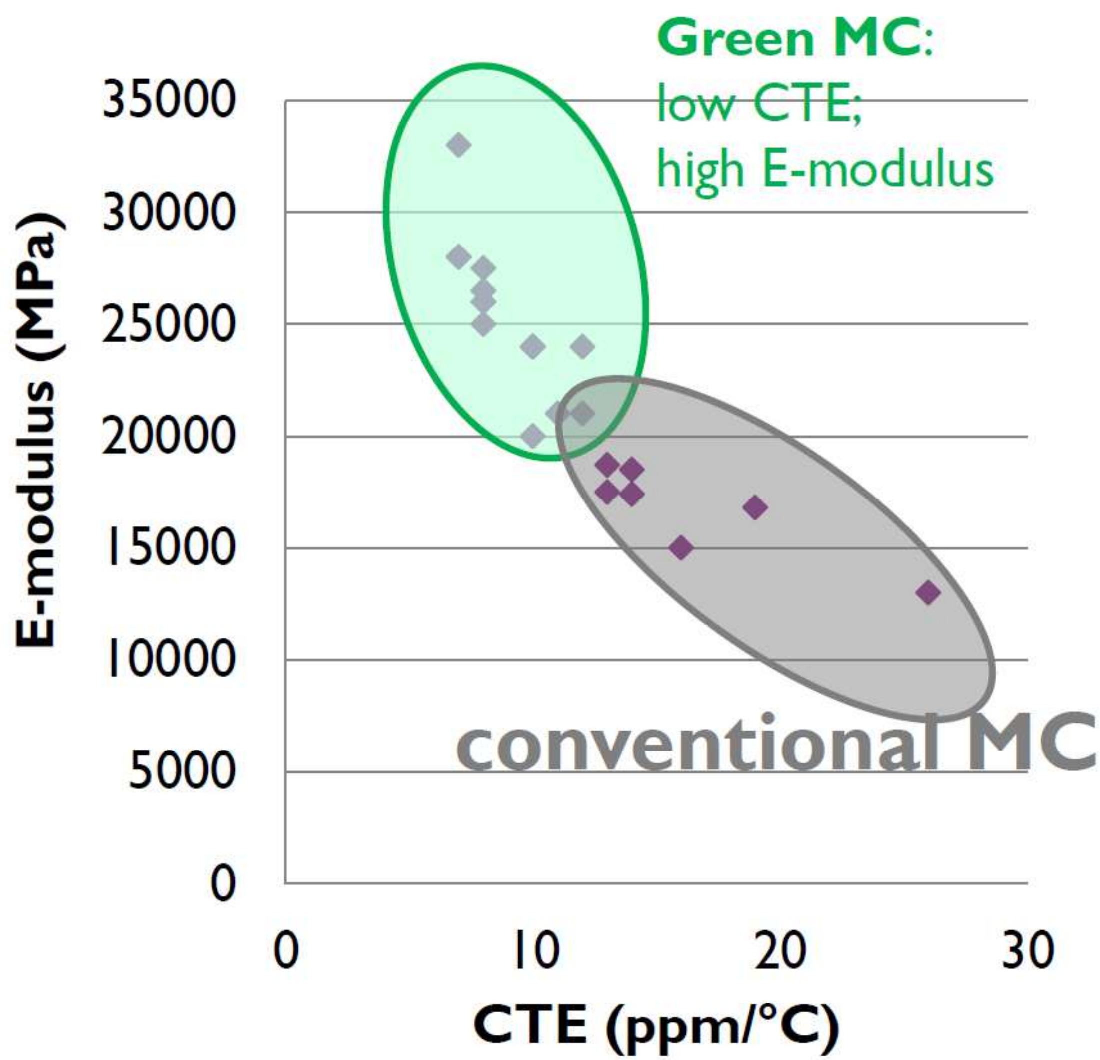

iNEMI Seminar "Impact of Green Mold Compound of First and Second Level Reliability Interconnect, 2013

State of Art

- Prior studies on reliability of Cu, Au and PCC wirebonds have quantified time-to-failure but damage mechanisms over test time has not been studied. [1][2][3].
- Failure in Au, Cu and PCC wirebond under high temperature was studied in prior studies, however, IMC growth and phase changes over time were not correlated with the change in electric properties of the device [3][4][5].
- Ag being one of the newer alternative to Au and Cu wires is not widely discussed in the literature[6].
- Evaluation of all wirebond material candidates under same test condition will enable fair comparison between the candidates

1. *Gan C., Ng E., Chan B., Classe F., Kwuanjai T., Hashim U., "Wearout reliability and intermetallic compound diffusion kinetics of Au and PdCu wires Used in Nanoscale Device Packaging", Journal of Nanomaterials, Vol 2013, Article ID 486373, pp1-9.*
2. *Goh C., Chong W., Lee T., Breach C., "Corrosion study and Intermetallics formation in Gold and Copper Wire Bonding in Microelectronics Packaging", Crystals Journal, Vol 3, 2013, pp 391-404.*
3. *Y. H. Tian, C. J. Hang, C. Q. Wang, G. Q. Ouyang, D. S. Yang, and J. P. Zhao, "Reliability and failure analysis of fine copper wire bonds encapsulated with commercial epoxy molding compound," Journal of Microelectronics Reliability., vol. 51, no. 1, pp. 157–165, 2011.*
4. *Abe H., Kang D., etc. all, "Cu Wire and Pd-Cu Wire Package Reliability and Molding Compounds", Proceedings of IEEE ECTC Conference, 2012, pp 1117-1123.*
5. *Yoo K., Uhm C., Kwon T., Cho J., Moon J., "Reliability Study of Low Cost Alternative Ag Bonding Wire with Various Bond Pad Materials", Proceedings of 11th IEEE EPTC Conference, 2009, pp 851- 857.*
6. *J. Xi et al., "Evaluation of Ag wire reliability on fine pitch wire bonding," IEEE 65th Electronic Components and Technology Conference (ECTC), San Diego, CA, 2015, pp. 1392-1395.*

Literature Review

Author	Reported Results
Vendevelde; 2011	Premature solder joint (SAC and SnPb) failures in TSOP packages molded with green EMC's using experimental and simulation results
Vendevelde; 2012	3D slice model of QFN devices to study effect of low CTE EMC on Cu wire reliability, reported damage in wire loop region
Soestbergen 2017	2D cross-sectional model of Cu wirebonded SOIC package. Reported delamination of EMC and stitch cracking of wires when green EMCs were used
Tee 2003; 2006	Reduction in QFN and BGA fatigue life due to reduction in CTE of the package using 3D FE model

Test Vehicle and Matrix

- 32 Pin QFN package wirebonded with 1mil Cu, wire on 0.9µm Al pad.
- Test Condition – AEC Q 100 T/C for grade 0 packages
- Scanning Parameters – 100kV, 10µA, 2400 images during 360° rotation
- Voxel Size – 2.06µm

Optical Image

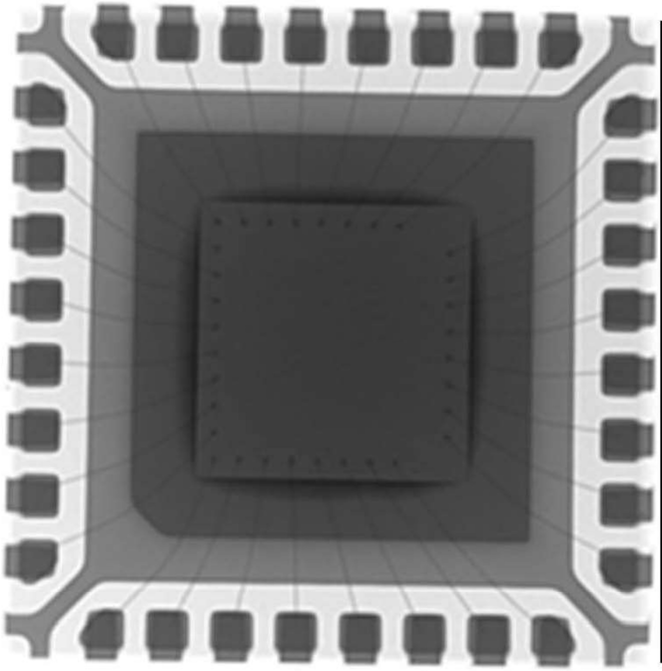

X-ray Image

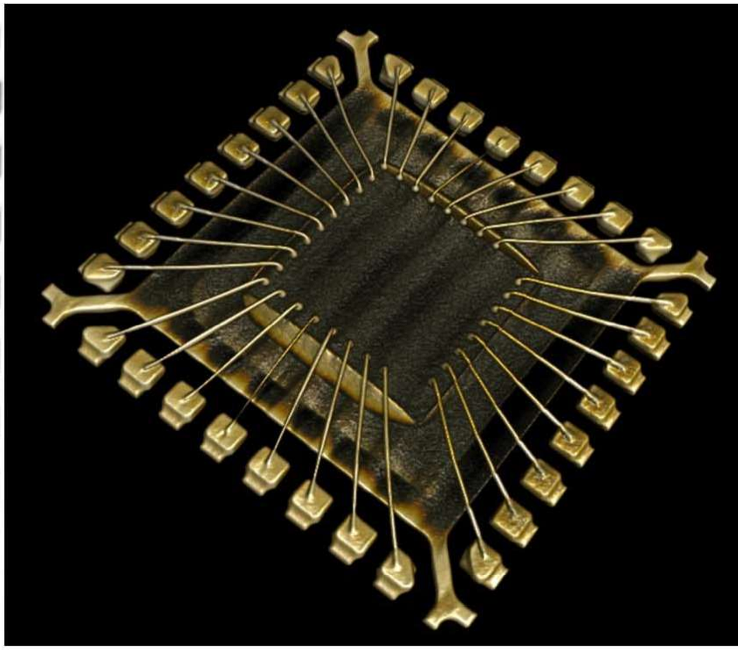

µ-CT Reconstruction

CT to Mesh Conversion

Image Segmentation
- ❑ Import DICOM Data
- ❑ Identify region-of-interest (ROI)

Volume Generation and Editing
- ❑ Poisson's Surface Reconstruction
- ❑ Quadratic Mesh Decimation
- ❑ Laplacian Smoothing
- ❑ Export .stl file

Assemble; FE Analysis Ready
- ❑ Assemble all .stl files
- ❑ Generate 3D mesh using Delaunay Triangulation
- ❑ Define material properties; BC’s

Image Segmentation

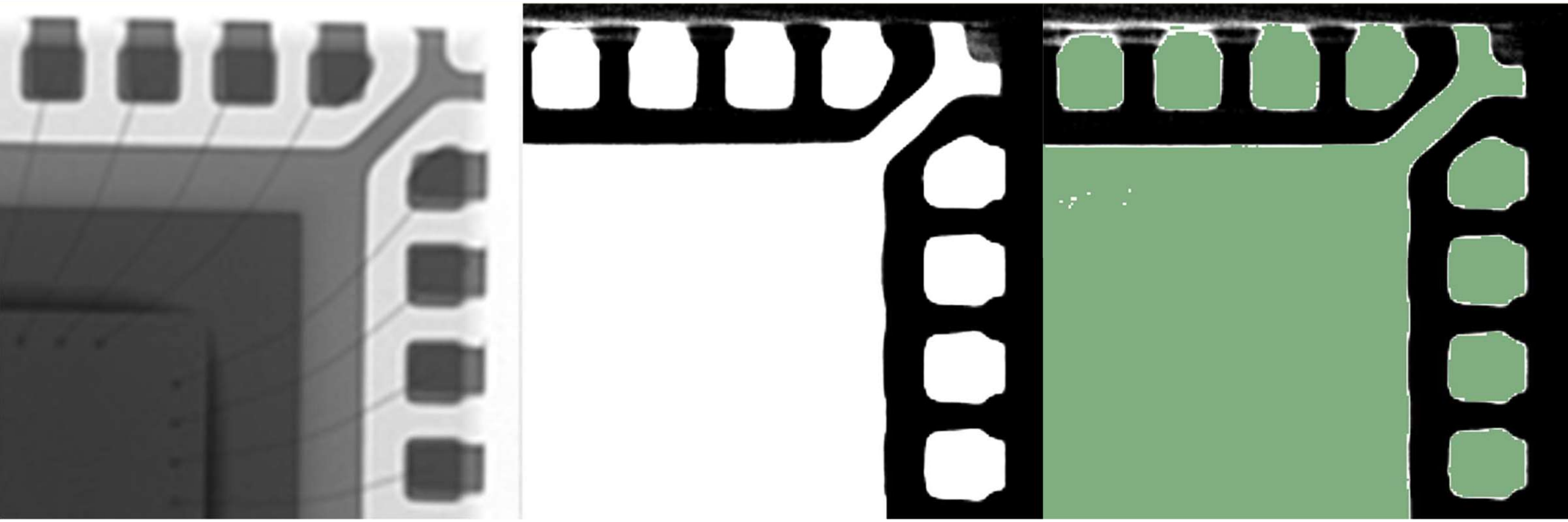

X-ray Boundary **DICOM Representation** **Selected Region**

- ❑ Define boundaries of the model and identify different features based on grayscale density of 3D DICOM dataset.
- ❑ Greyscale range is selected based on the density of the material to be extracted. Selected area is marked in green

Poisson's Surface Reconstruction

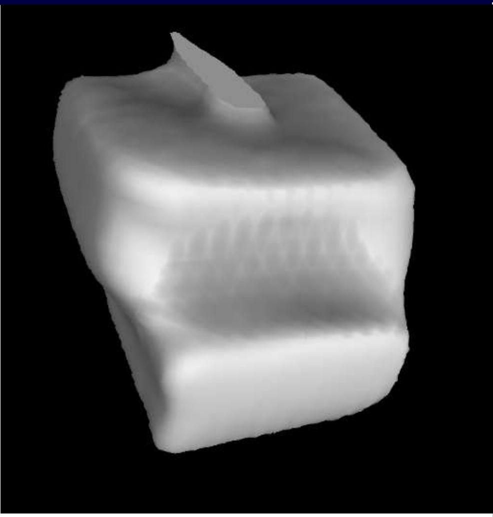

CT Representation

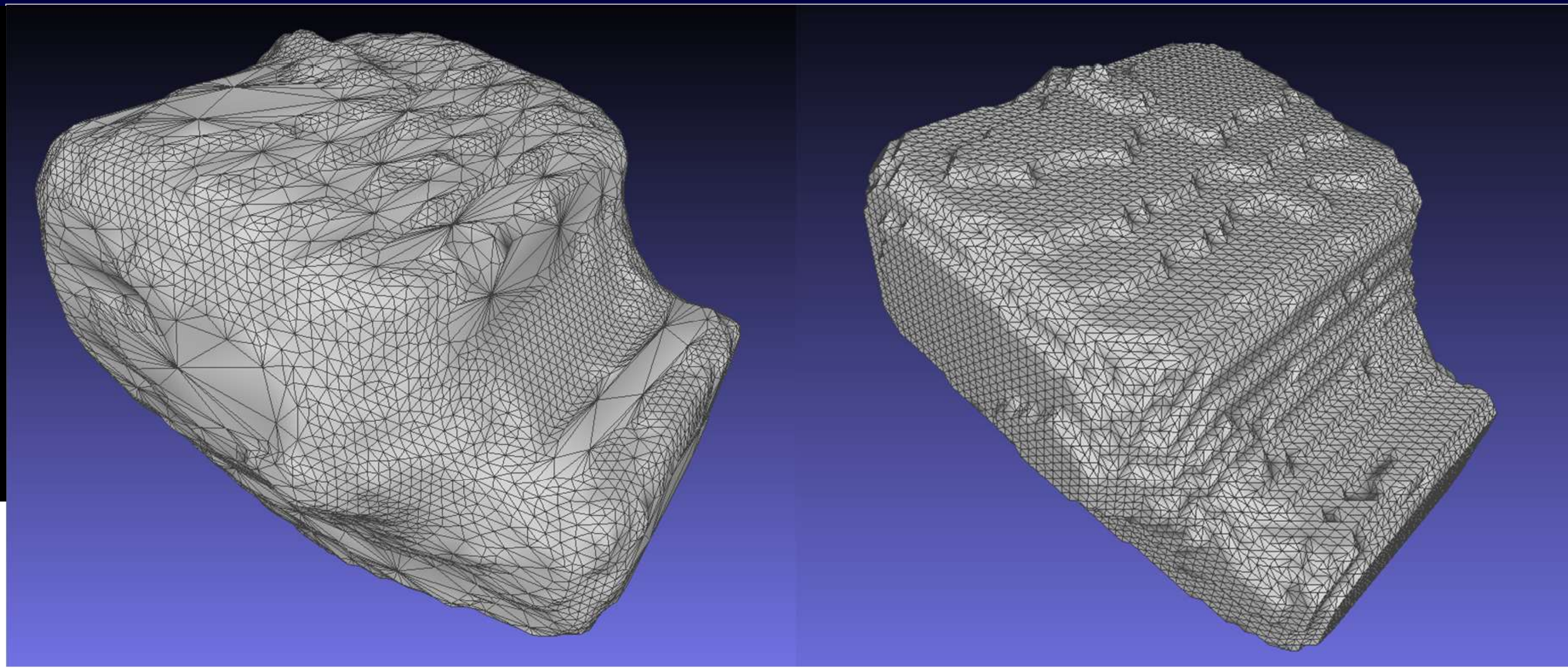

Pre **Post**

Surface Reconstruction

- Define water-tight surface using Poisson surface reconstruction technique.
- This step regularizes mesh and removes artificial defects generated during CT scanning process.

Mesh Decimation and Smoothing

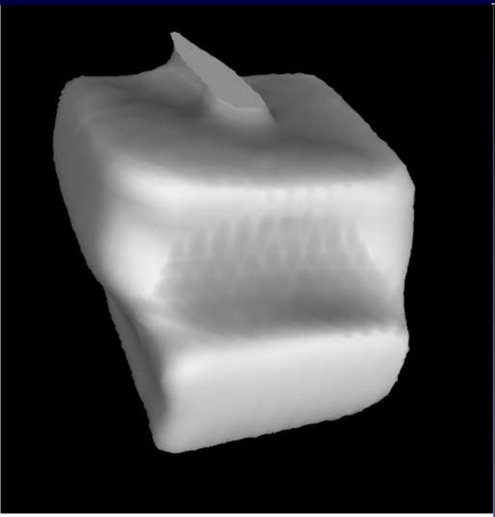

CT Representation

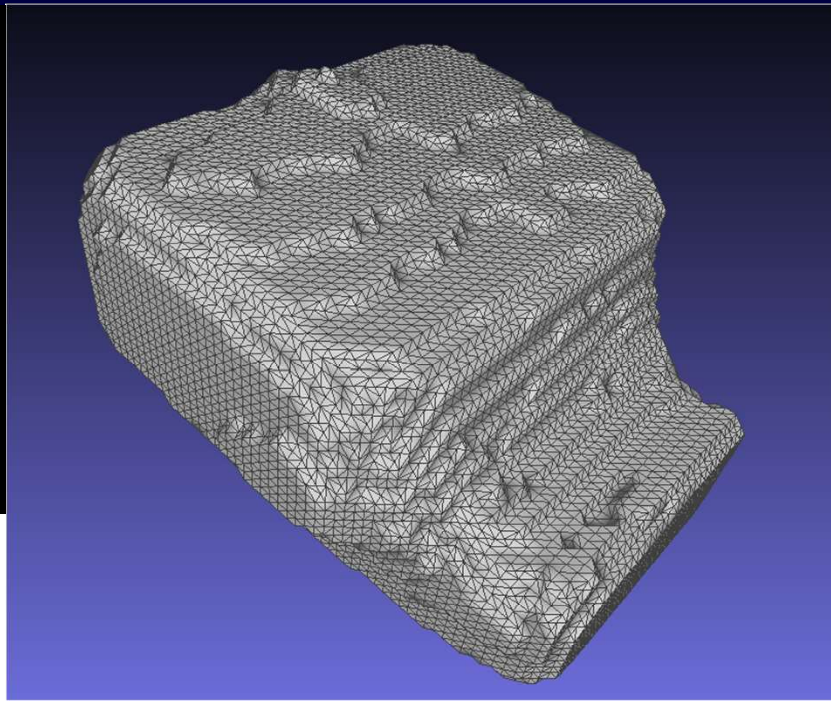

Pre Analysis

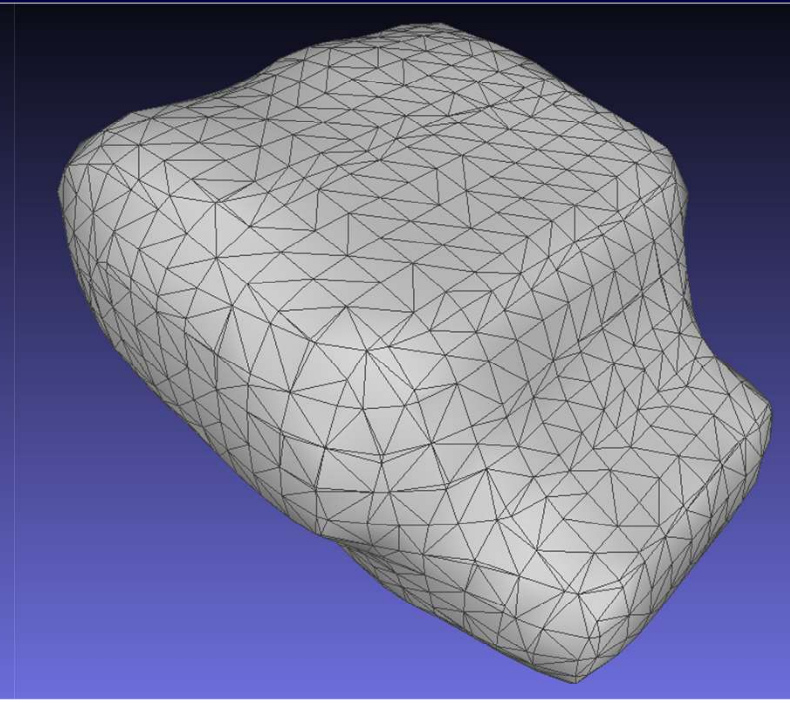

Post Analysis

- ❑ Number of elements are reduced without loosing surface definition to make model lighter and easy for calculations
- ❑ Perform Laplacian smoothing operation to improve the surface finish and the mesh.

Model Assembly

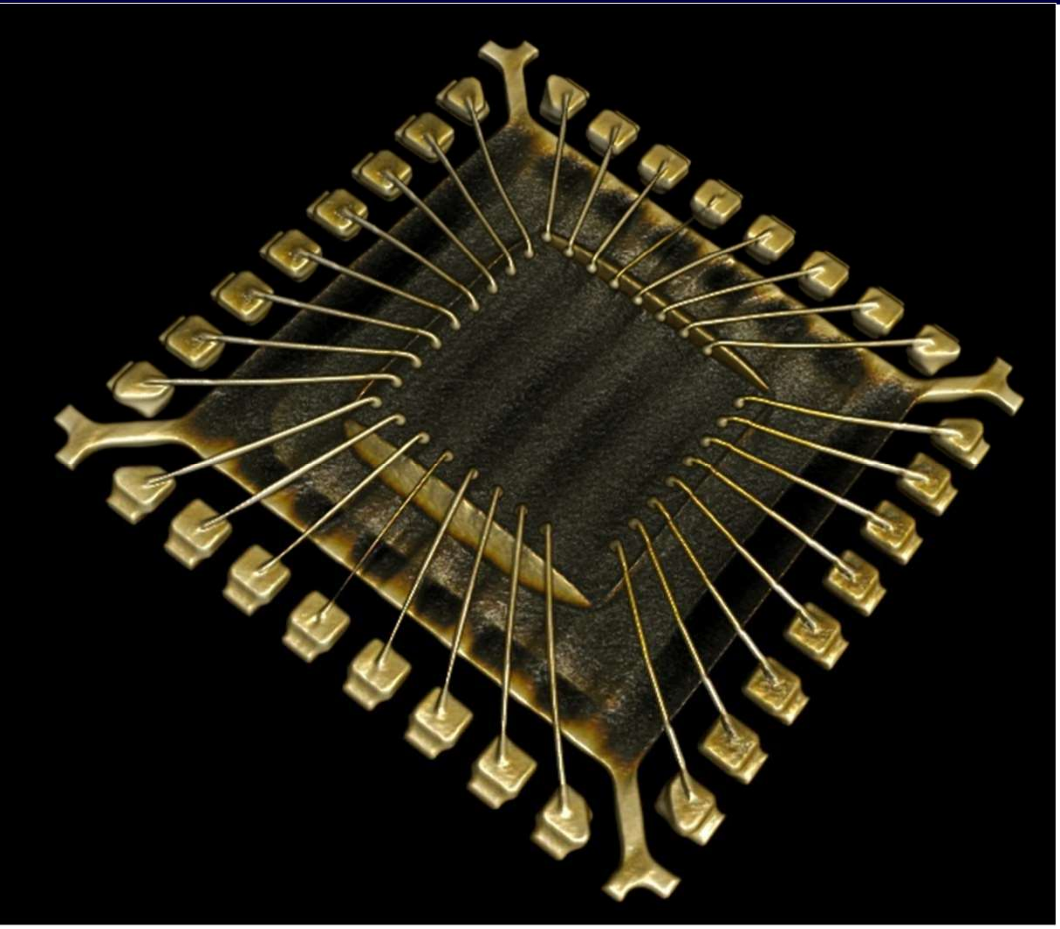

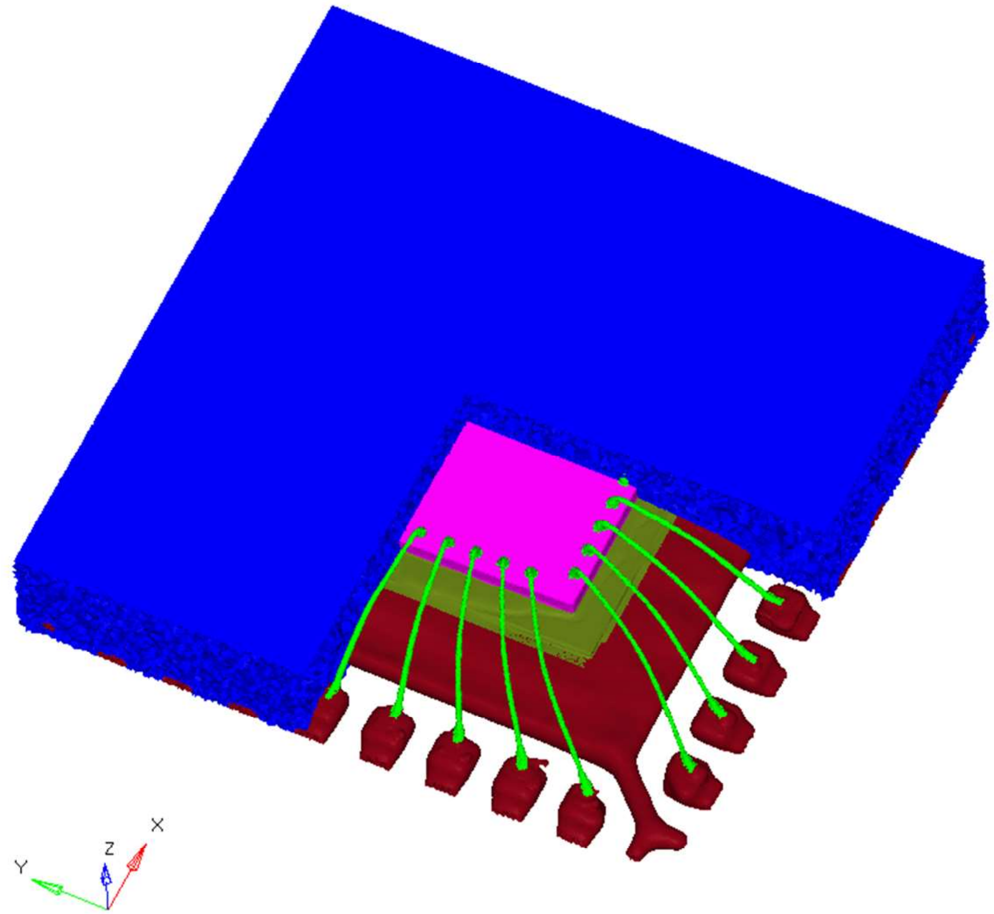

Component	Original	Modeled
Chip (mm)	2.00*2.00	2.03*2.03
Ball Bond (µm)	69.85	70.95
Cu Wire (µm)	25.40	26.97

Model Assembly

Ball Bond and Wedge Bond

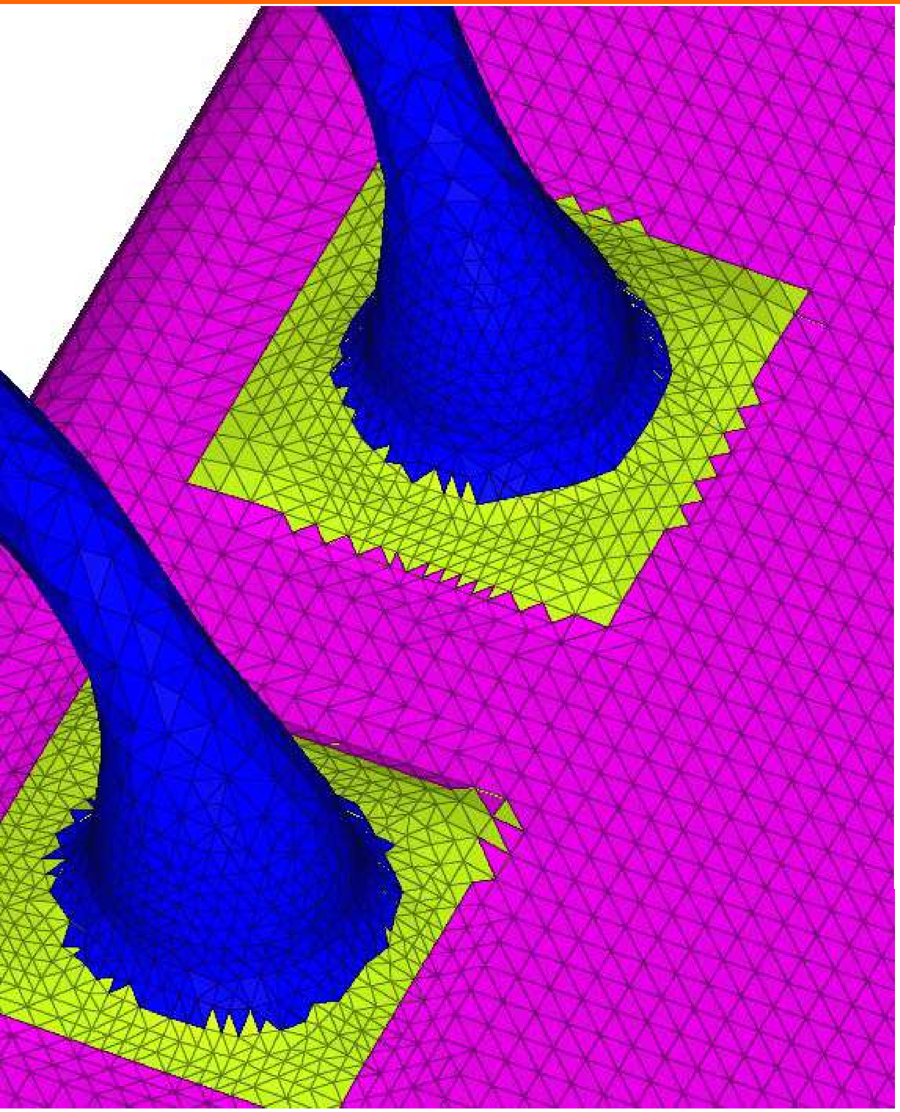

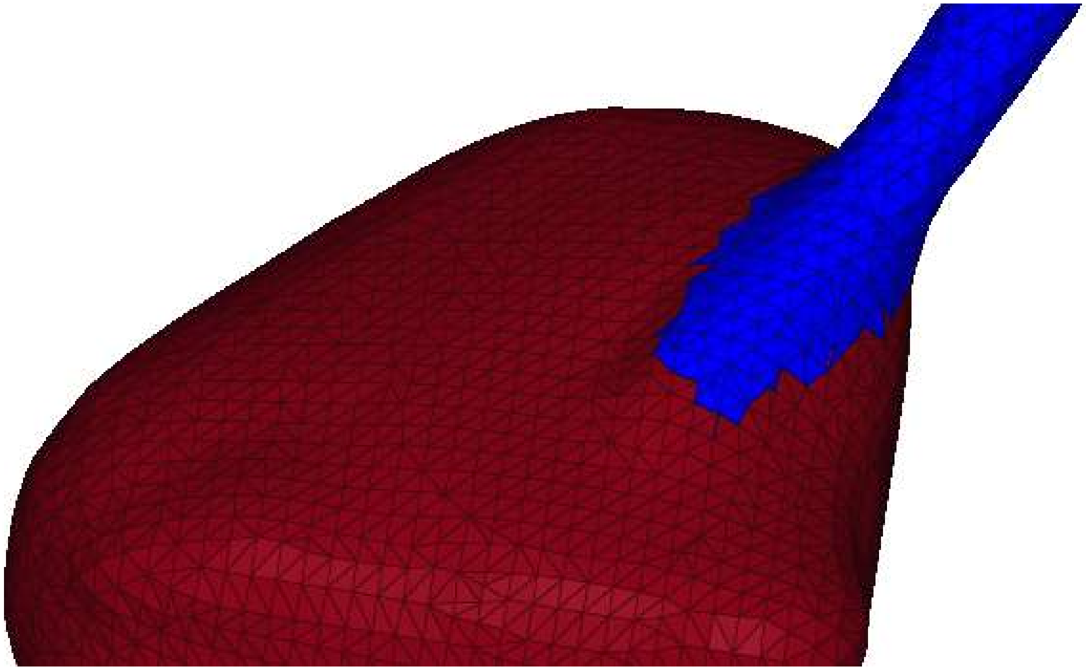

Model Assembly

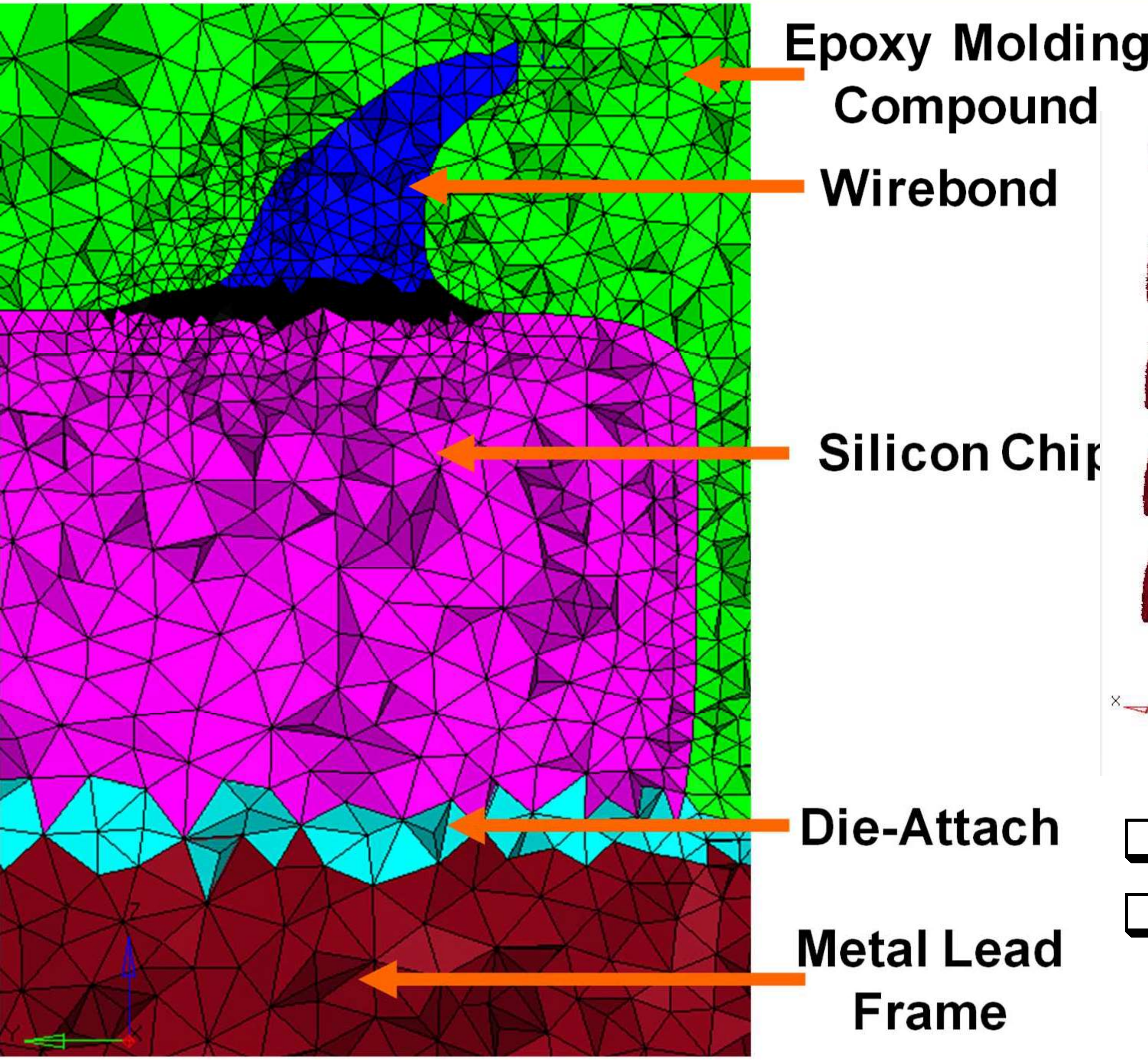

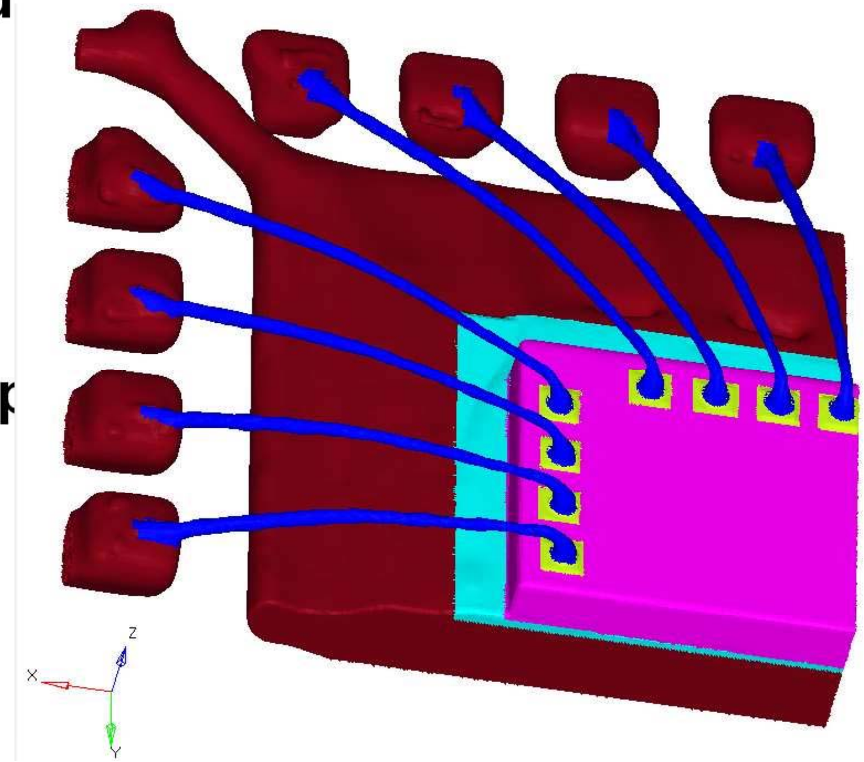

- Elem Count – 5,007,566
- Elem type – C3D4

Material Properties

Component	Material	E (GPa)	CTE (ppm)	Yield Strength (MPa)
Lead Frame	C194 Alloy	121	16.7	
Die-attach	CRM-1076NS	10	45	
Chip	Silicon	163	3.5	
Wire	Copper	129	16.3	310
Pad	Aluminum	68	24	
Epoxy Molding Compounds	A	30	7	
	B	26.5	8	
	C	24	10	
	D	21	12	
	E	18.5	14	
	F	15	16	

1. B. Vandevelde et.al., "Early fatigue failures in copper wire bonds inside packages with low CTE green mold compounds," *2012 4th ESITC Conference*, Amsterdam, Netherlands, 2012, pp. 1-4.
2. P. Lall, et.al., "Model for BGA and CSP reliability in automotive underhood applications," 53rd ECTC Conf. 2003, pp. 189-196.
3. Intel Packaging Handbook, Chapter 5 Physical constants of IC package materials, 2000.
4. http://www.olinbrass.com/sites/default/files/downloads/Olin-Brass-Copper-Alloy-C194-Data-Sheet.pdf

Thermal Cycling Profile

- AEC Q100 Standard for Grade 0 Packages – -40°C to 150°C
- Ramp – 20min; Dwell – 10 min.
- Time/Cycle – 60 min.

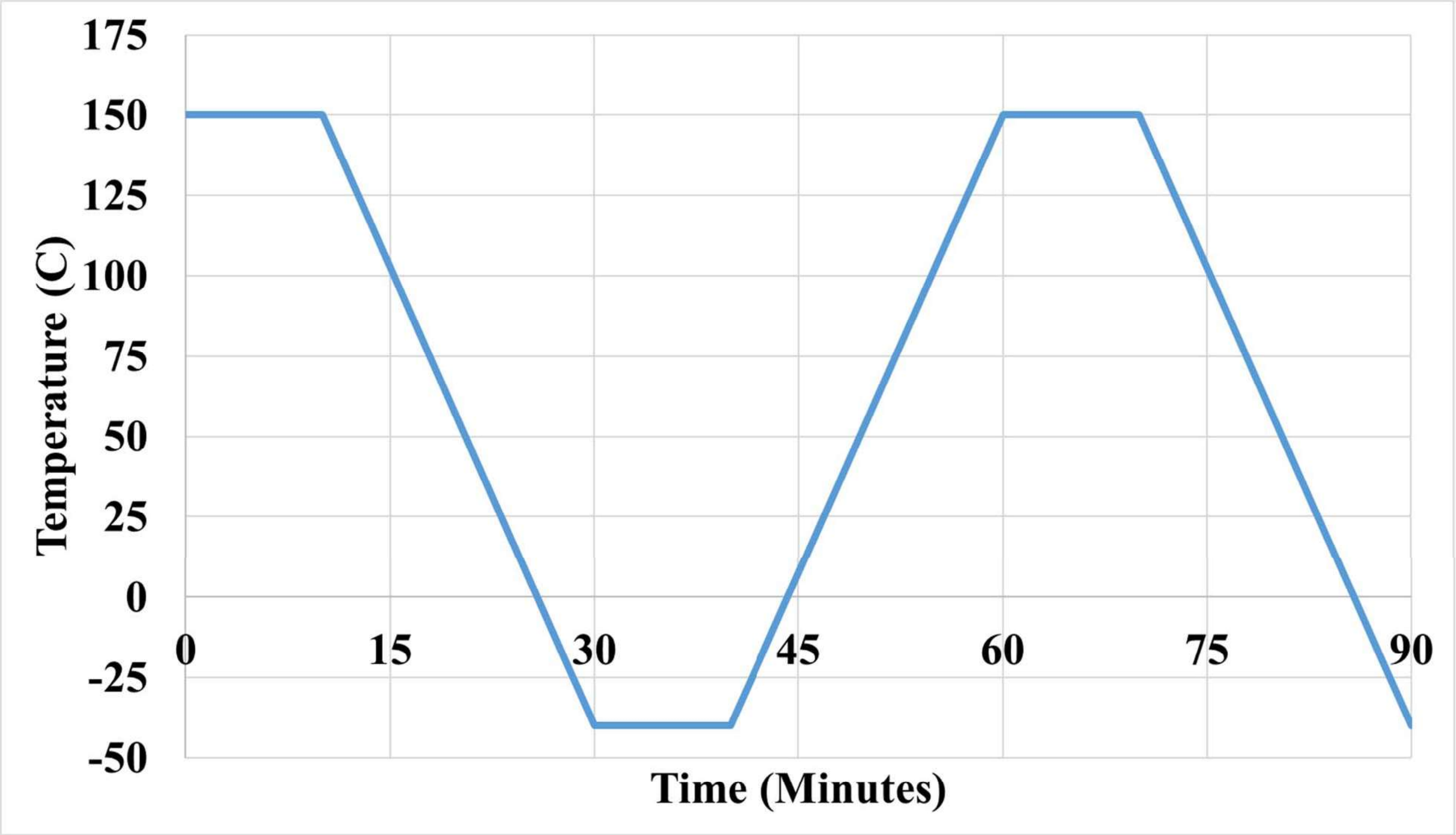

cave³

NSF Center for Advanced Vehicle and Extreme Environment Electronics

AUBURN UNIVERSITY

Results

Strains on Chip During Cooldown Phase

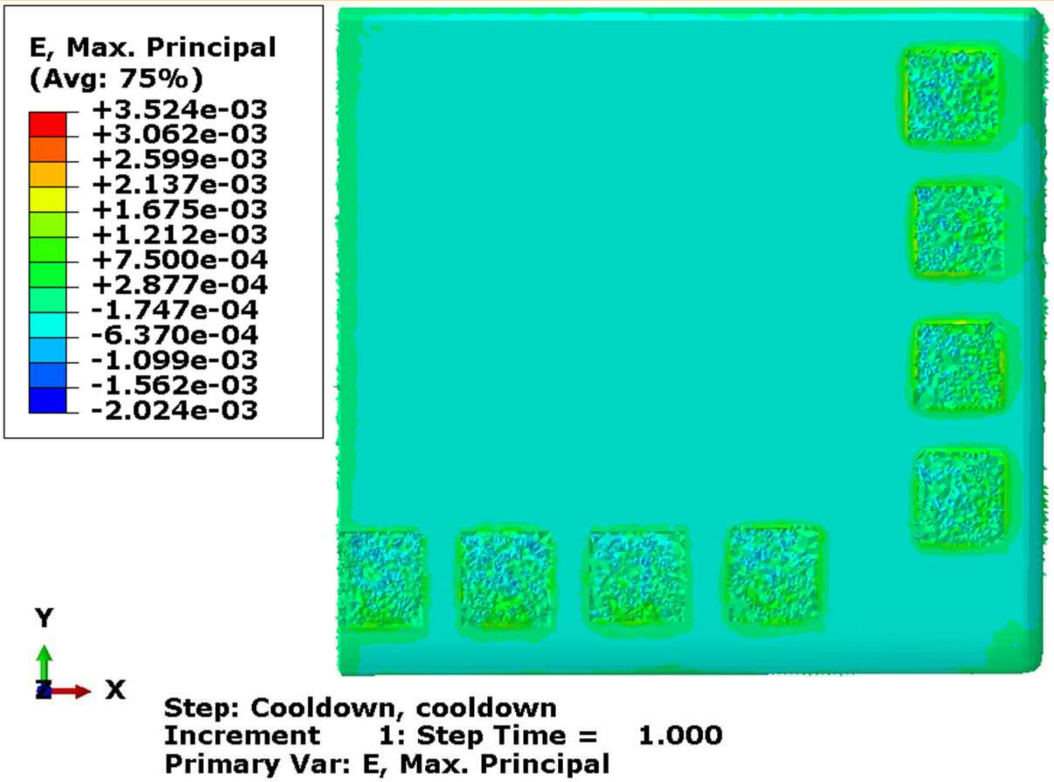

Molded with EMC A

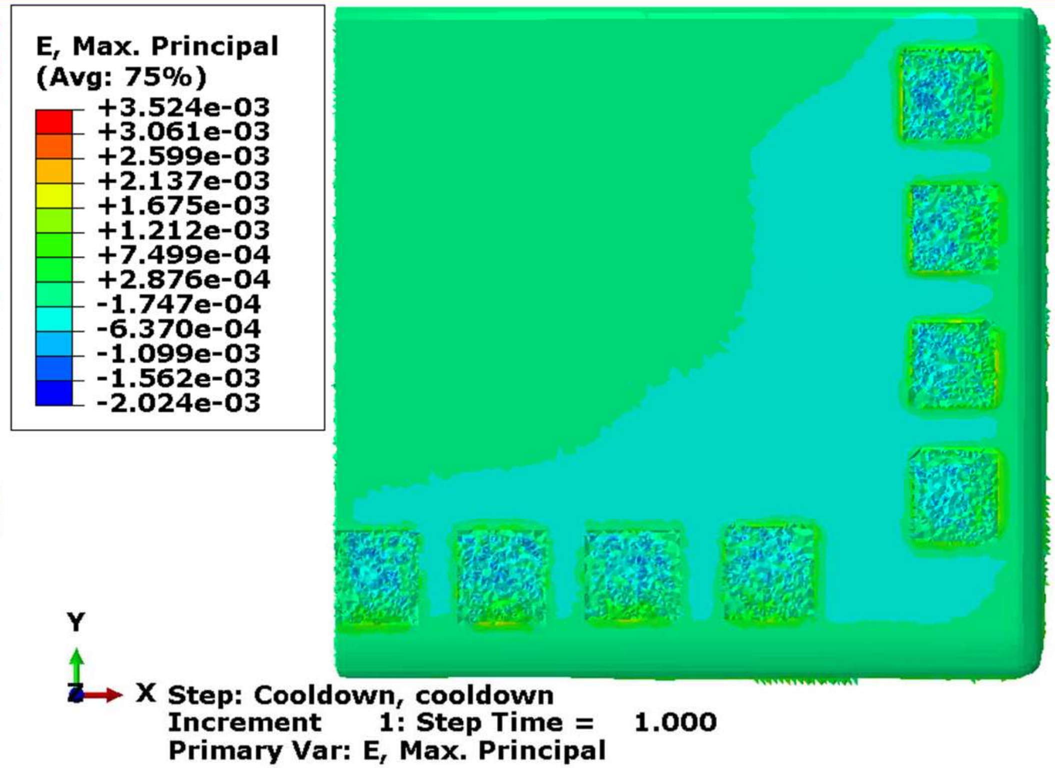

Molded with EMC F

- Chip molded with green CTE EMCs have lower risk of delamination related failure and could be more suitable for *ultra-low-k* dielectric materials.

Results

Strains on Leads-EMC Interface Cooldown Phase

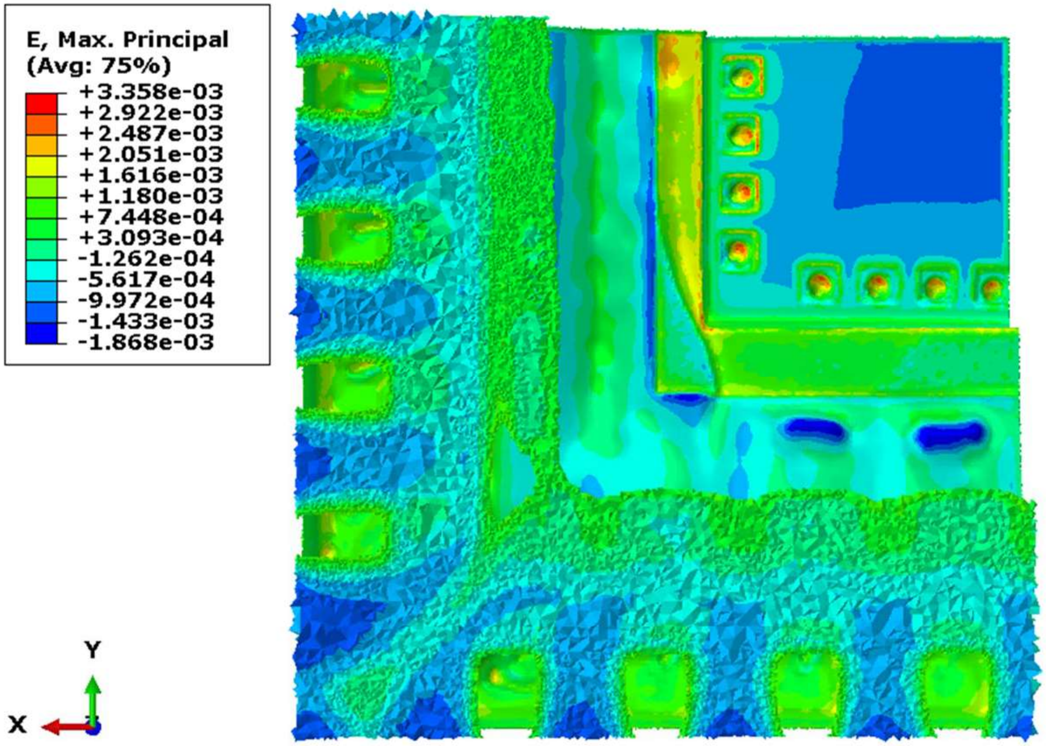

Molded with EMC A

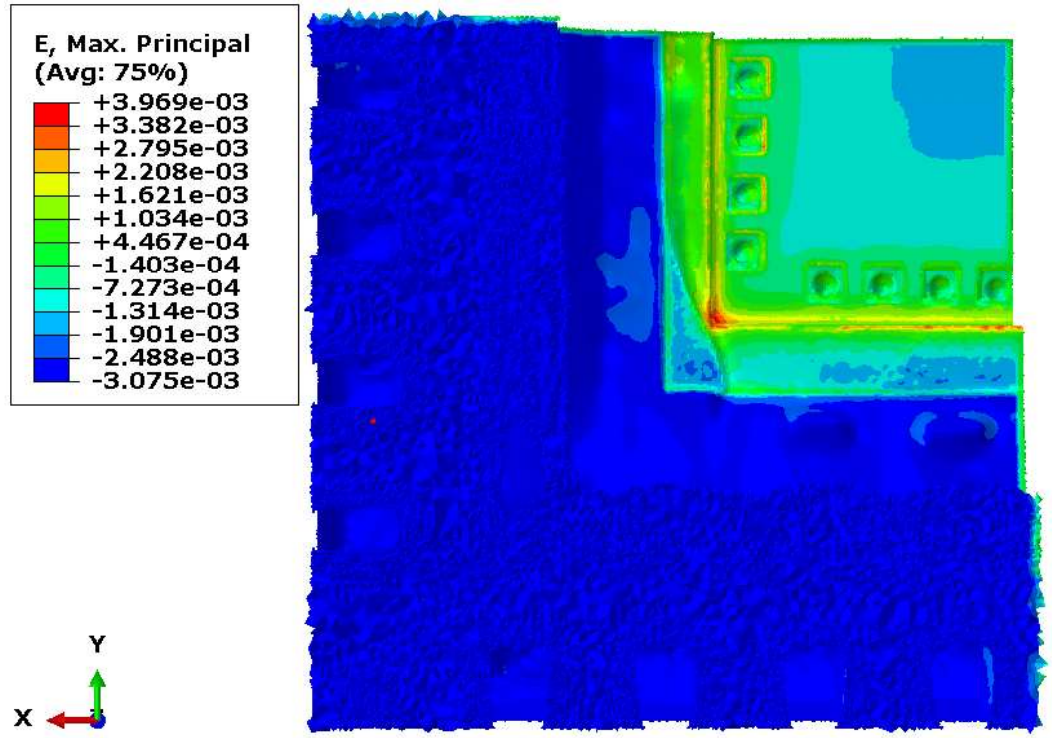

Molded with EMC F

- ❑ Strains at the leads-EMC interface were highest for EMC A. Green EMCs could be highly susceptible for delamination related premature failures and need careful evaluation of interfacial properties.

Results

Stresses on WBs during Cooldown Phase

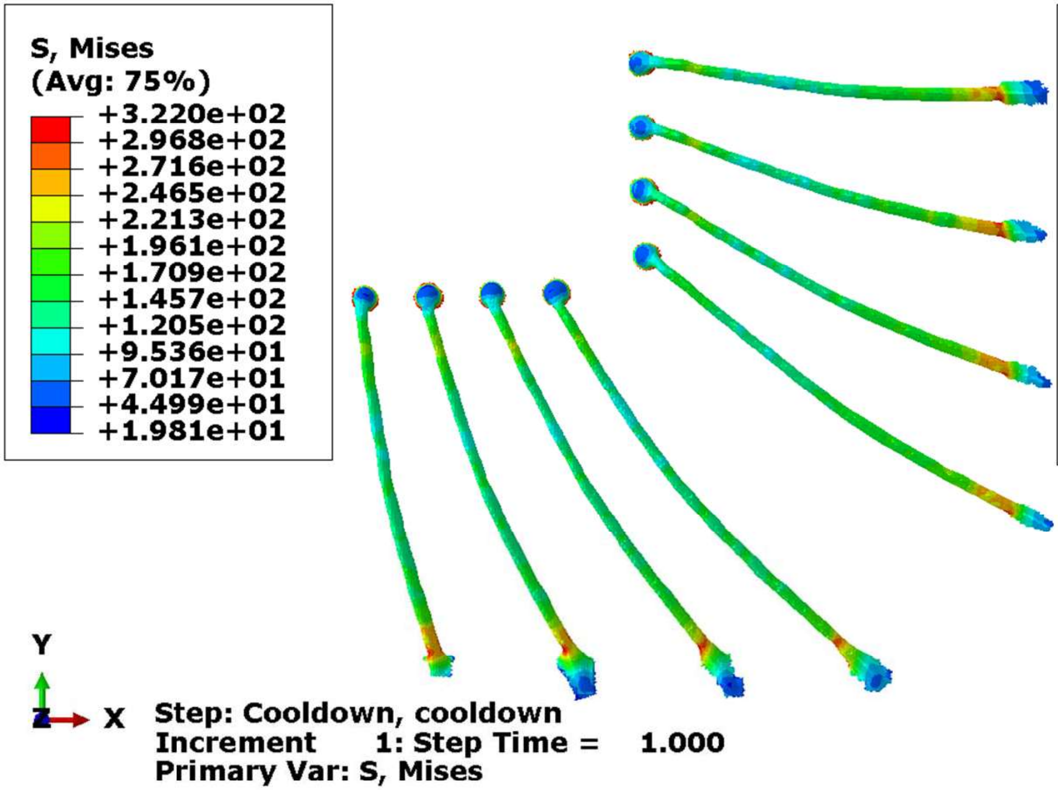

Molded with EMC A

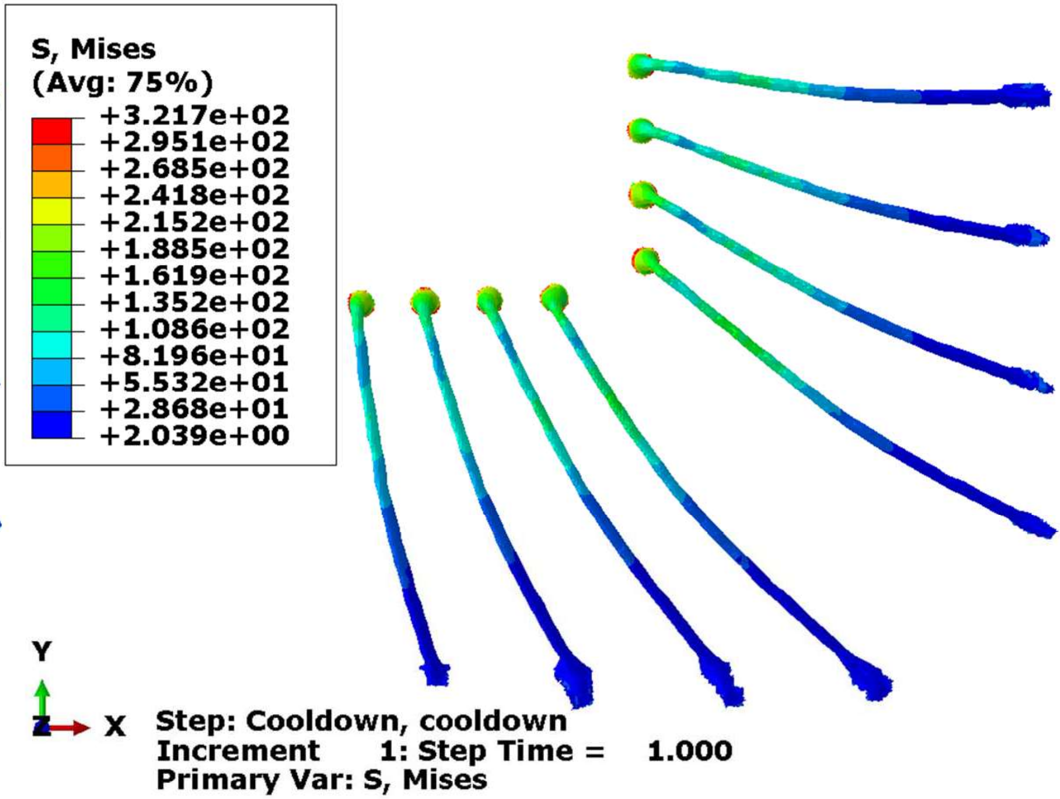

Molded with EMC F

- ❑ Highest von-mises stresses were observed at the wedge bond for green EMCs. Regular EMCs do not show excessive stresses at the wedge bond.

Results

Principal Stress along the length of Wire Bond

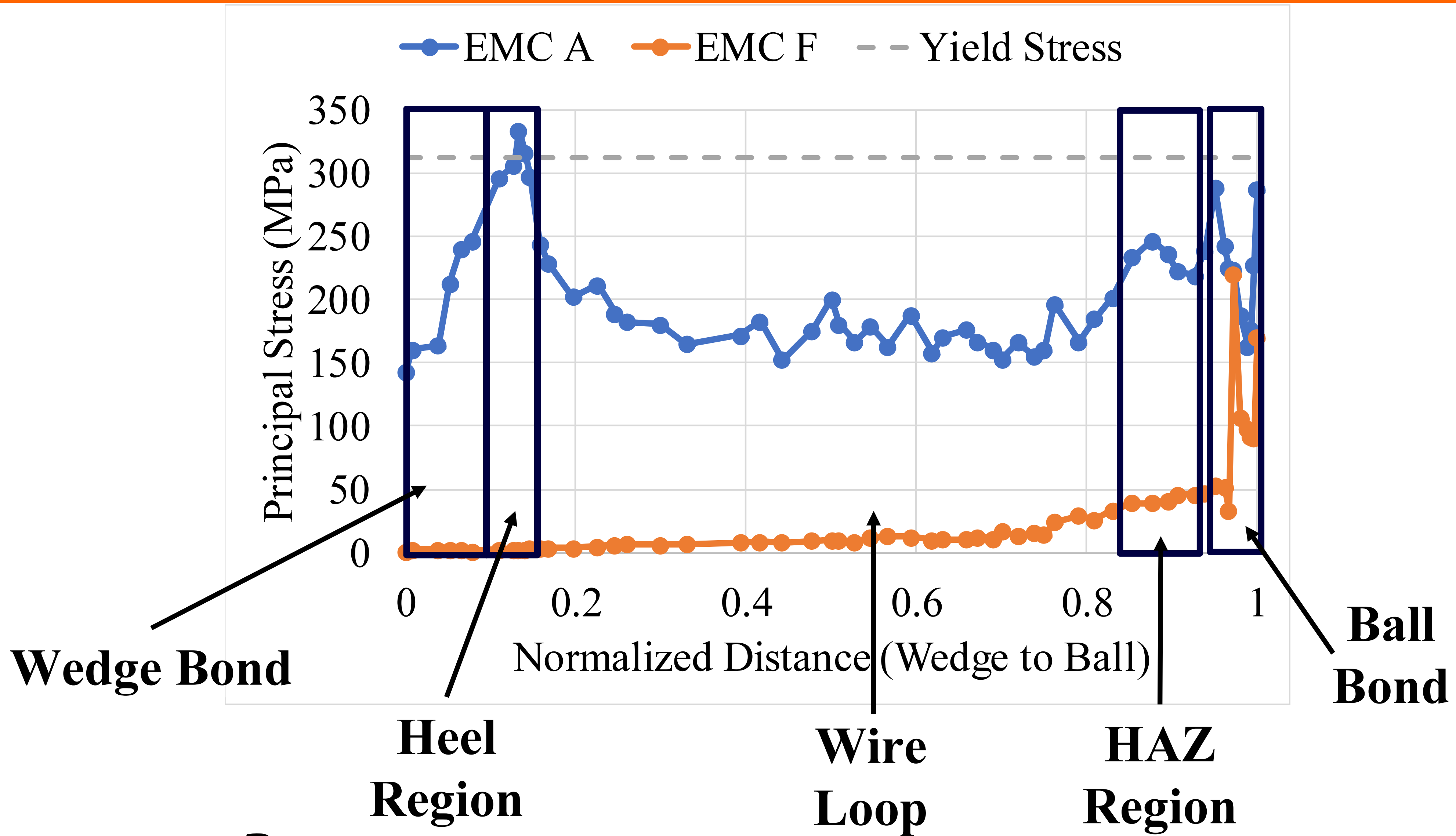

cave³

NSF Center for Advanced Vehicle and Extreme Environment Electronics

AUBURN UNIVERSITY

Results

Effective Plastic Strain after 1 complete cycle

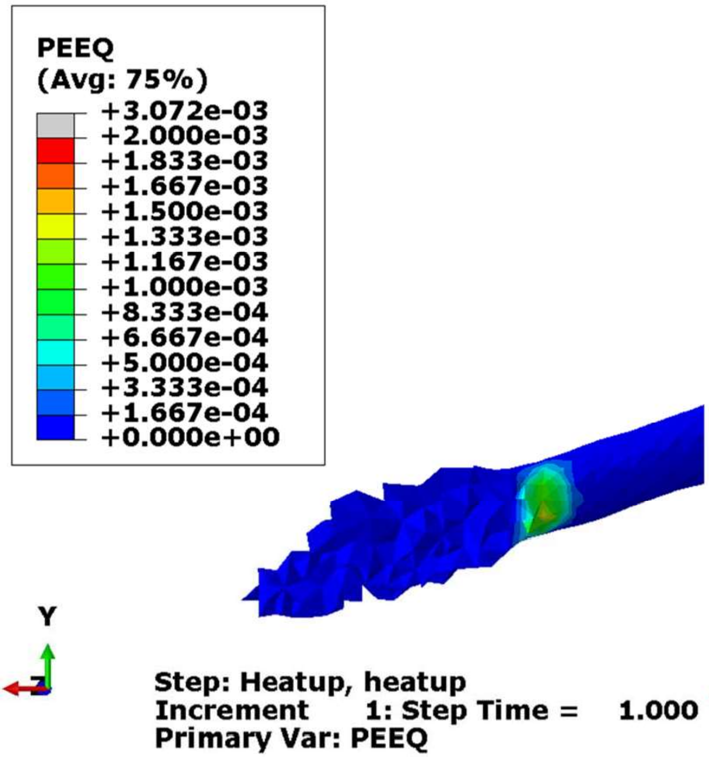

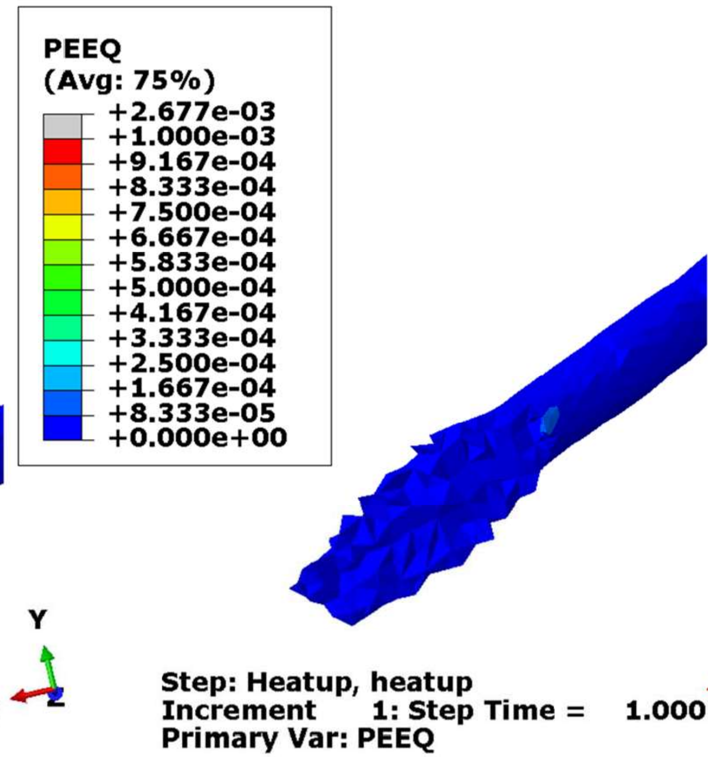

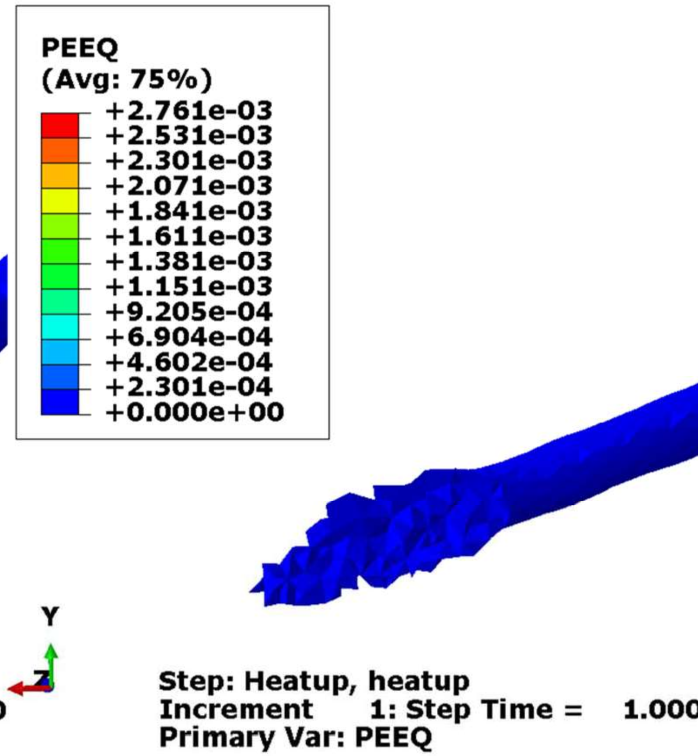

	EMC A	EMC C	EMC F
CTE (ppm)	7	10	16
E (GPa)	30	24	15

Results

Damage Variation Within Package

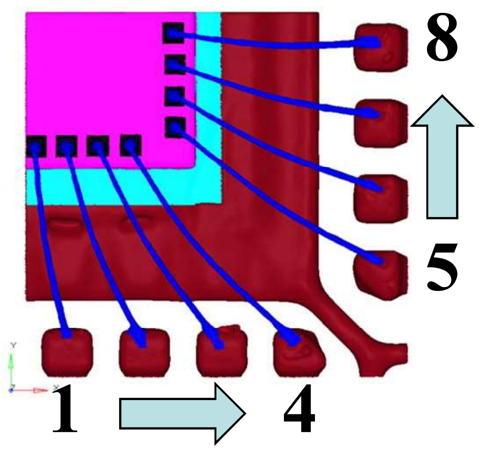

- Wirebond numbers follow counter-clockwise direction as shown in figure.
- WB 4 showed highest plastic deformation in all cases due to higher DNP.

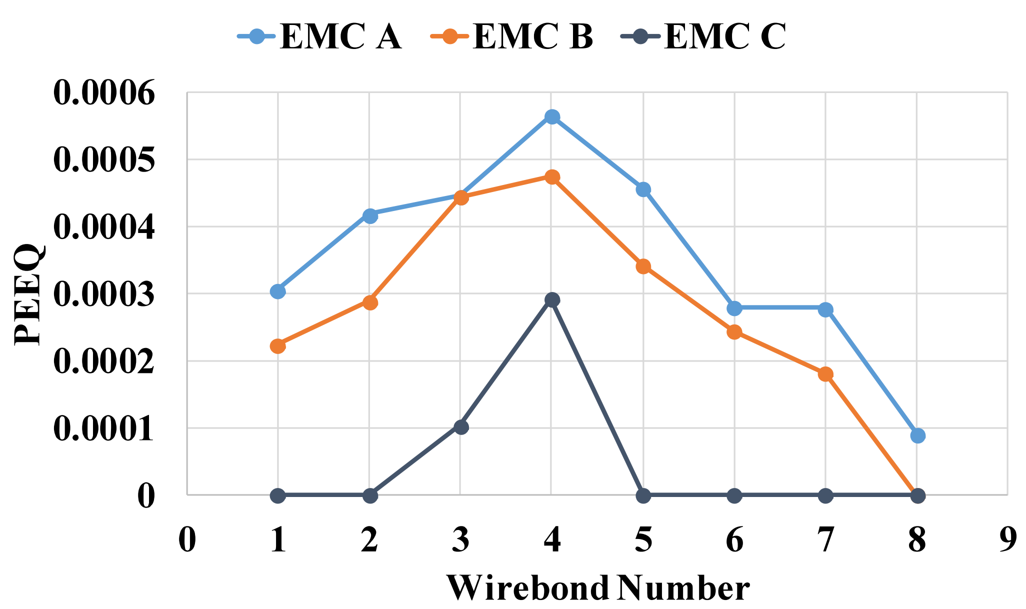

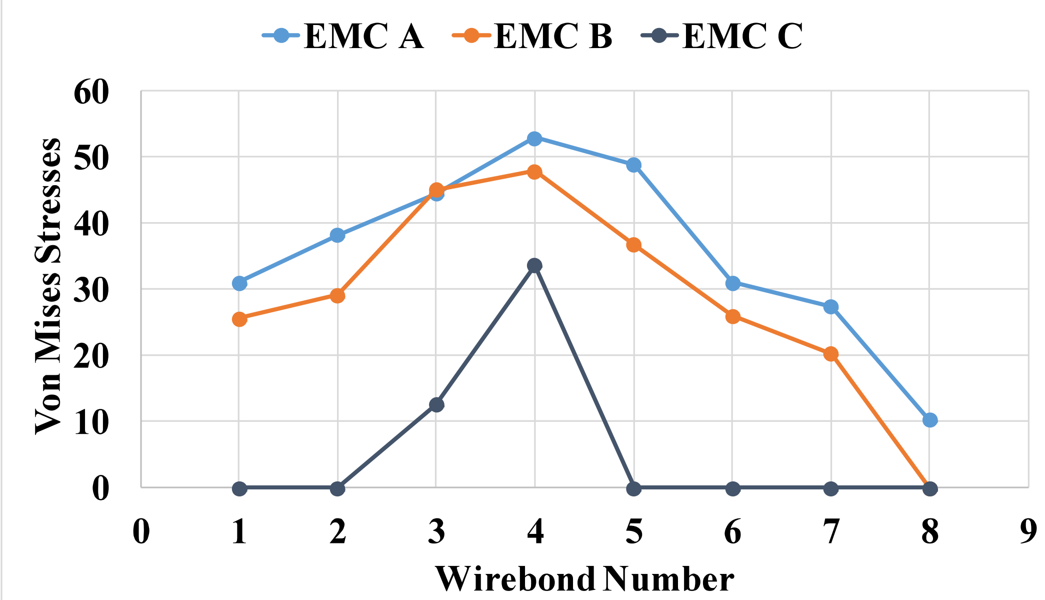

Results – After 1 Complete Cycle

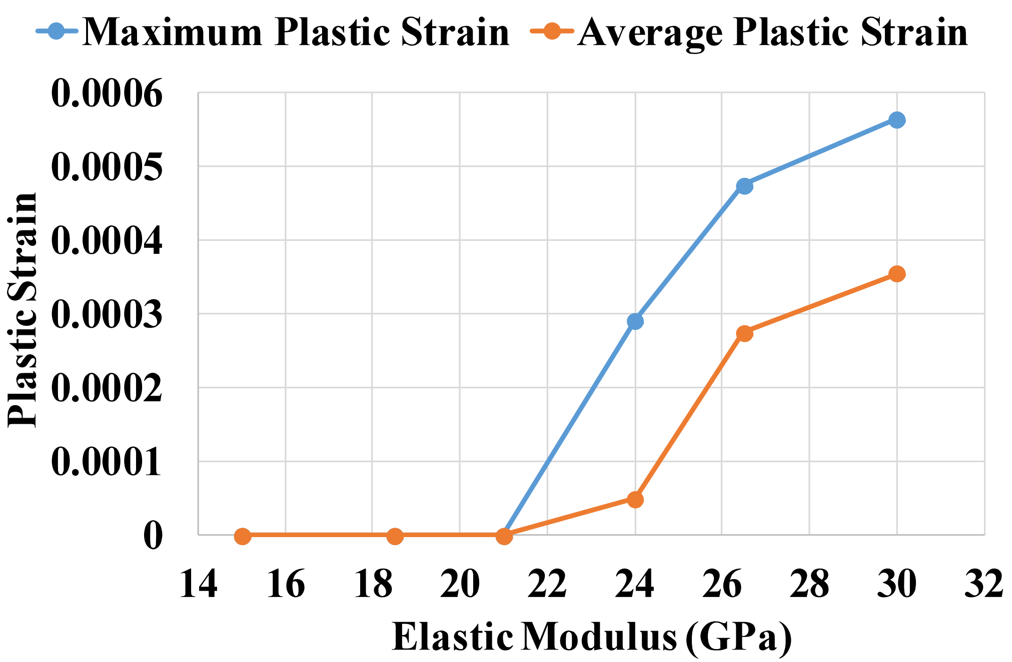

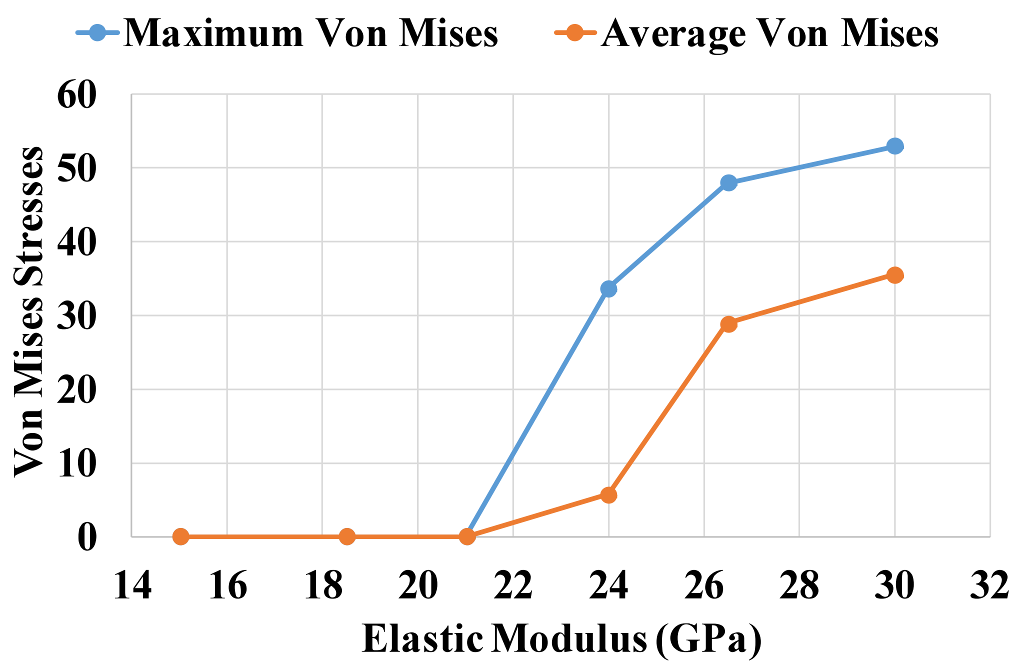

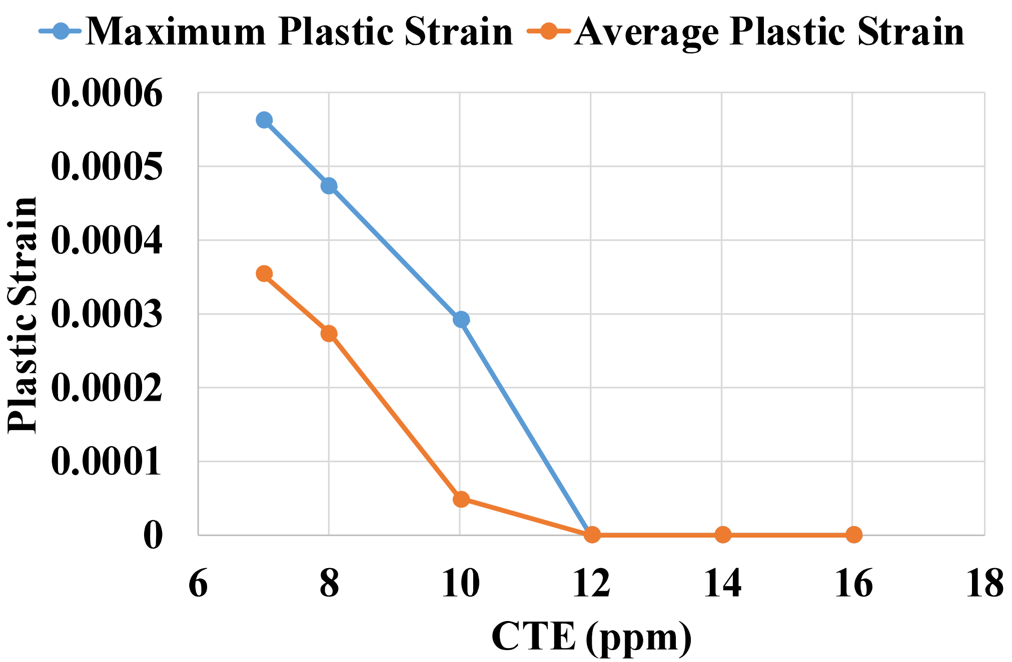

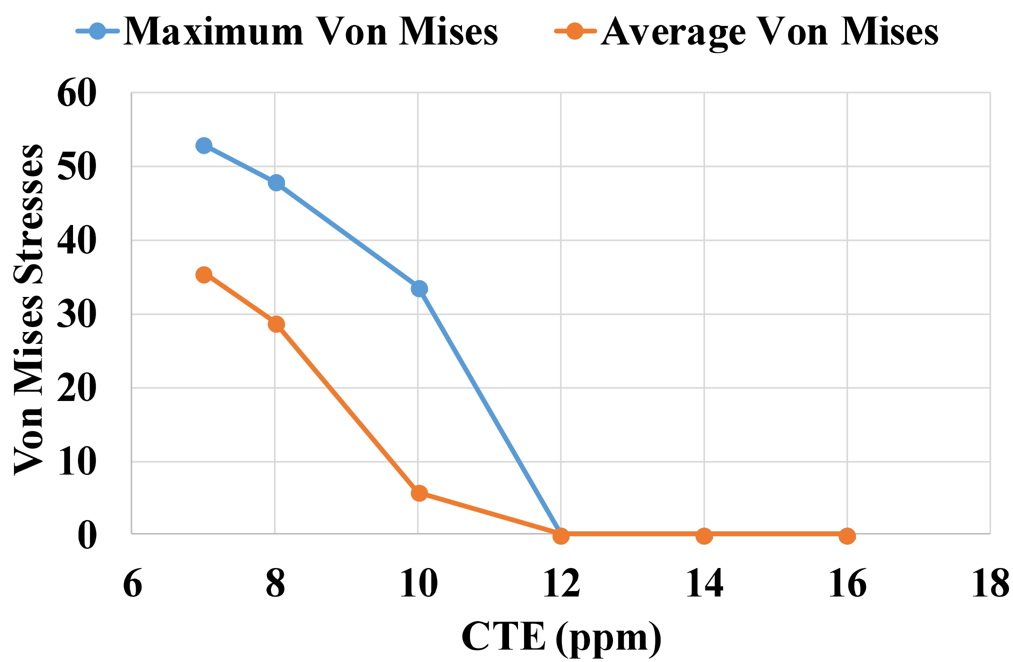

Summary and Conclusions

- In this work, 32 pin QFN assembly was scanned using X-ray-CT system and the scanned data was used to build FE model. True geometry of the wirebond, lead frame, pad was captured in the model.

- Correlation between material properties of EMC with plastic strain and von mises stresses on various components was established successfully for the QFN type packages.

- EMC with lowest CTE and highest E caused highest plastic deformation at wedge bond. EMCs D, E and F with higher CTE proved to be more reliable. Delamination related failures in the green EMCs needs to be further evaluated.

Moving Boundary Model based on the electrochemical measurements of Cu and Cu-Al IMCs

Y. Luo, P. Lall

- Introduce an electrochemical approach to the quantification of Cu-Al wire bond micro-galvanic corrosion under high humidity environmental conditions

- Build a life-prediction model of Cu-Al wire bond interconnect

New Approach of WB Corrosion Modeling

current

Assumption of unchanged corrosive environment & unchanged corrosion front

Constant chlorine concentration, Tafel parameters

Constant corrosion rate of Cu-Al IMC layer

new

Assumption of time-dependent corrosive environment due to chlorine transport & moving corrosion front

Time-dependent chlorine concentration, Tafel parameters

Time-dependent corrosion rate of Cu-Al IMC layer

Flowchart of Corrosion Modeling

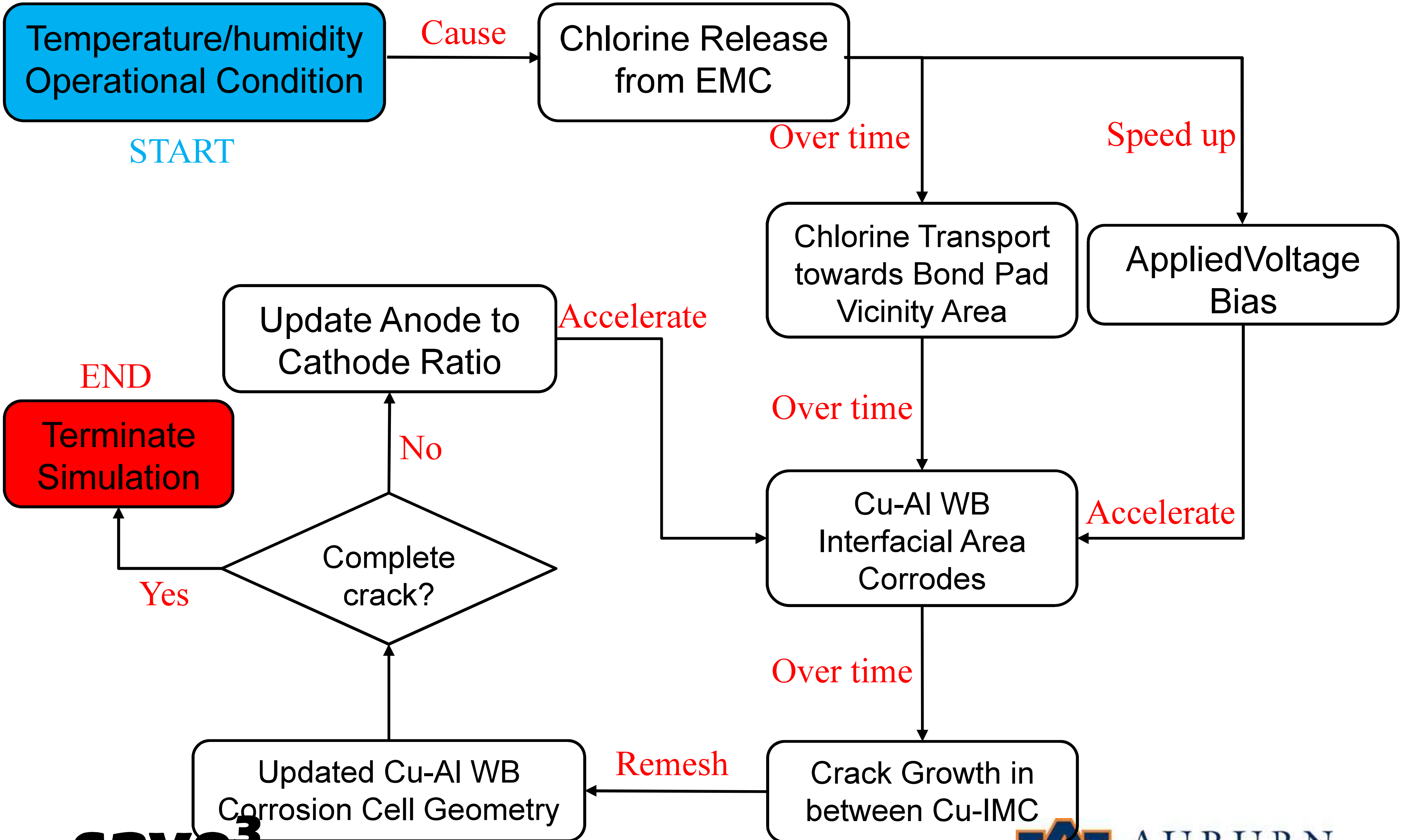

Cu-Al Wire Bond Corrosion Modeling

Epoxy Mold Compound
pH
Diffusion Coefficient
Ionic Mobility
Chlorine Release Rate

Cu-Al Wire Bond
Electrochemical Properties
IMC Thickness
Wire Bond Size

Operational Environment
Temperature
Relative Humidity
Electric Bias

↓

Time-Dependent FEM Multiphysics Solver

↓

Crack Growth Simulation

↓

RUL Prediction

Modeling Geometry

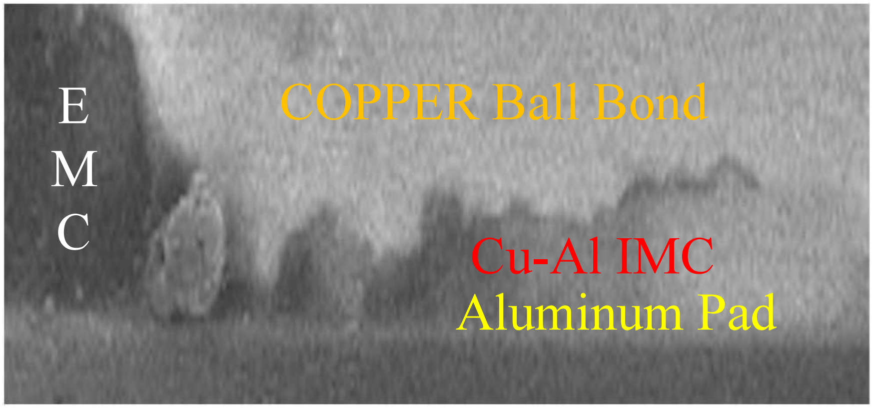

SEM cross section image of WB corrosion

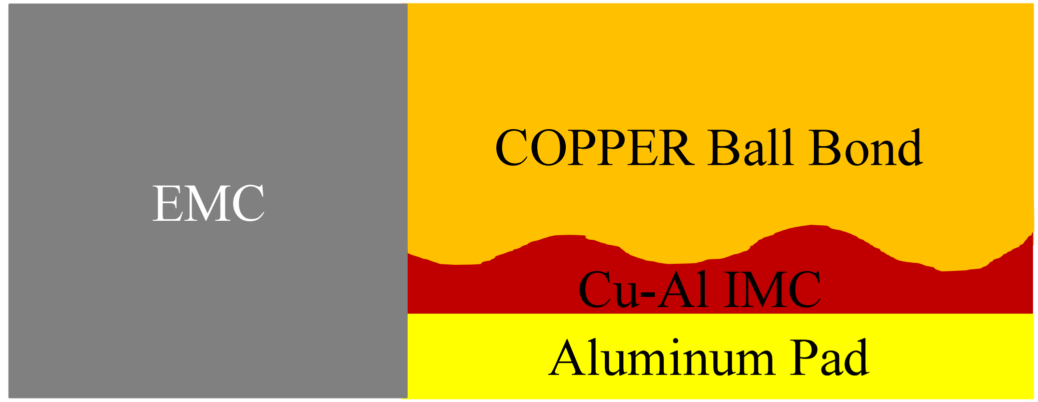

model geometry (free of corrosion)

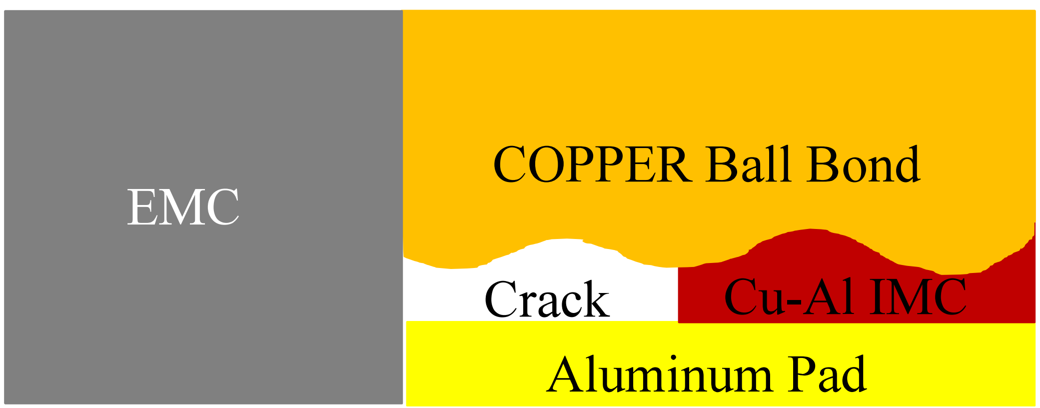

model geometry (corrosion propagation)

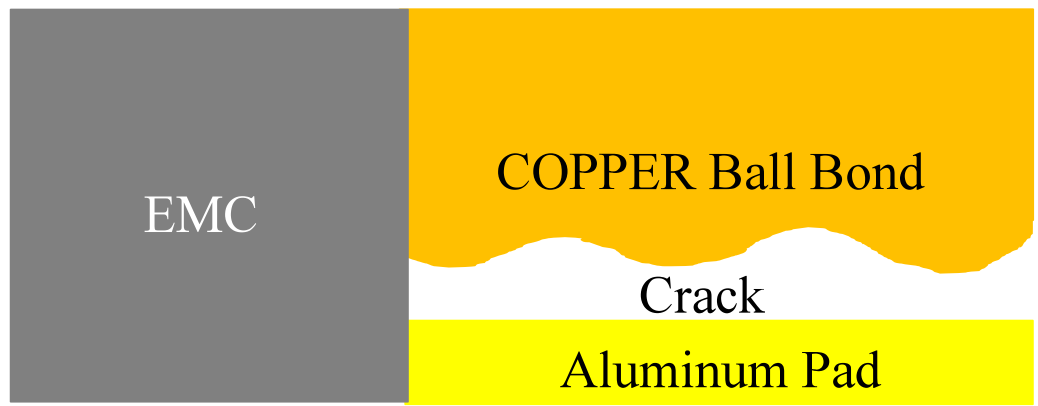

model geometry (WB failure)

Demonstration of Geometry Evolution

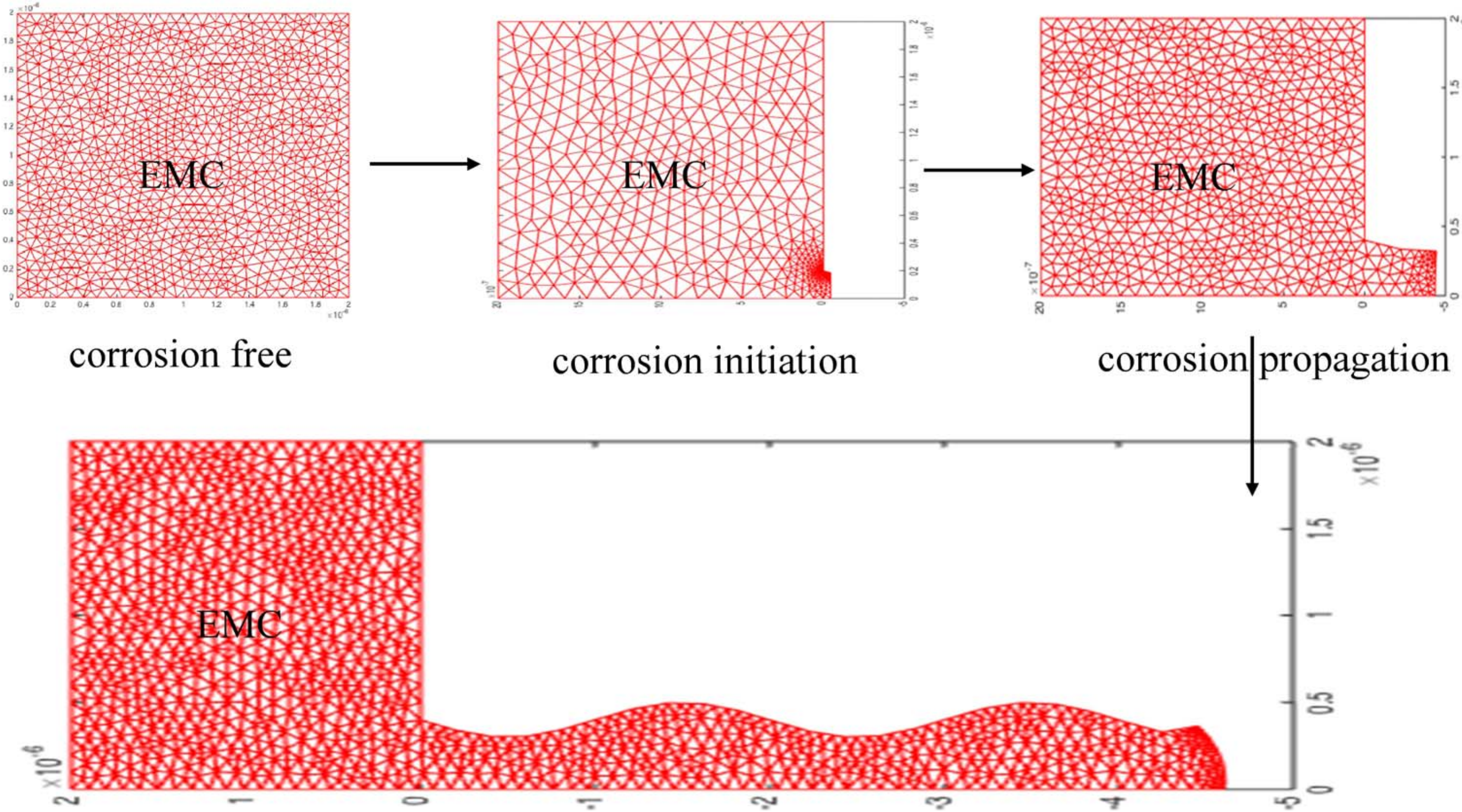

further corrosion propagation

Nernst Planck Equation

NP governs the transport of chlorine in EMC

$$\frac{\partial c}{\partial t} = \nabla \cdot (D \nabla c) + z\mu \nabla \cdot (c \nabla V)$$

J: ionic flux
D: diffusion coefficient
c: concentration
z: electron number
μ: ionic mobility
V: electric potential
t: aging duration

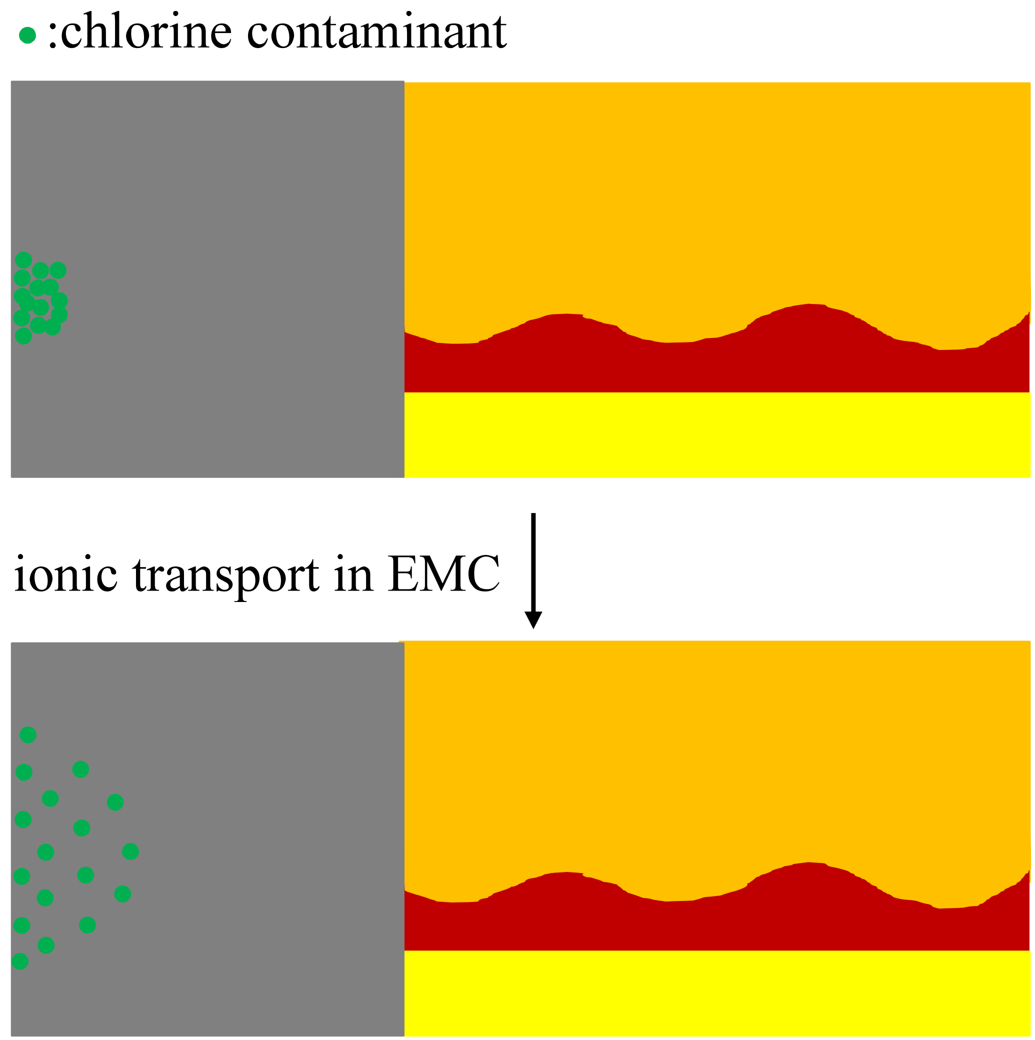

Butler-Volmer B.C.

BV B.C. predicts the corrosion rate of Cu-Al IMC

$$\nabla^2 V = 0$$

$$\nabla_n V = -j_{a(c)}(V)/\sigma$$

$$j_c = j_{0c} * \left(e^{\frac{E_c - V}{\alpha_c}} - e^{\frac{E_c - V}{-\beta_c}}\right)$$

$$j_a = j_{0a} * \left(e^{\frac{E_a - V}{\alpha_a}} - e^{\frac{E_a - V}{-\beta_a}}\right)$$

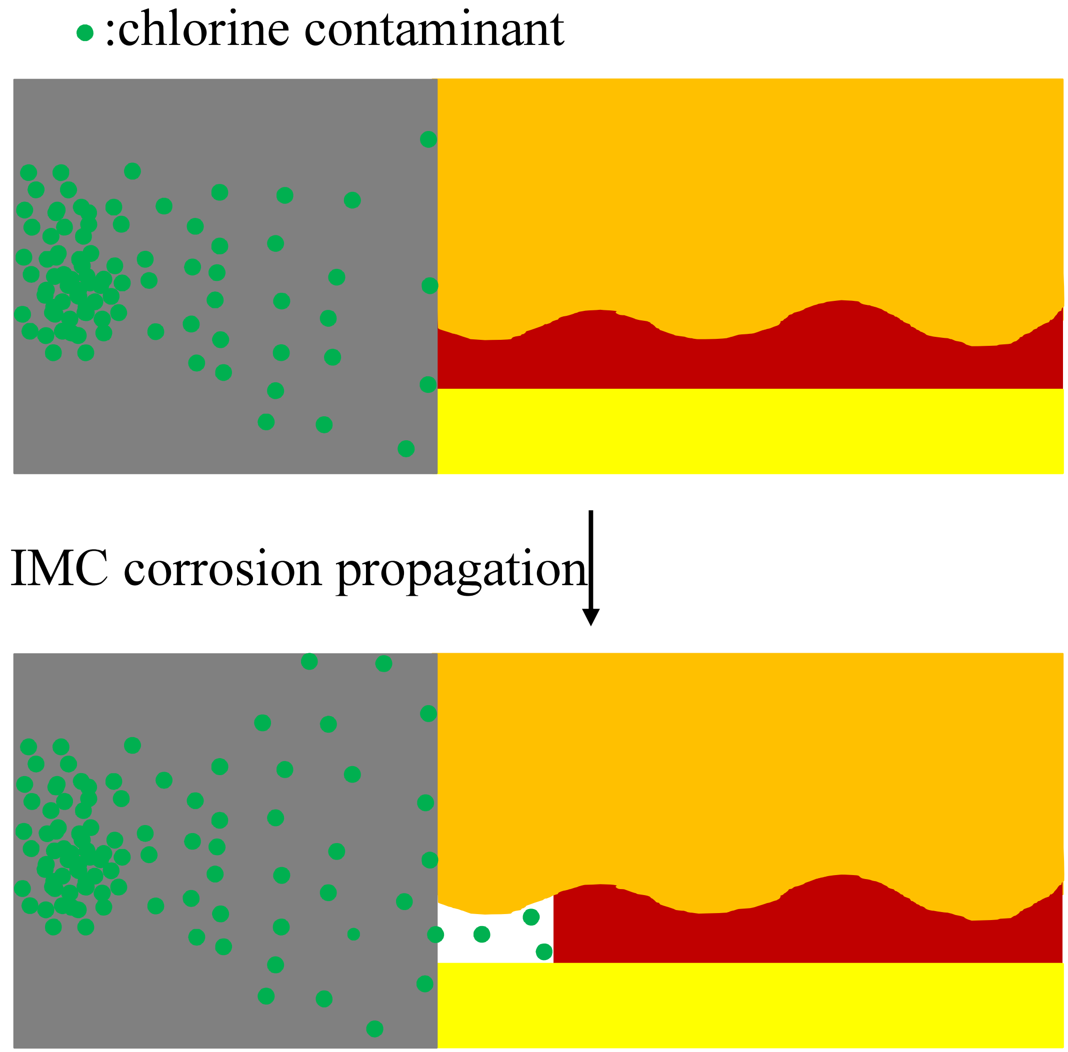

ja, jc: anodic/cathodic corrosion current density
j0a, j0c: anodic/cathodic free corrosion current density
Ea, Ec: anodic/cathodic open circuit potential
alpha, beta: Tafel parameters
sigma: electrolyte conductivity

FEM Approach to Solve PDEs

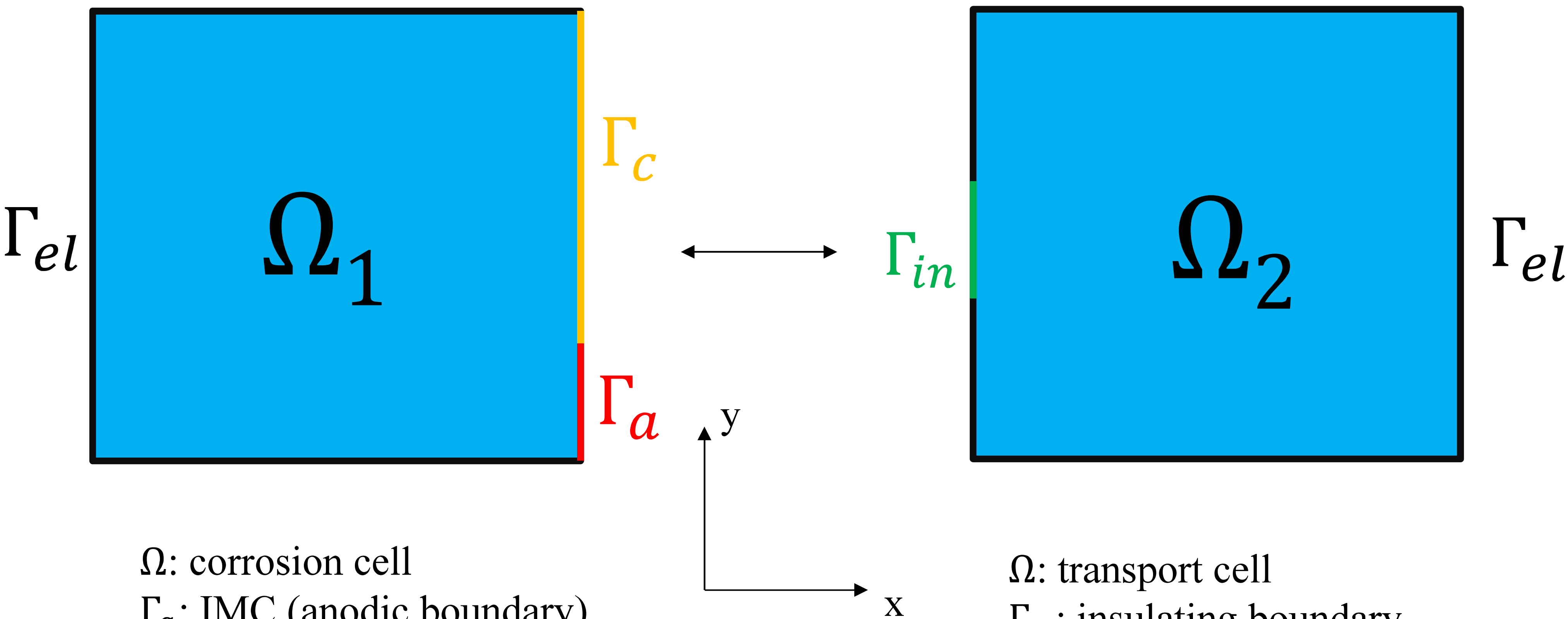

Ω: corrosion cell
Γ_a: IMC (anodic boundary)
Γ_c: Cu (cathodic boundary)
Γ_{el}: insulating boundary

Ω: transport cell
Γ_{el}: insulating boundary
Γ_{in}: influx boundary

Gauss–Seidel Iterative Approach

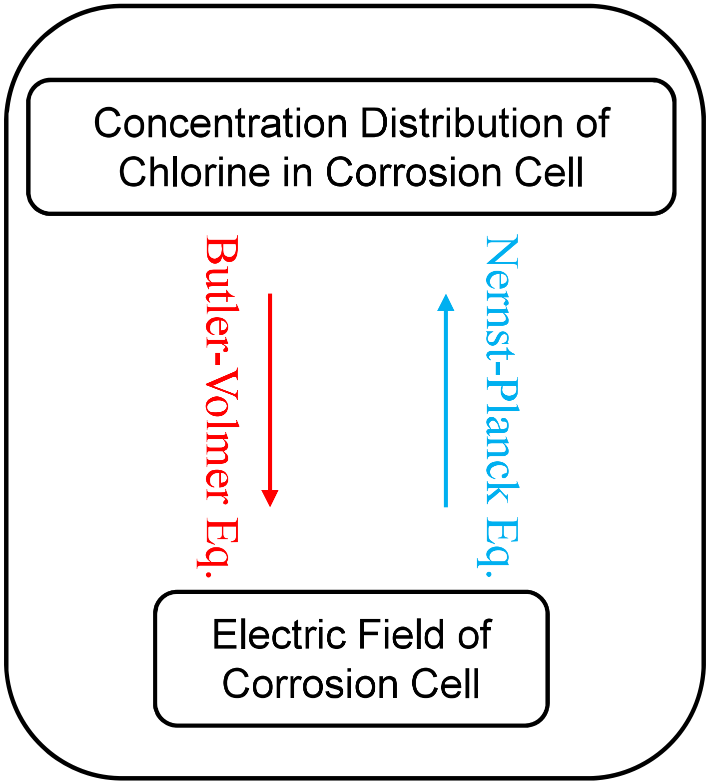

Coupled Nonlinear PDEs

Gauss–Seidel Iterative Method

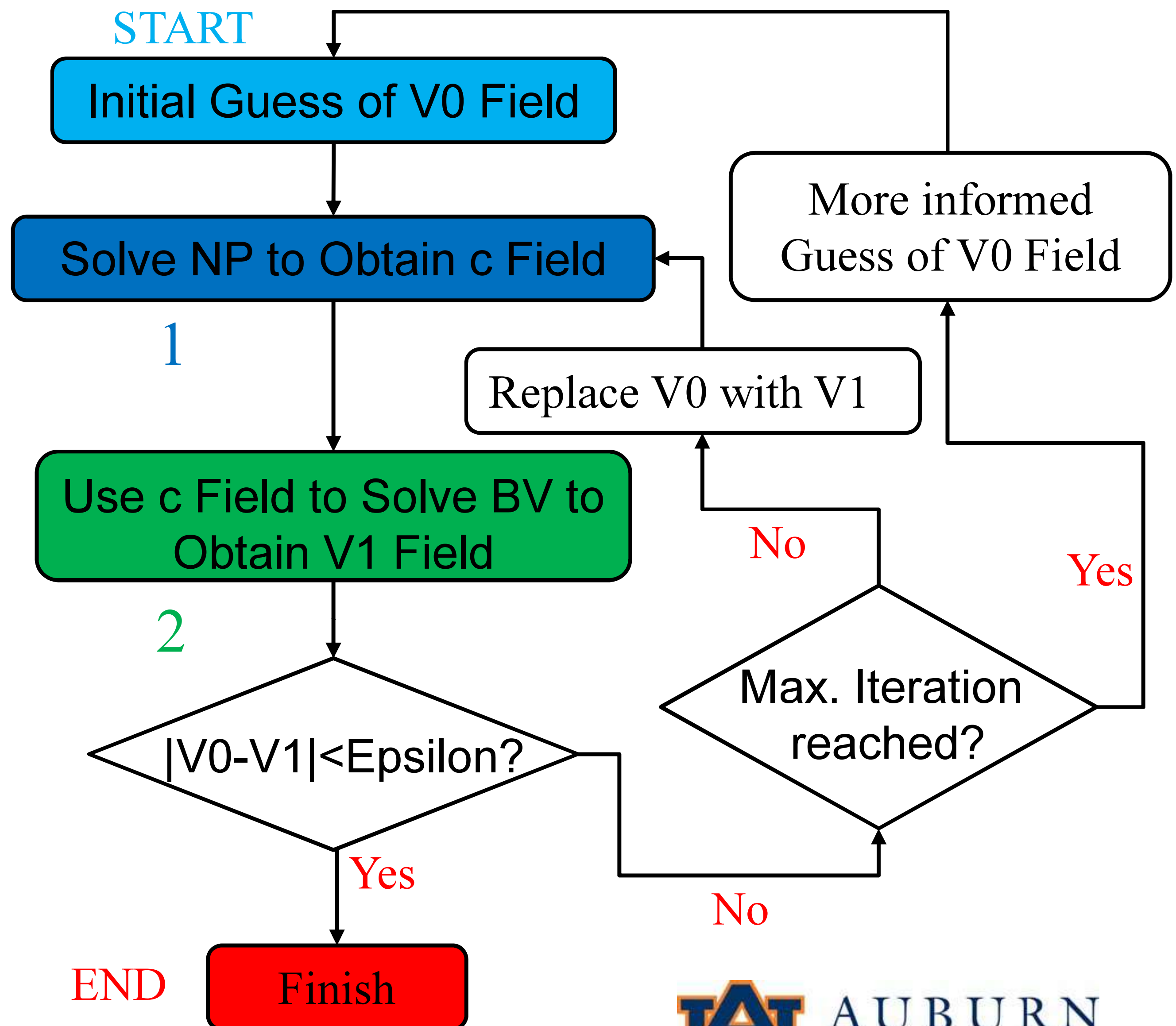

FEM Approach to Solve N.P.

$$\frac{\partial c}{\partial t} = \nabla \cdot (D\nabla c) + z\mu\nabla \cdot (c\nabla V)$$

$$\iint_{\Omega_e} [N]^T [N]\{\frac{\partial c}{\partial t}\} dxdy = -\iint_{\Omega_e} [\nabla N]^T D [\nabla N]\{c\} dxdy - \iint_{\Omega_e} [\nabla N]^T z\mu\nabla V [N]\{c\} dxdy$$ Domain Discretization

$$M_{ij}^e = -D\iint_{\Omega_e} \left[\frac{\partial N_i}{\partial x}\frac{\partial N_j}{\partial x} + \frac{\partial N_i}{\partial y}\frac{\partial N_j}{\partial y}\right] dxdy$$

$$G_{ij}^e = -z\mu\nabla V\iint_{\Omega_e} \left[\frac{\partial N_i}{\partial x}N_j + \frac{\partial N_i}{\partial y}N_j\right] dxdy$$

$$A_{ij}^e = \iint_{\Omega_e} N_i N_j dxdy$$

$$\frac{\partial\{c\}}{\partial t}[A] = [M]\{c\} + [G]\{c\}$$

$$\int_{t_l}^{t_{l+1}} \frac{\partial\{c\}}{\partial t}[\mathrm{A}]\mathrm{dt} = \int_{t_l}^{t_{l+1}} [\mathrm{M}]\{\mathrm{c}\}\mathrm{dt} + \int_{t_l}^{t_{l+1}} [\mathrm{G}]\{\mathrm{c}\}\mathrm{dt}$$ Time Discretization

$$(c_{t_{l+1}} - c_{t_l})[\mathrm{A}] = [\mathrm{M}]c_{t_{l+1}}(t_{l+1} - t_l) + [\mathrm{G}]c_{t_{l+1}}(t_{l+1} - t_l)$$ Backward Euler

$$([\mathrm{A}] - [M]\Delta t - [G]\Delta t)c_{t_{l+1}} = [\mathrm{A}]c_{t_l}$$

FEM Approach to Solve B.V.B.C.

PDE with nonlinear B.C

$$\nabla^2 V = 0$$

$$\nabla_n V = -j_{a(c)}(V)/\sigma$$

$$j_c = j_{0c} * \left(e^{\frac{E_c - V}{\alpha_c}} - e^{\frac{E_c - V}{-\beta_c}}\right)$$

$$j_a = j_{0a} * \left(e^{\frac{E_a - V}{\alpha_a}} - e^{\frac{E_a - V}{-\beta_a}}\right)$$

Taylor's series

$$f(V) = j_a, g(V) = j_c$$

$$f(V_0^e + \delta^e) \simeq f(V_0^e) + f'(V_0^e) * \delta^e$$

$$g(V_0^e + \delta^e) \simeq g(V_0^e) + g'(V_0^e) * \delta^e$$

Newton-Galerkin method

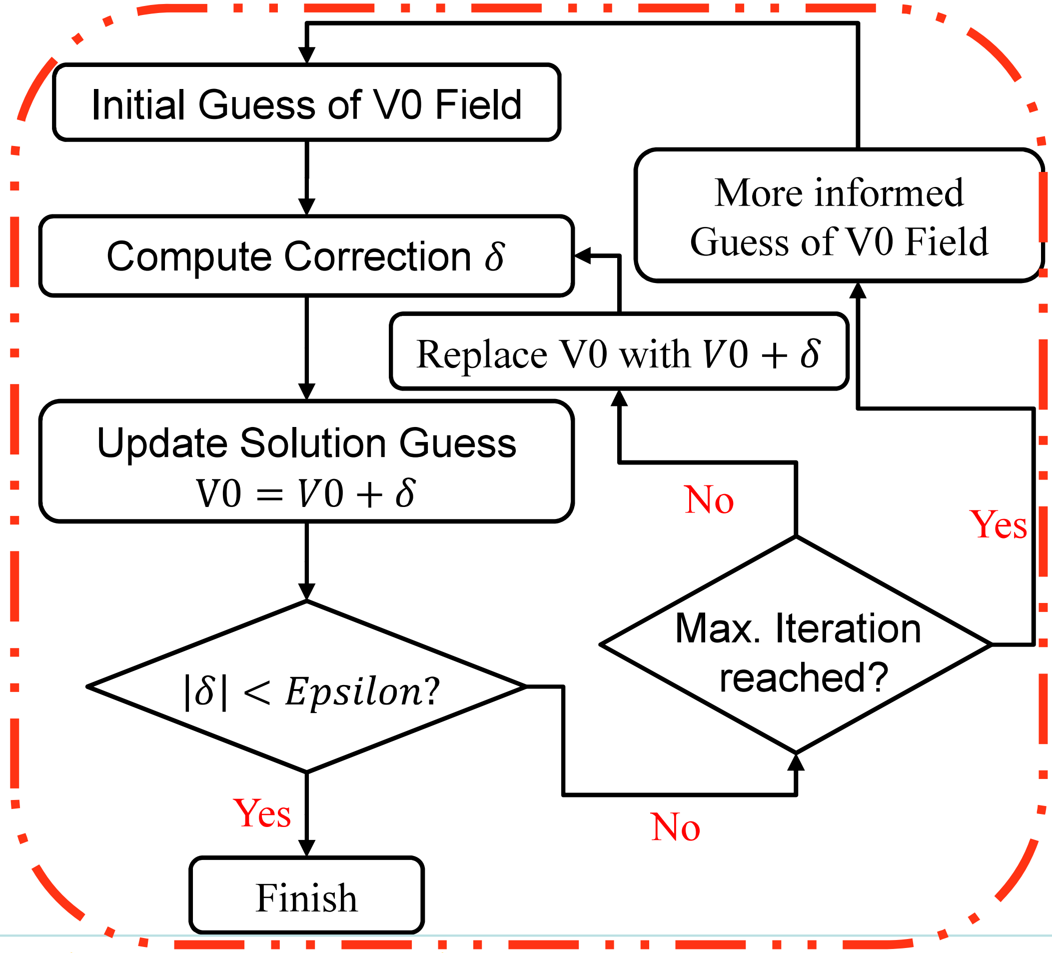

$$\left(M_{ij}^e - \frac{1}{\sigma}\int_{\Gamma_a} N_i f'(V_0^e)\,dl - \frac{1}{\sigma}\int_{\Gamma_c} N_i g'(V_0^e)\,dl\right)\{\delta^e\} = \frac{1}{\sigma}\int_{\Gamma_a} N_i f(V_0^e)\,dl + \frac{1}{\sigma}\int_{\Gamma_c} N_i g(V_0^e)\,dl - M_{ij}^e V_0^e$$

$$K\{X\} = b$$

PDE Result Verification for N.P.

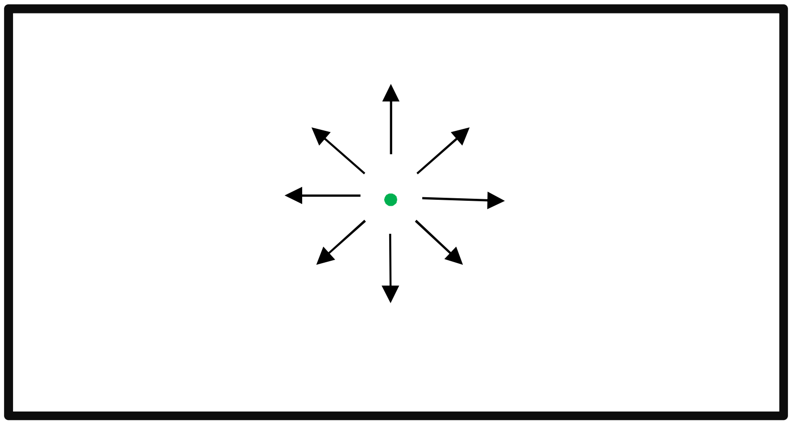

$D=10^{-10} m^2/s$
$c=10 mol/m^2$

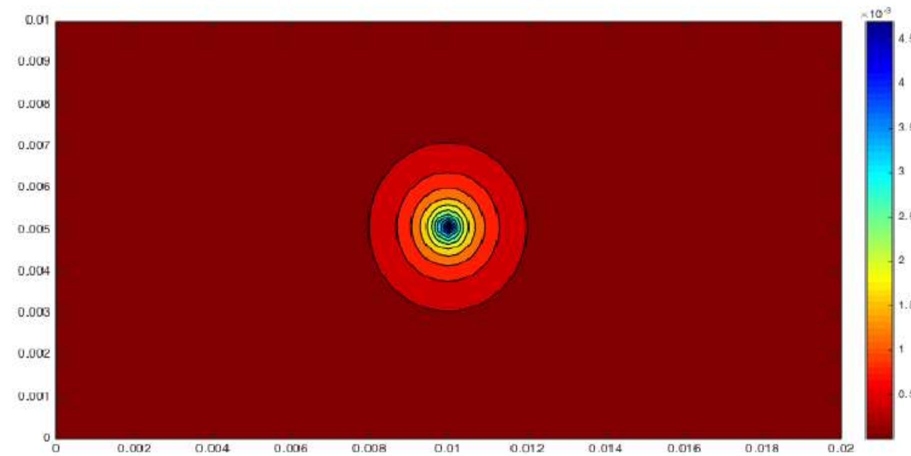

t=10000s

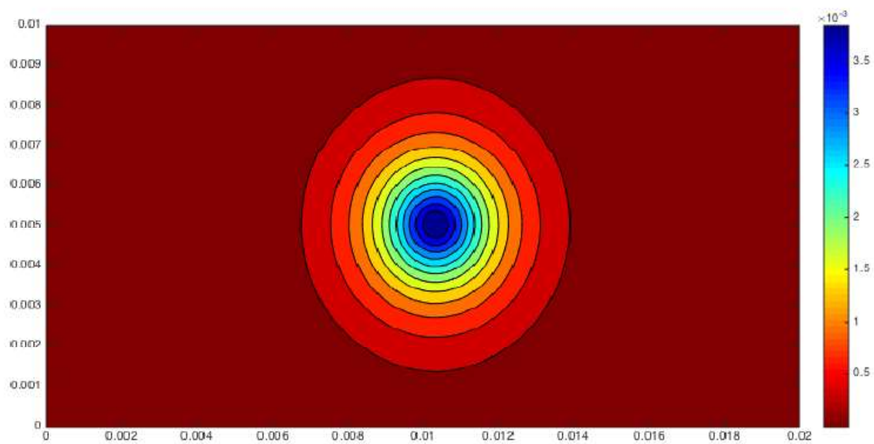

t=20000s

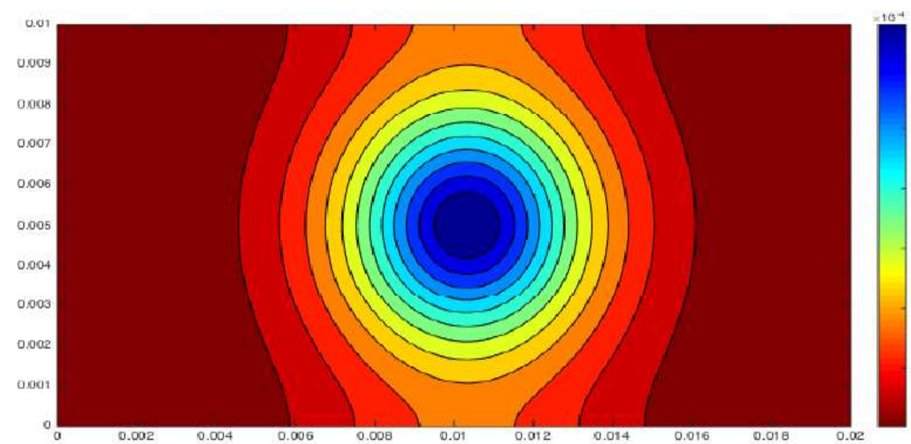

t=40000s

PDE Result Verification for N.P.

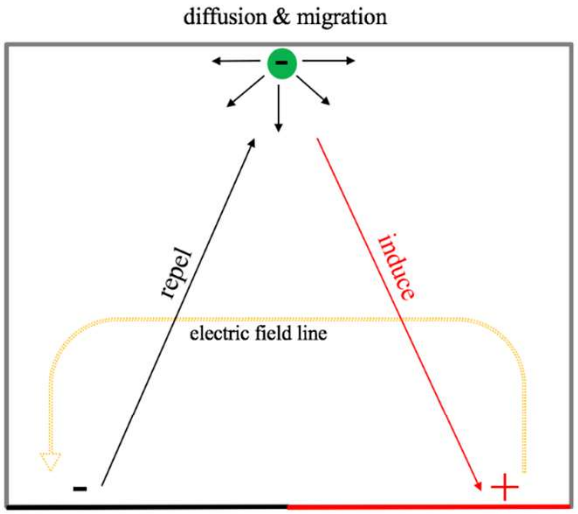

$D=10^{-17} m^2/s$
$\mu=10^{-15} m^2/(V \cdot s)$
influx= $10^{-12} mol/(m^2 \cdot s)$

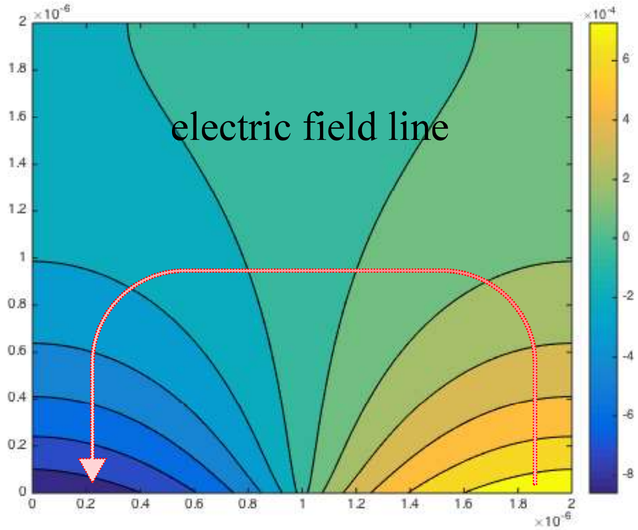

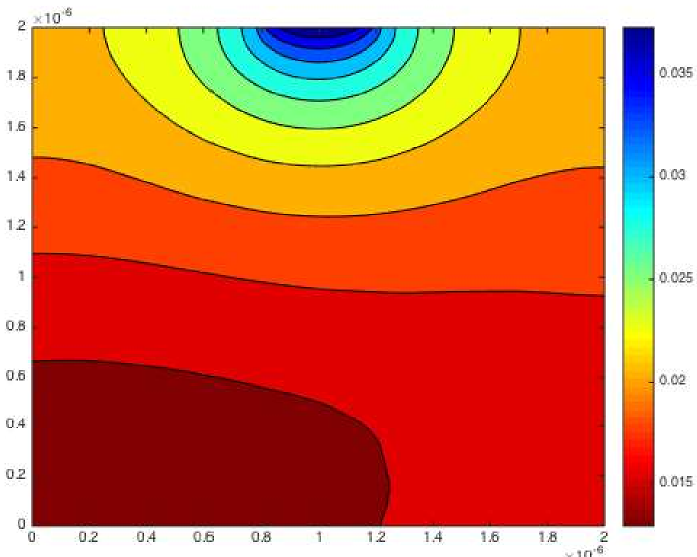

Concentration field @ t=10^5s

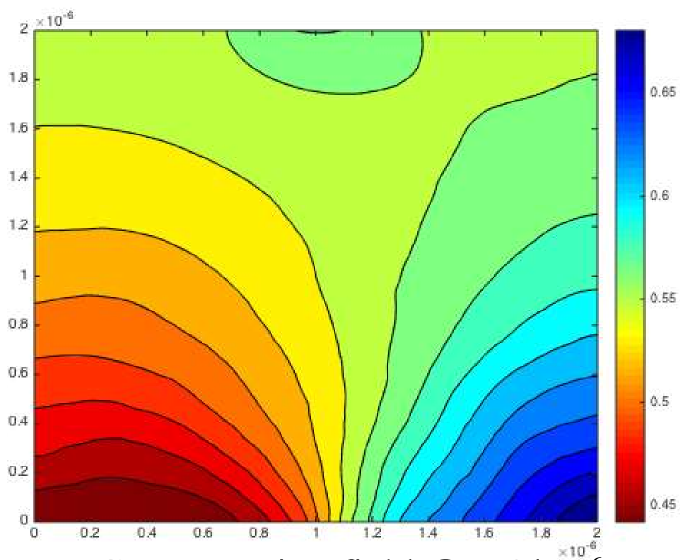

Concentration field @ t=$2*10^6$s

PDE Result Verification for B.V.B.C

FEM Program Output

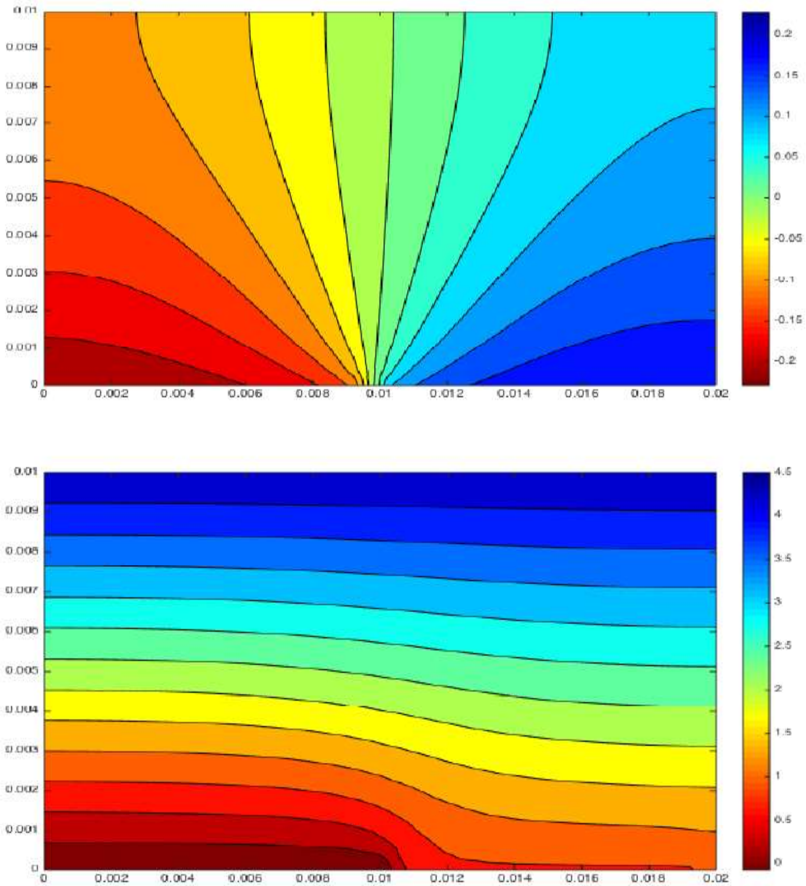

Published Simulation Results

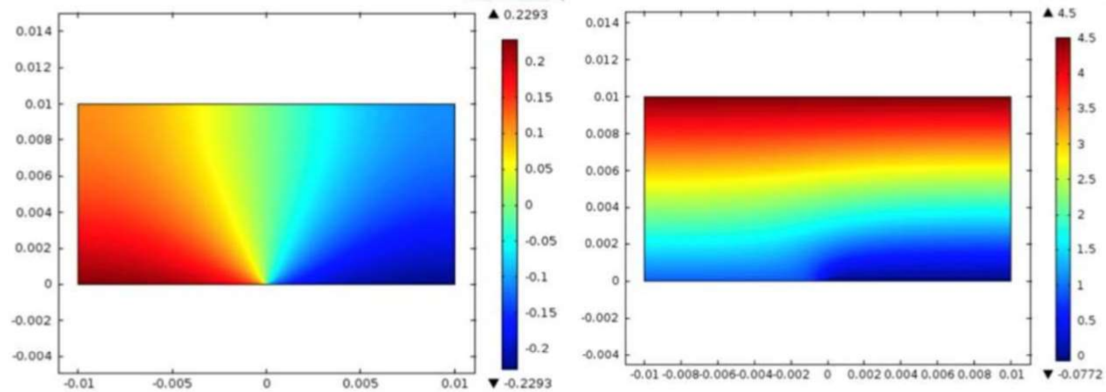

Property	Value	Units
Tafel Parameters:		
α_A anodic reaction of metal A	0.05	V
α_B anodic reaction of metal B	0.05	V
β_A cathodic reaction of metal A	0.05	V
β_B cathodic reaction of metal B	0.05	V
σ conductivity of the electrolyte	10	$\Omega^{-1}m^{-1}$
$i_{0,(A)}$ free current density of metal A	1	Am^{-2}
$i_{0,(B)}$ free current density of metal B	1	Am^{-2}
a surface length of metal A	0.01	m
b surface length of metal B	0.01	m
w thickness of the electrolyte	0.01	m
$\phi_{0,(A)}$ free corrosion potential of metal A	0.5	V
$\phi_{0,(B)}$ free corrosion potential of metal B	-0.5	V

Input data used for model validation

A Finite Difference Numerical Analysis of Galvanic Corrosion for Semi-Infinite Linear Coplanar Electrodes, P.Doig
Finite Element Modeling of Galvanic Corrosion of Metals , *E. Gutierrez-Miravete*

WB Interfacial Corrosion Front Tracking

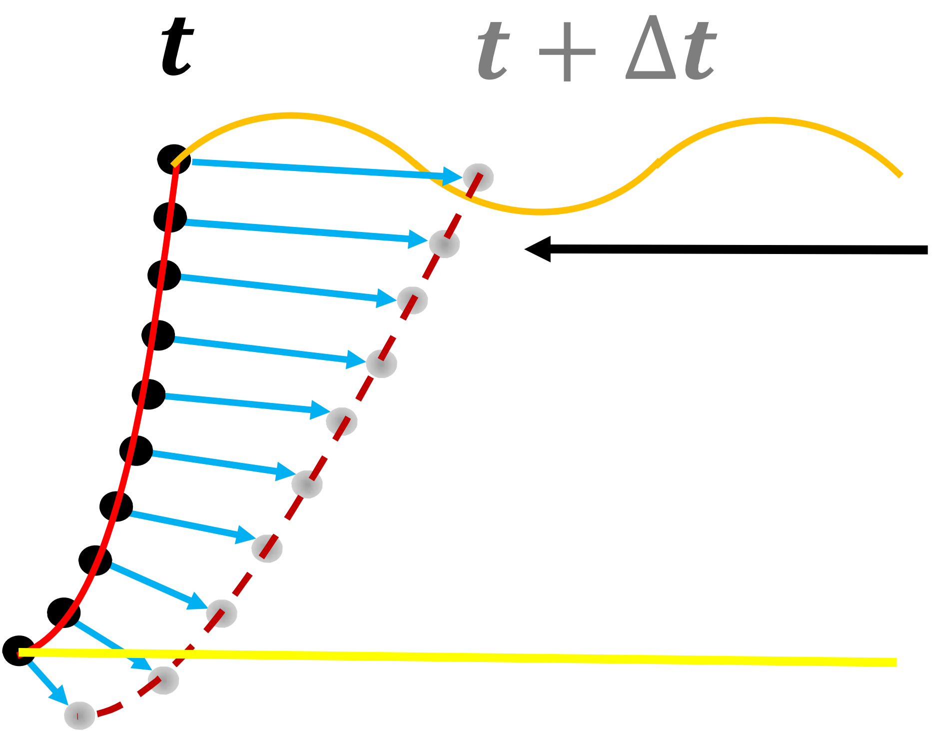

Using **Faraday's Law** to Compute Nodal Displacements on the Corrosion Front

$$v = \frac{M}{zF\rho} j$$

v is corrosion rate (m/s), M is molar mass of IMC (g/mol), F is Faraday's constant, z is electron number and ρ is density of IMC (kg/m^3)

- nodes on current-state corrosion boundary
- next-state corrosion boundary nodes projection
- current-state corrosion boundary
- next-state corrosion boundary projection
- step direction and length
- copper ball bond/IMC layer interface
- aluminum pad/IMC layer interface

WB Interfacial Corrosion Front Tracking

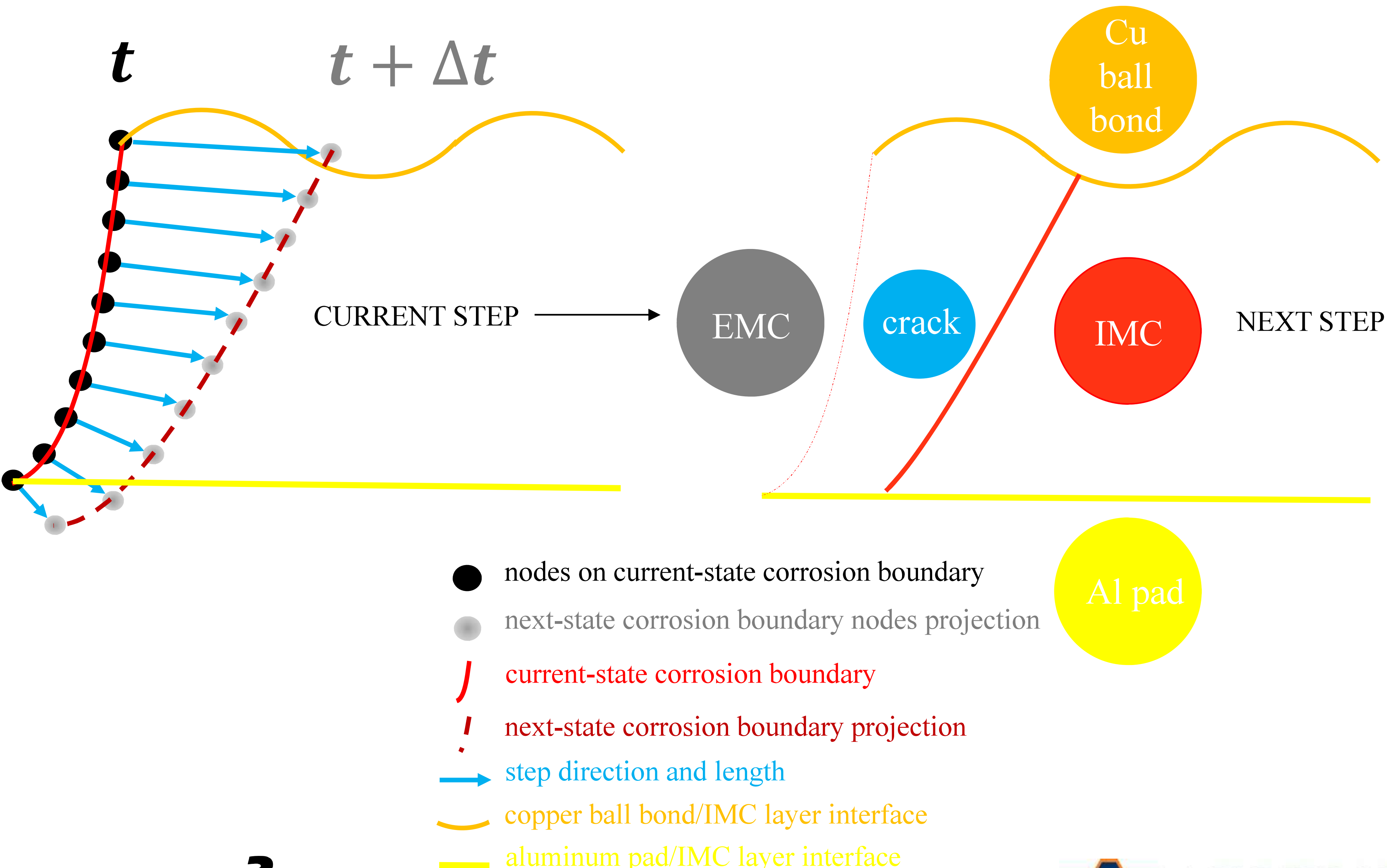

WB Interfacial Corrosion Front Tracking

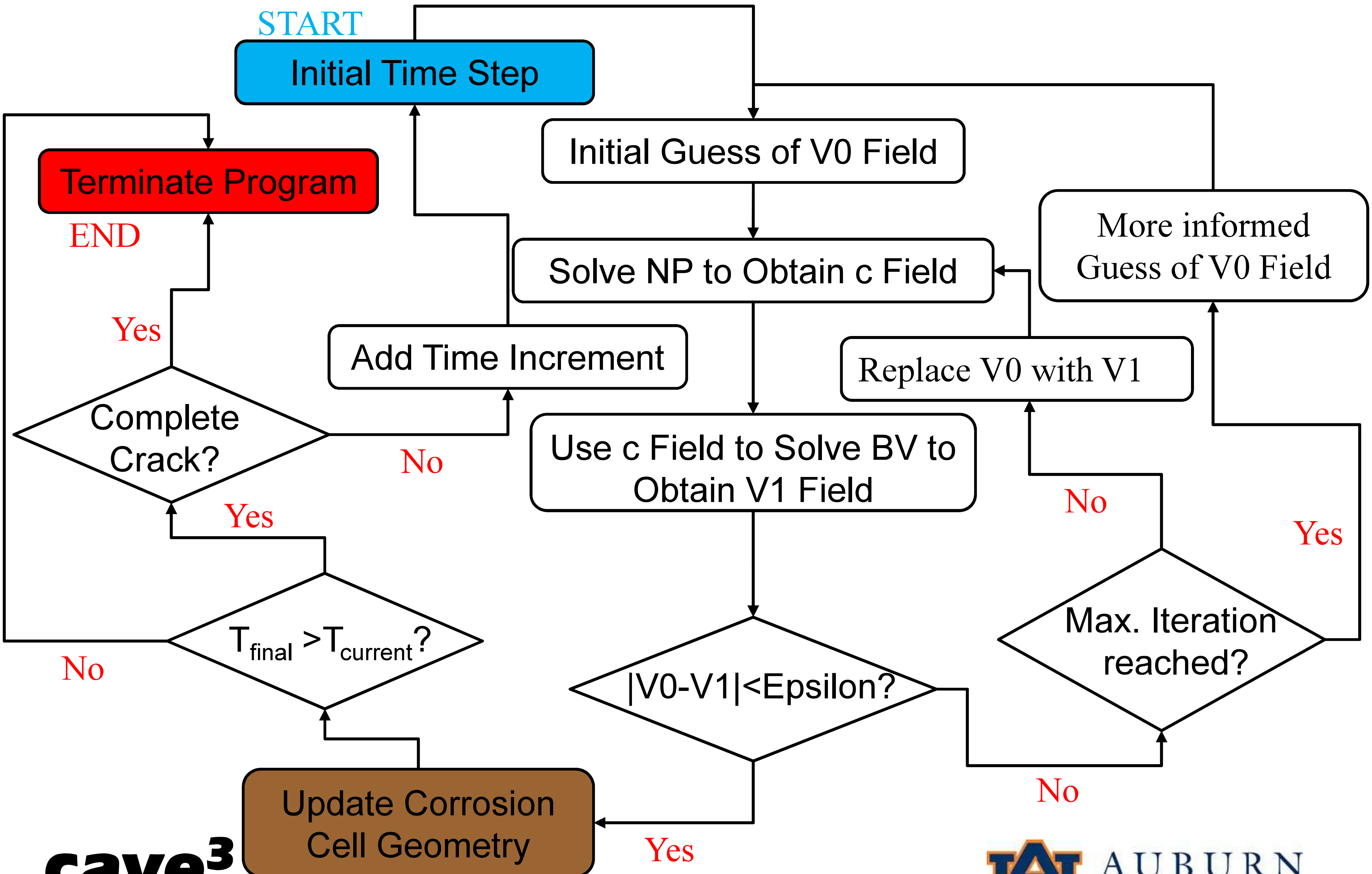

Model Inputs & Output

Inputs

- Temperature
- Relative humidity level
- Electric bias
- pH
- Diffusion Coefficient of chlorine
- Mobility of chlorine
- EMC chlorine release rate
- Tafel parameters of copper
- Tafel parameters of Cu-Al IMC
- Cu-Al wire bond radius
- Cu-Al IMC thickness

Output

- Crack Growth(RUL) as a function of aging duration

EMC Chlorine Release Rate Test

Diffusion Cell Test Setup

Fick's Law

$$J = {\color{red}D}\nabla c$$

J: ionic flux
D: diffusion coefficient
c: concentration

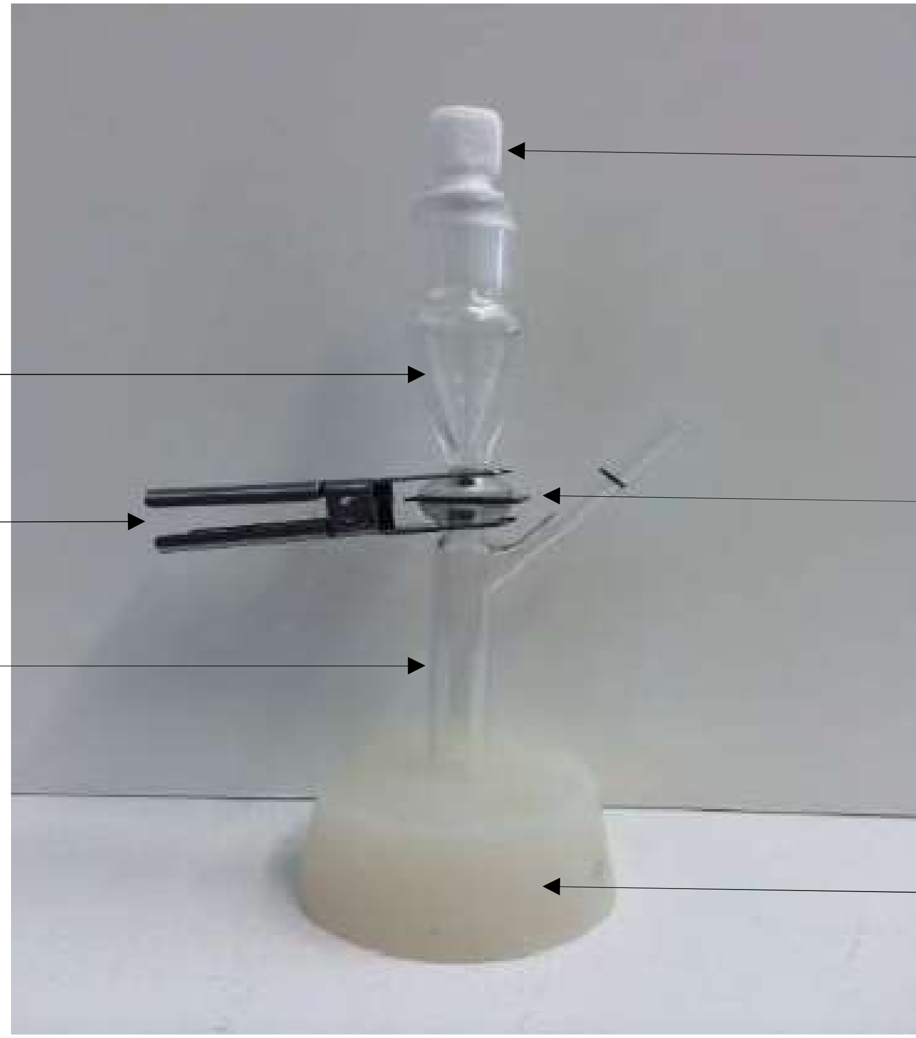

stopper

upper chamber

clamp

lower chamber

pedestal

Ionic Mobility Cell Test

Nernst-Planck Equation

$$J = D\nabla c + z\mu c\nabla V$$

J: ionic flux
D: diffusion coefficient
c: concentration
z: electron number
μ: ionic mobility
V: electric potential
t: aging duration

∇V to be determined

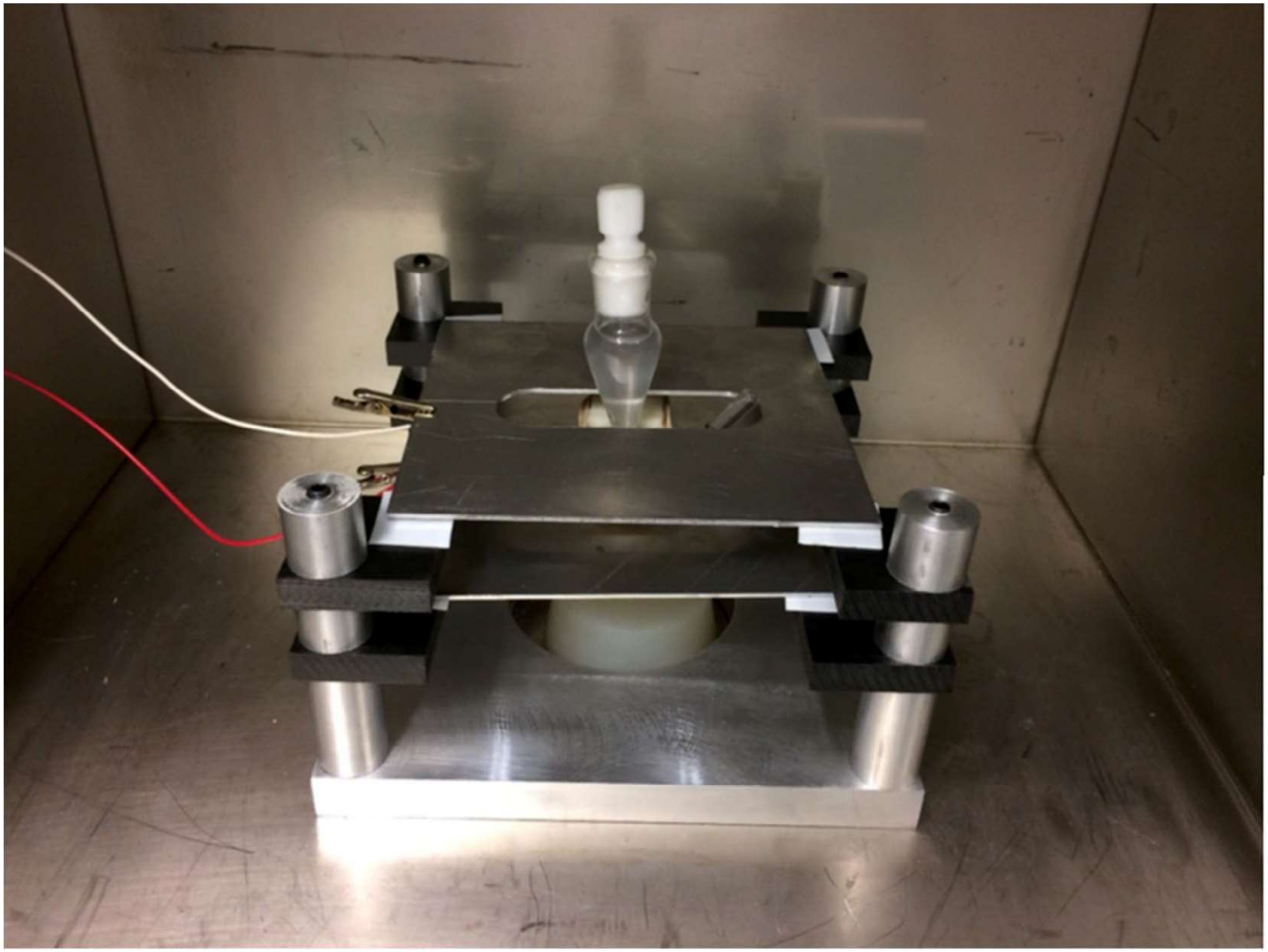

Calculation of ∇V across Sample EMC

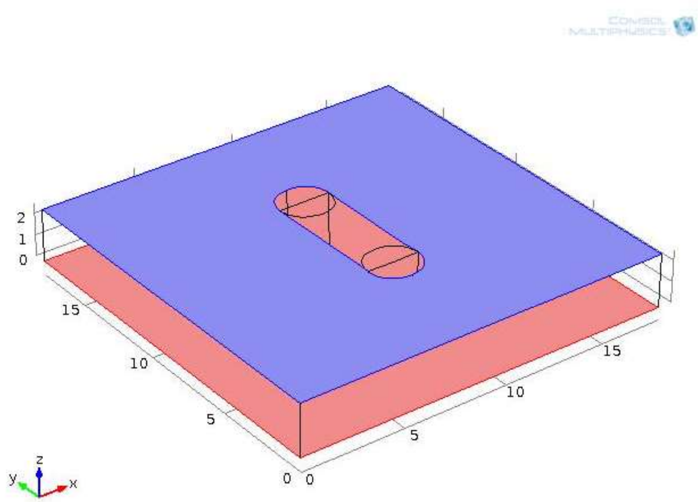

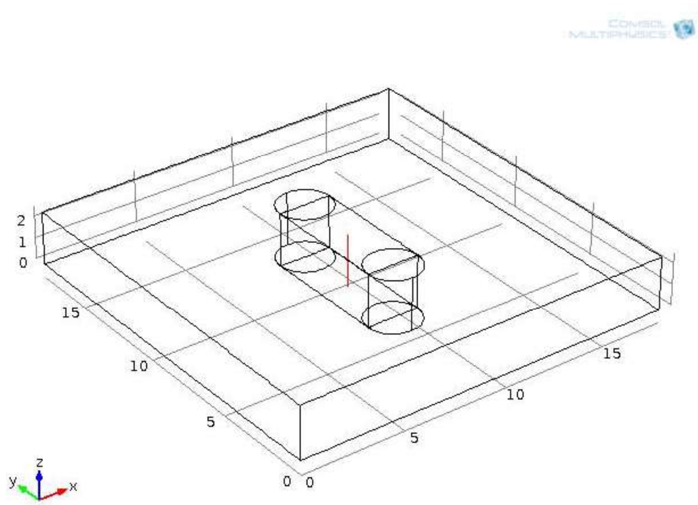

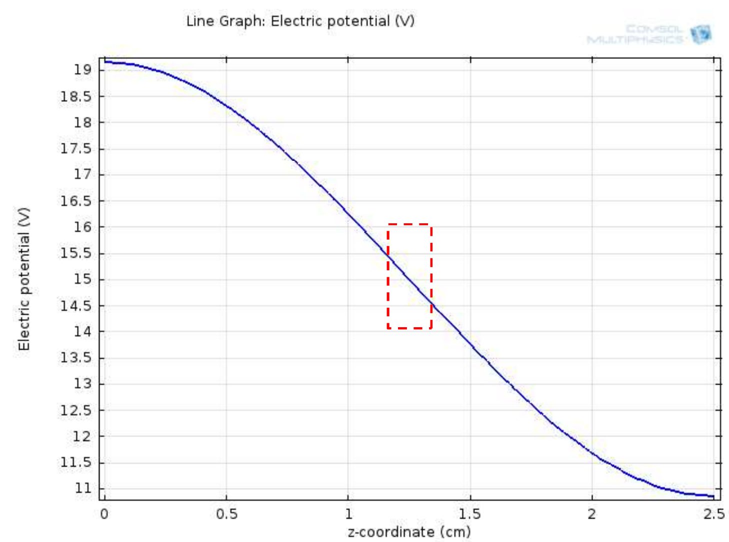

Electrochemical Polarization Test

3-electrode electrochemical cell setup

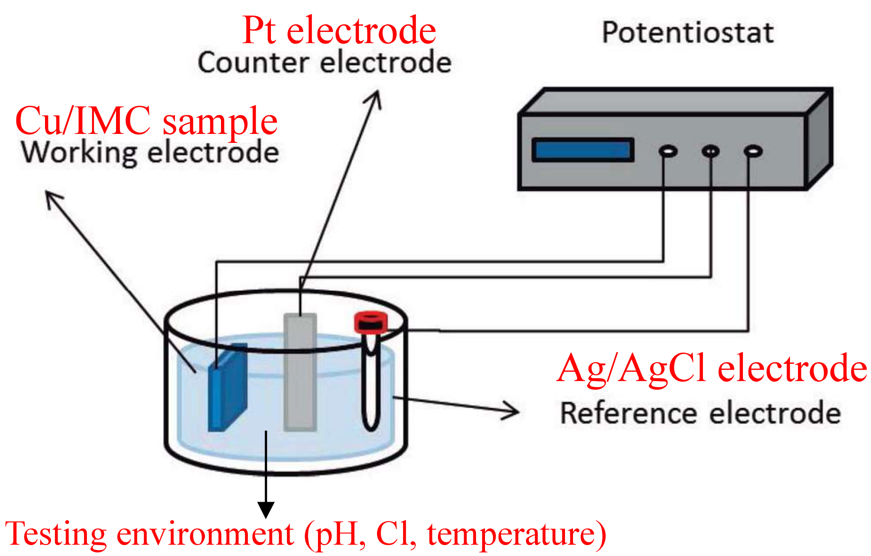

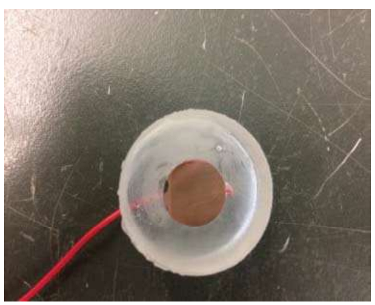

Cu test sample

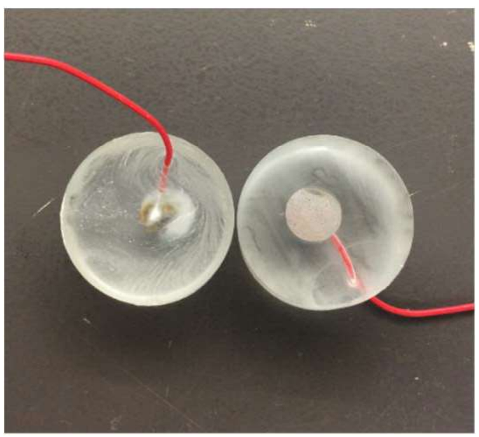

CuAl IMC test sample

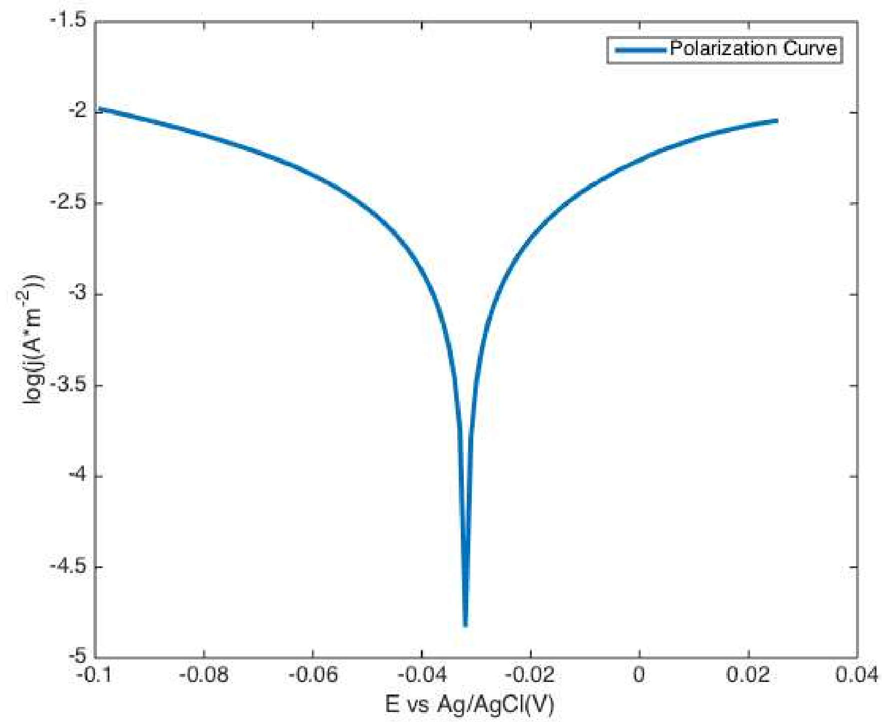

sample result of polarization curve

Tentative Simulation of WB Failure

Inputs

- Diffusion Coefficient of chlorine ($1*10^{-10}cm^2/s$)
- Mobility of chlorine ($1*10^{-8}cm^2/(V.s)$)
- EMC chlorine release rate (1ppm/day)
- OCP of copper (0V vs Ag/AgCl)
- OCP of Cu-Al IMC (-0.5V vs Ag/AgCl)
- Free corrosion current density of copper ($0.1A/cm^2$)
- Free corrosion current density of copper ($0.1A/cm^2$)
- Tafel Slope alpha of Cu (0.1)
- Tafel Slope beta of Cu (0.1)
- Tafel Slope alpha of Cu-Al IMC (0.1)
- Tafel Slope beta of Cu-Al IMC (0.1)
- Cu-Al wire bond radius (35microns)
- Cu-Al IMC thickness (200nm)
- Voltage bias (1V)

Crack Growth & RUL Prediction

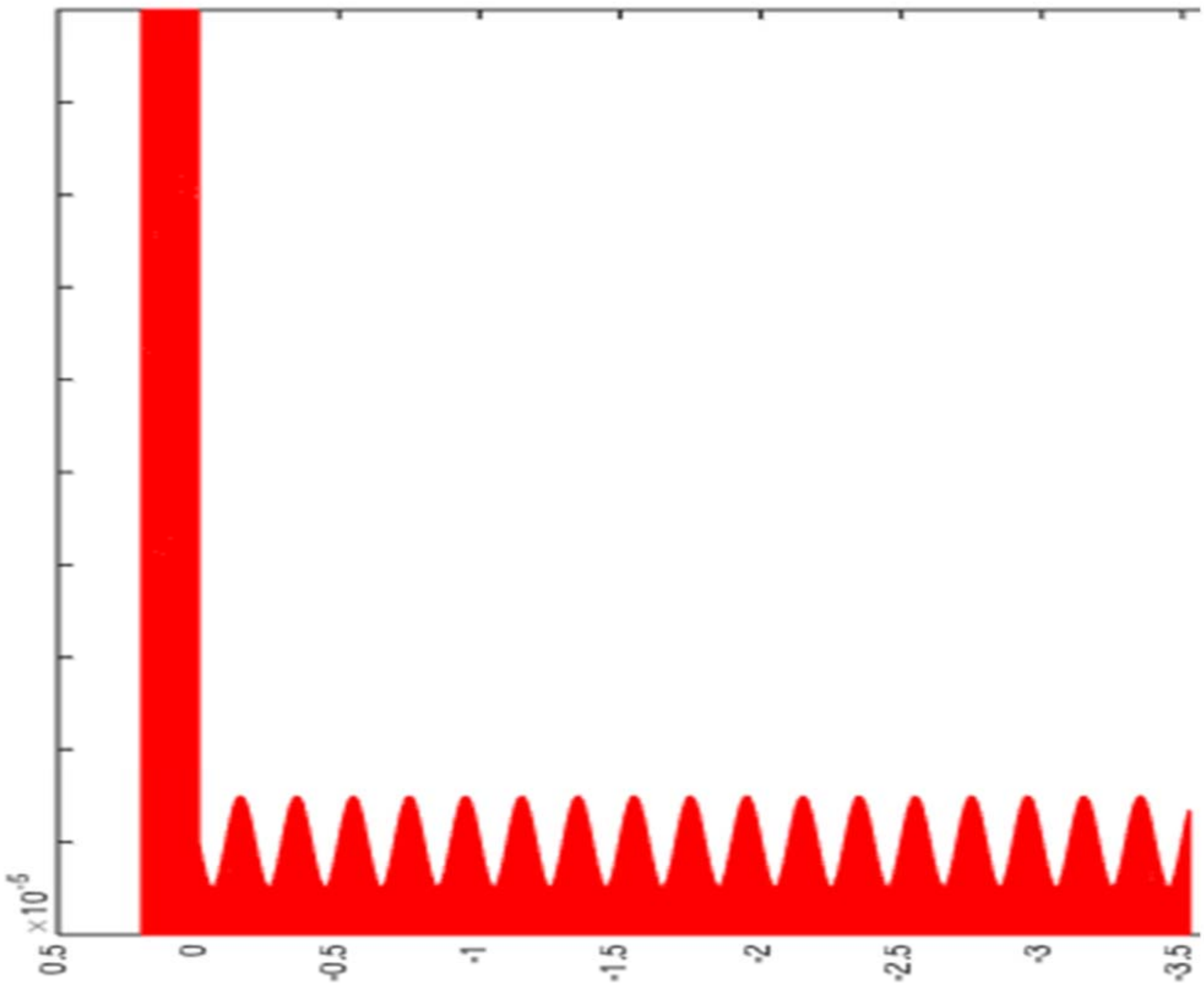

Crack Growth & RUL Prediction

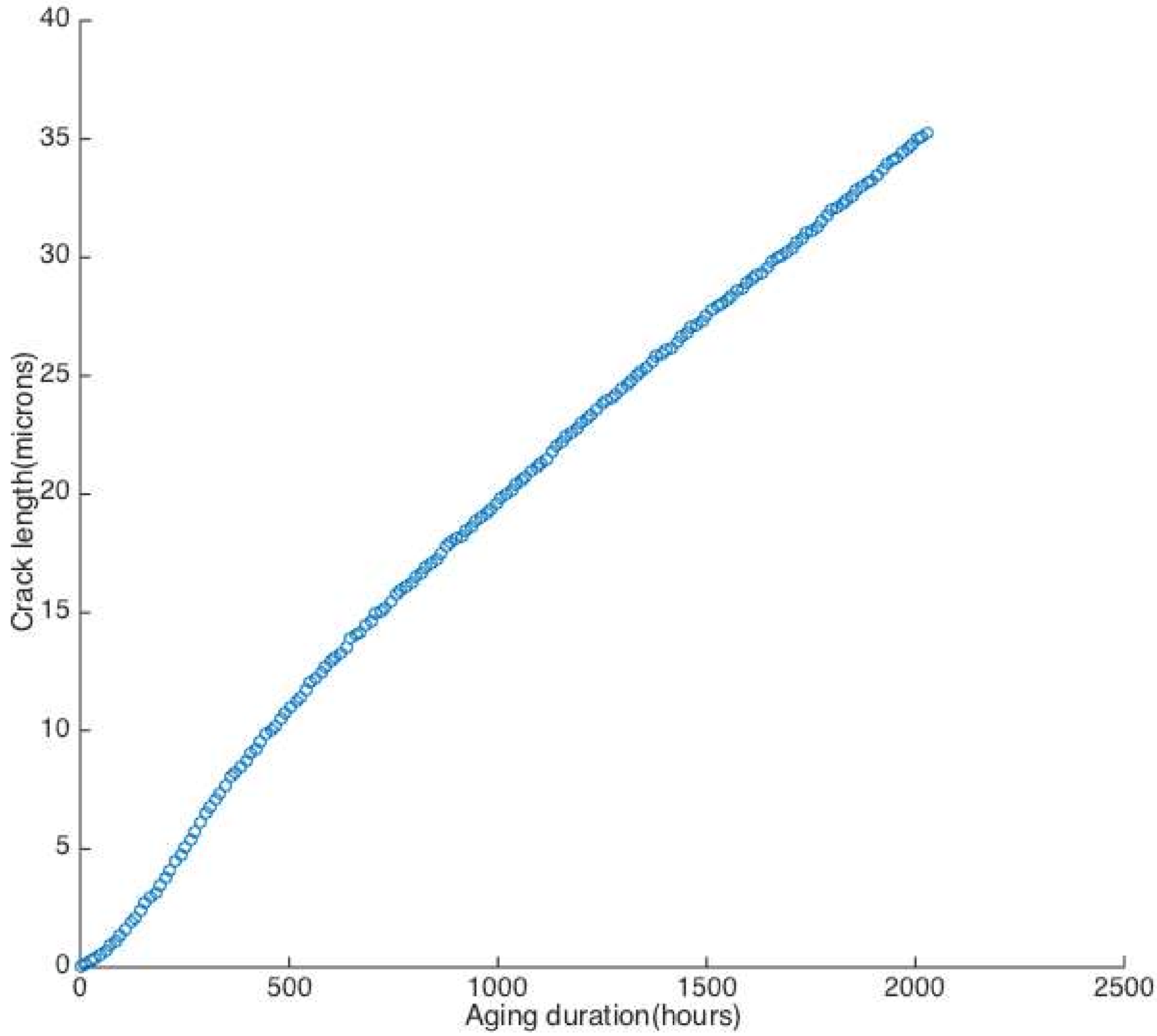

Chlorine Transport & WB Failure

Built-in Chlorine Contamination Tests (130°C/100%RH)

Test Sample

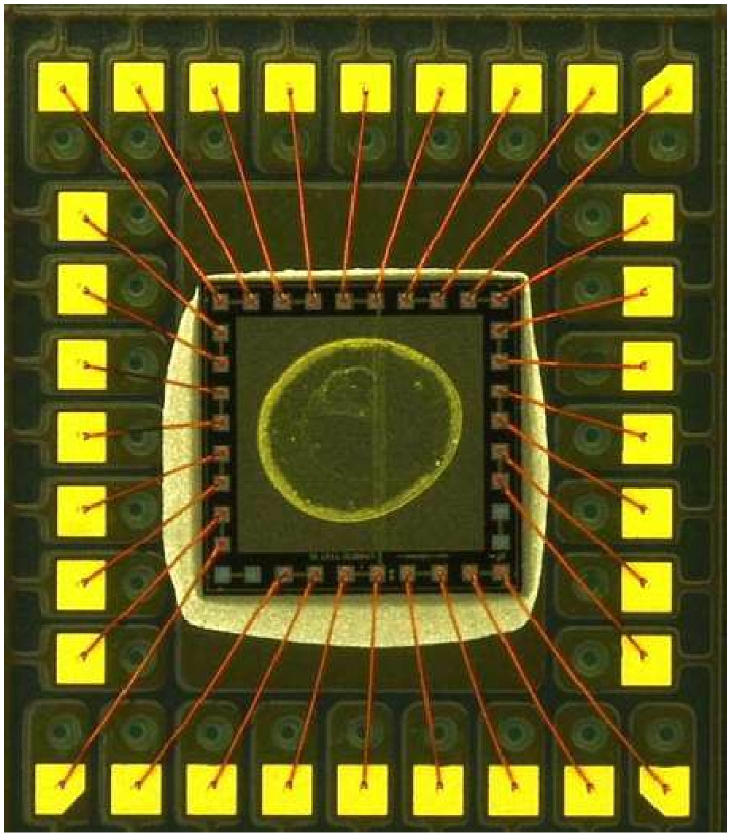

32-pin CSP with 16 pairs of Cu-Al wire bonds in the peripheral area and KCl drop on the top of die

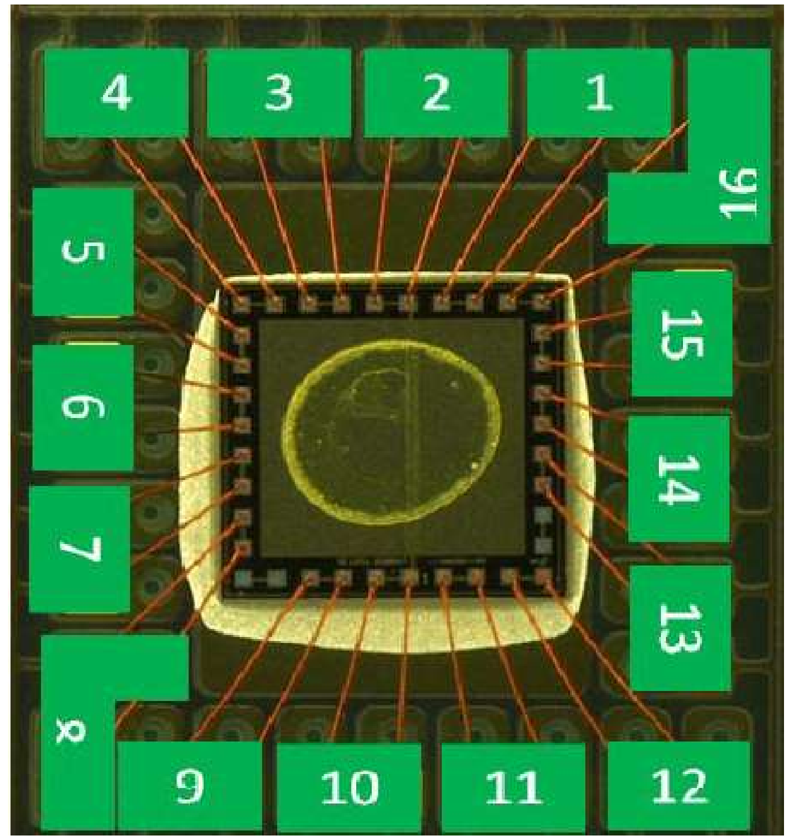

individual WB pairs are numbered and electric resistance of them are measured periodically

Chlorine Transport & WB Failure

Built-in Chlorine Contamination Tests (130°C/100%RH)

Sample #1

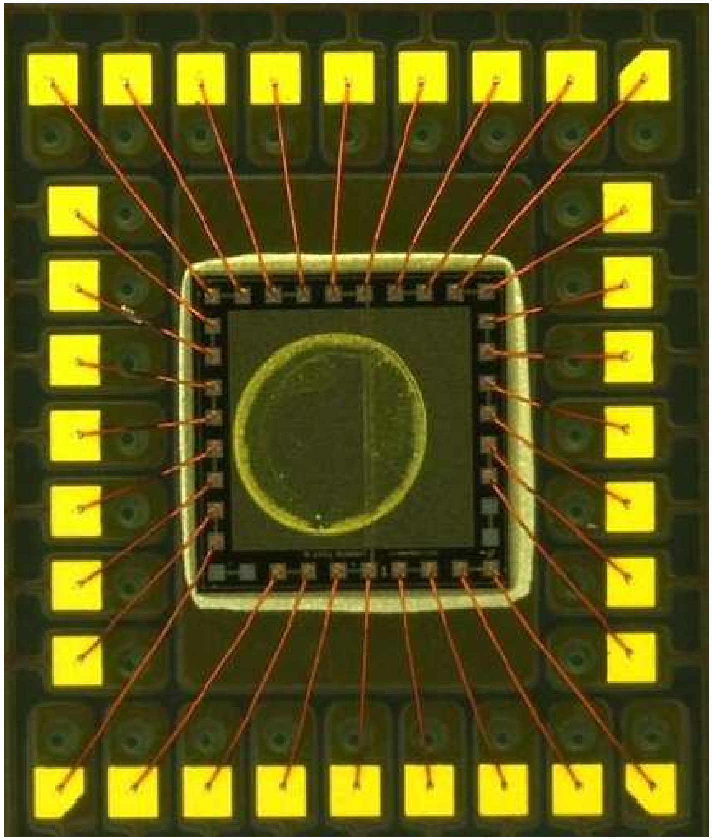

Resistance Measurements

# of PIN	Time zero	24 hr 130C/100 %RH parr bomb	48 hr 130C/100 %RH parr bomb	72hr 130C/10 0%RH parr bomb	96hr 130C/100 %RH parr bomb	120hr 130C/100 %RH parr bomb
#1	0.3552	0.3625	0.3632	38K	M	M
#2	0.3624	0.3665	0.3596	M	M	M
#3	0.3584	0.3531	0.4825	0.45K	M	M
#4	0.3493	0.3508	0.6983	M	M	M
#5	0.3379	0.3429	M	M	M	M
#6	0.3422	0.9427	13.35	M	M	M
#7	0.3285	0.3313	0.8K	M	M	M
#8	0.3513	0.3487	348.13	0.51K	M	M
#9	0.3533	0.3596	0.3523	0.3624	0.3644	M
#10	0.3462	0.3511	0.3628	0.3584	M	M
#11	0.3742	0.3634	0.3553	0.3521	M	M
#12	0.3629	0.3638	0.3745	0.3678	M	M
#13	0.3585	0.3455	0.3658	0.3695	M	M
#14	0.3365	0.3452	0.3356	0.3328	16K	16K
#15	0.3277	0.3312	0.3188	0.3266	M	M
#16	0.3524	0.3489	0.3529	0.3514	0.3527	M

Chlorine Transport & WB Failure

Built-in Chlorine Contamination Tests (130°C/100%RH)

Sample #2

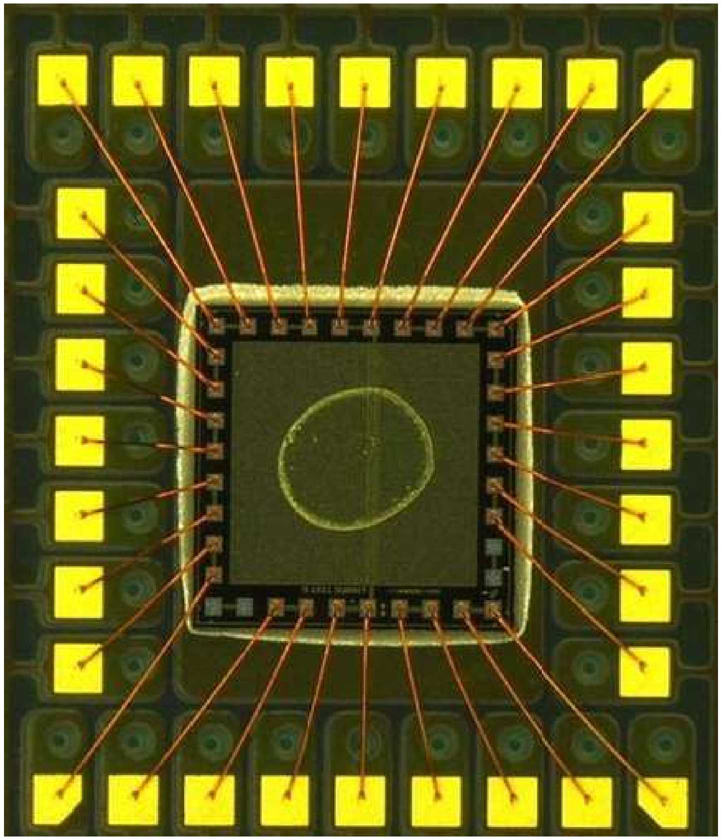

Resistance Measurements

# of PIN	Time zero	24 hr 130C/100 %RH parr bomb	48 hr 130C/100 %RH parr bomb	72hr 130C/100 %RH parr bomb	96hr 130C/100 %RH parr bomb
#1	0.3721	0.3742	0.3623	0.3624	0.3556
#2	0.3588	0.3622	0.3672	0.3597	0.3564
#3	0.3562	0.3485	0.3464	0.3422	0.3442
#4	0.3648	0.3612	0.3688	0.3633	0.5839
#5	0.3413	0.3408	0.3514	0.3467	M
#6	0.3386	0.3356	0.3229	0.3319	M
#7	0.3378	0.342	0.3527	0.3462	M
#8	0.3744	0.3647	0.3632	0.3705	17.05
#9	0.3663	0.3635	0.3659	0.3559	M
#10	0.3574	0.3542	0.3541	0.3435	28.51
#11	0.3563	0.3521	0.3284	0.3541	M
#12	0.3662	0.3633	0.3781	0.3439	0.9026
#13	0.3682	0.3647	0.3562	0.3526	M
#14	0.345	0.3541	0.3447	0.3487	M
#15	0.3375	0.3372	0.3326	0.3335	8.56
#16	0.3629	0.3589	0.3663	0.3688	97.33

Summary and Conclusions

- An electrochemical approach is introduced to calculating micro-galvanic corrosion rate at Cu-Al wire bond interface under temperature humidity environmental conditions

- An multiphysics model is developed to quantify effect of different environmental factors on Cu-Al bond pad interfacial corrosion rate

High Strain Rate Properties of SACQ Solder after Prolonged Thermal Aging up to 6-Months

V. Yadav, P. Lall

- ❑ Investigate the effect of 6-Month thermal aging on mechanical properties and compare results with SAC105 and SAC305.
- ❑ To investigate the High Strain Rate (10-75 per sec) behavior of SAC-Q Lead free alloy at high operating temperature (25°C–200°C).
- ❑ Measure the mechanical properties including Ultimate Tensile Strength (UTS) and Young's Modulus (E) for SAC-Q solder alloys.
- ❑ Compute the Anand's parameters of SAC-Q using Stress-Strain curves.
- ❑ Verify the accuracy of the predictive model with experimental data.

SAMPLE PREPARATION

Specimen dimension

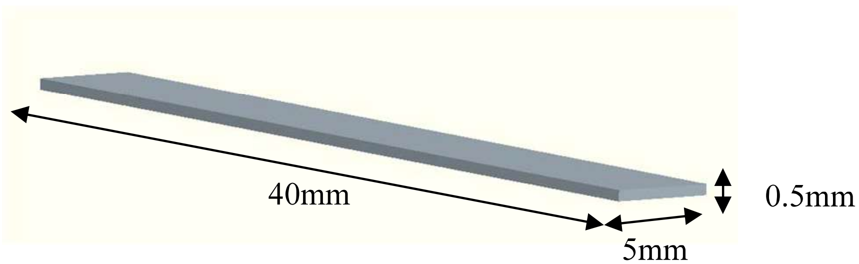

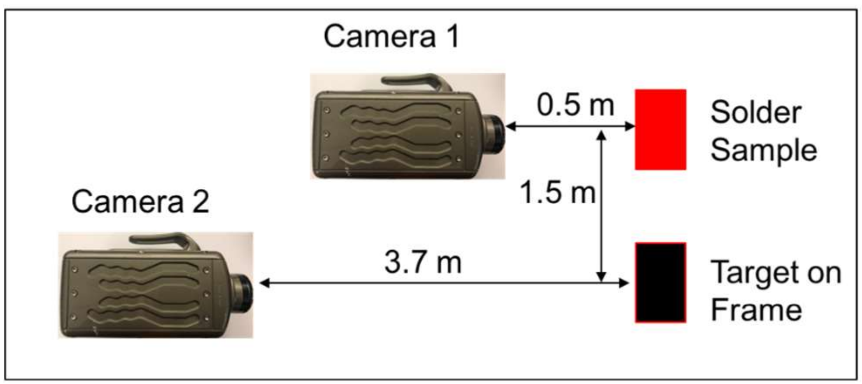

Test Setup

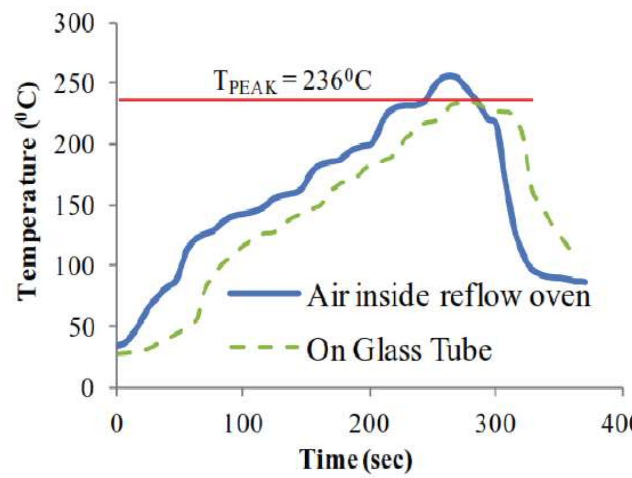

Reflow Profile

Composition & Test Matrix

	% Contents			
Element	SAC-Q	SAC105	SAC305	SAC405
Sn	92.7	98.5	96.5	95.5
Ag	3.4	1.0	3.0	4.0
Cu	0.5	0.5	0.5	0.5
Bi	3.4	0.0	0.0	0.0

Table: Test Matrix

Aging Duration (in Days)	Operating Temp.	Strain Rate (per sec)			
		10 / sec	35 / sec	50 / sec	75 /sec
0	25, 50, 75, 100, 125, 150, 175, & 200 °C	X	X	X	X
30		X	X	X	X
60		X	X	X	X
120		X	X	X	X
180		X	X	X	X

Stress-Strain Curve:

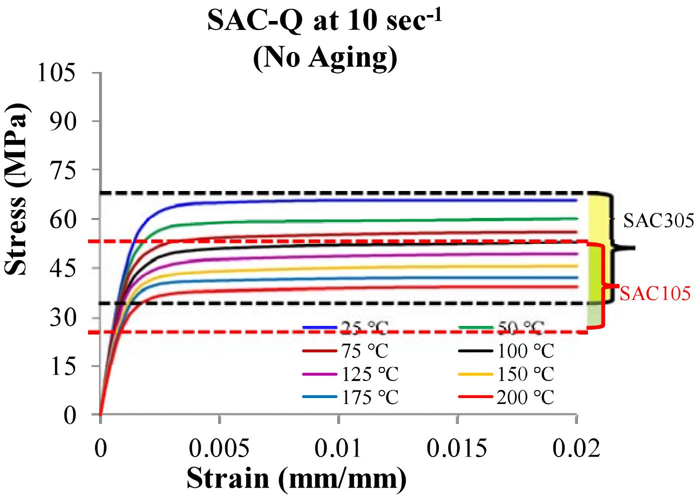

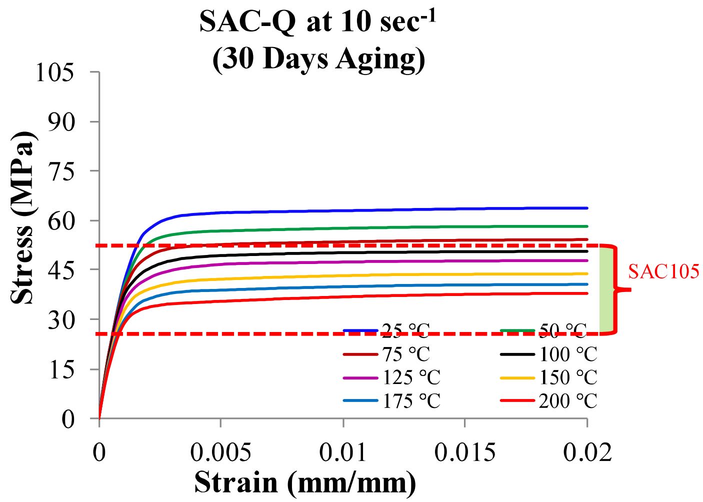

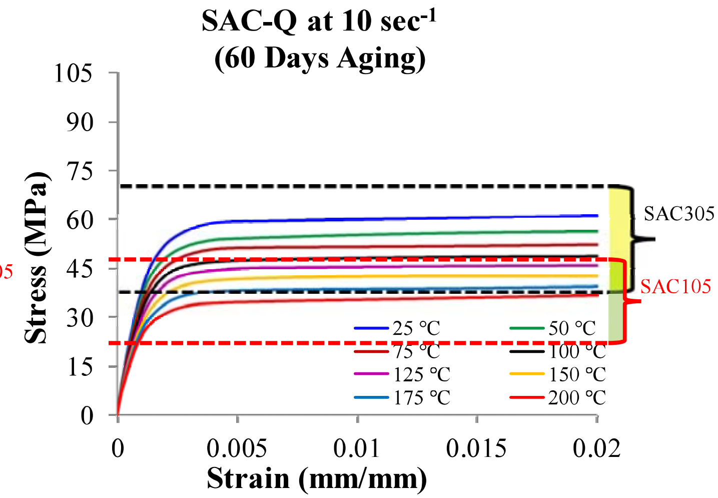

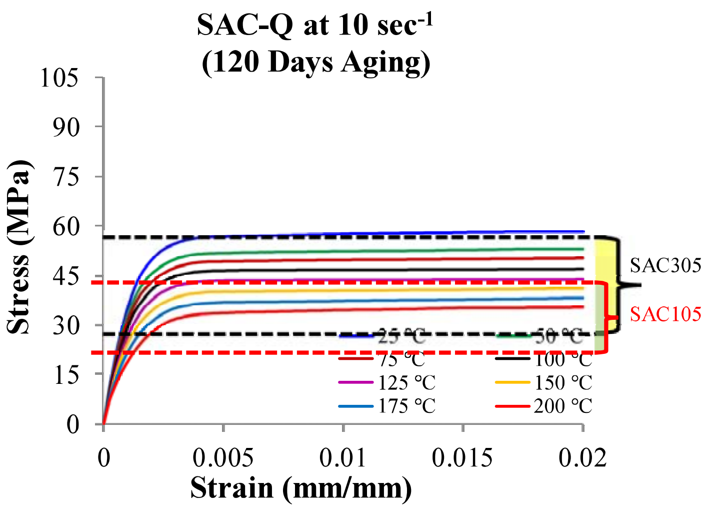

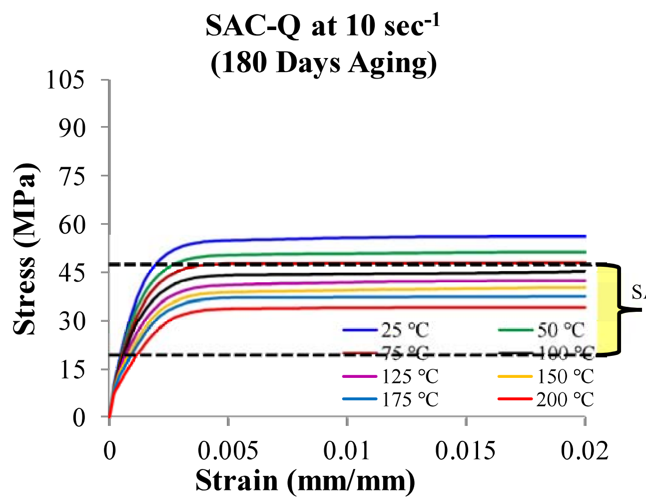

Stress-Strain Curve:

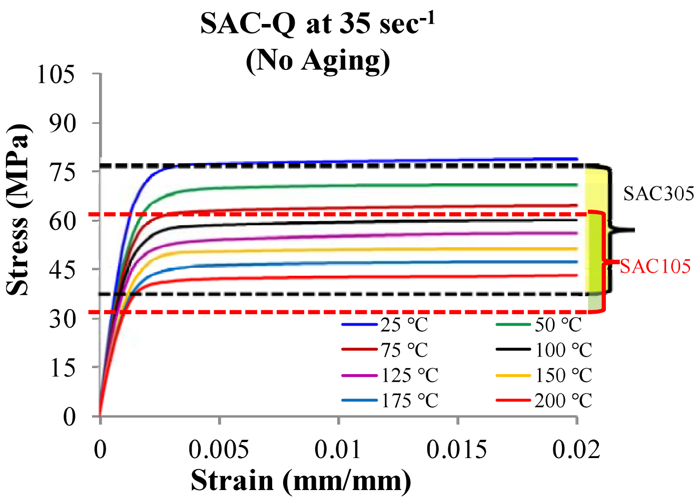

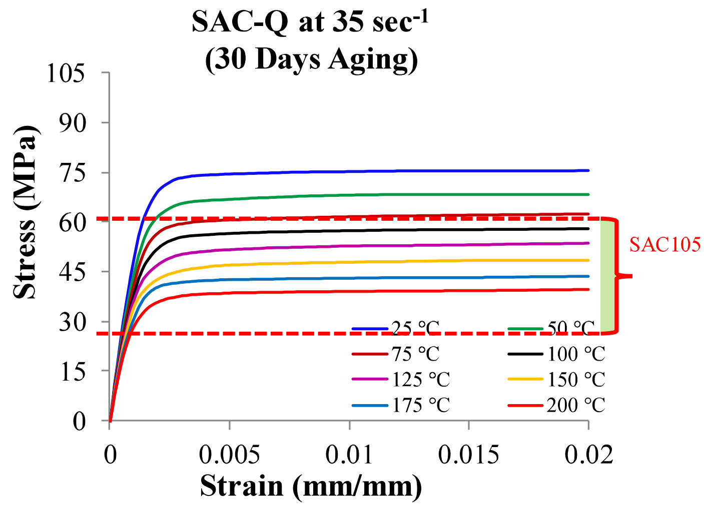

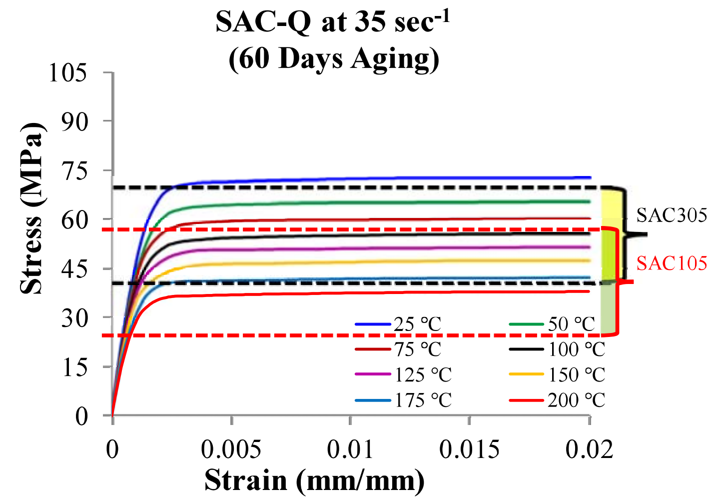

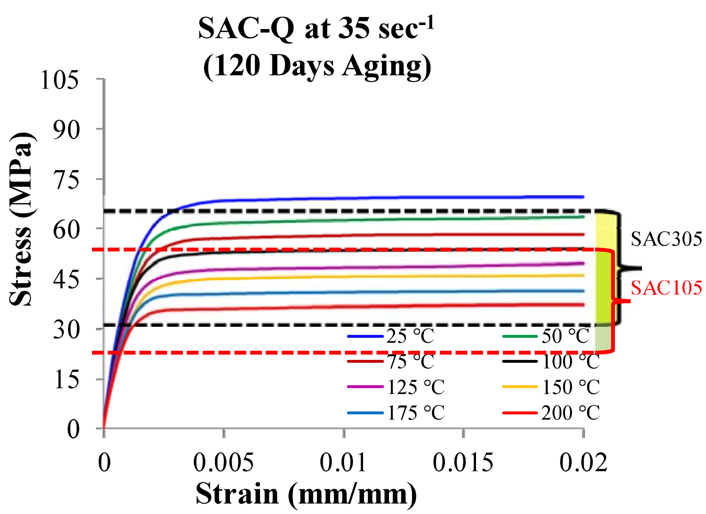

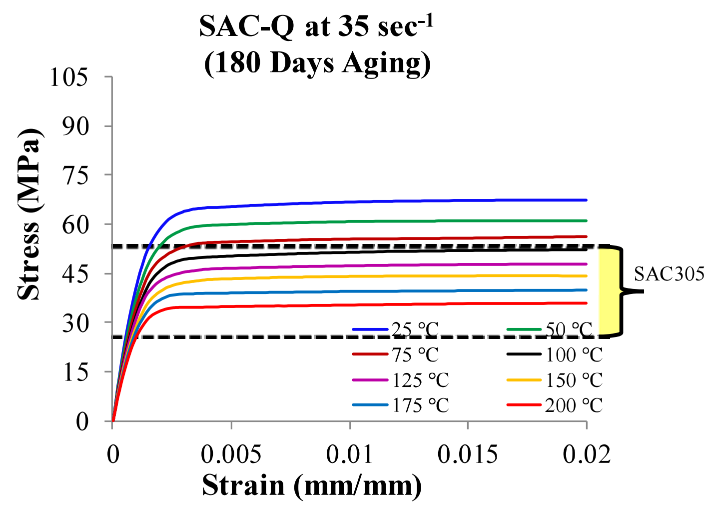

Stress-Strain Curve:

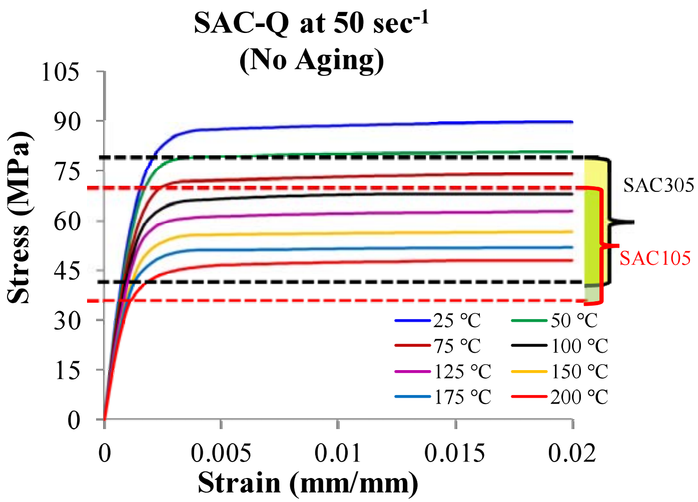

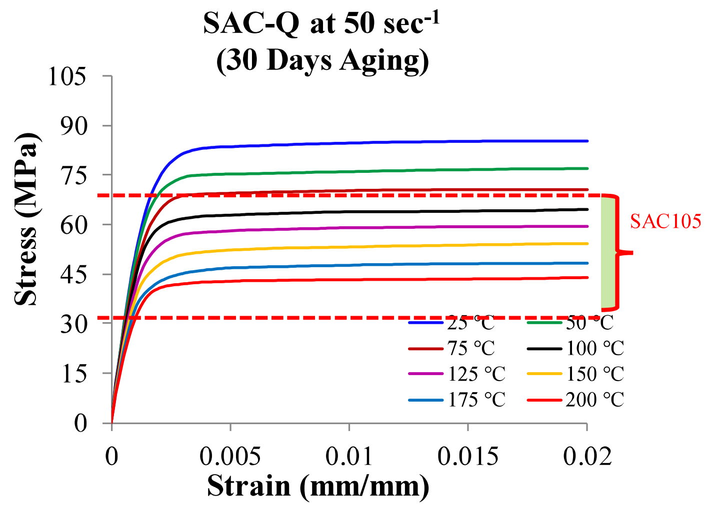

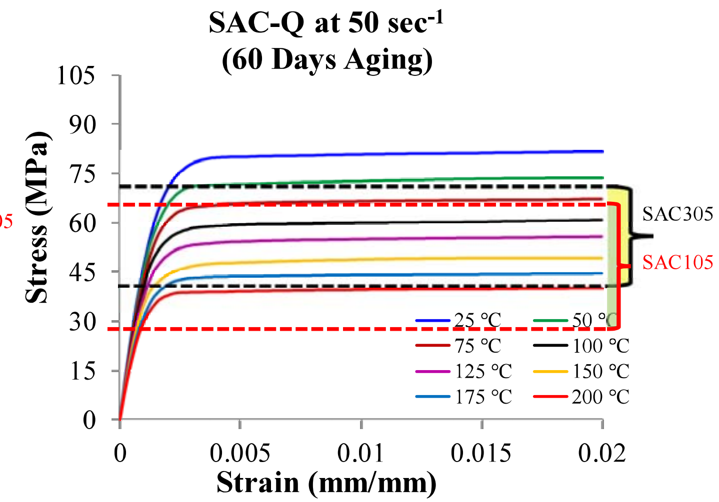

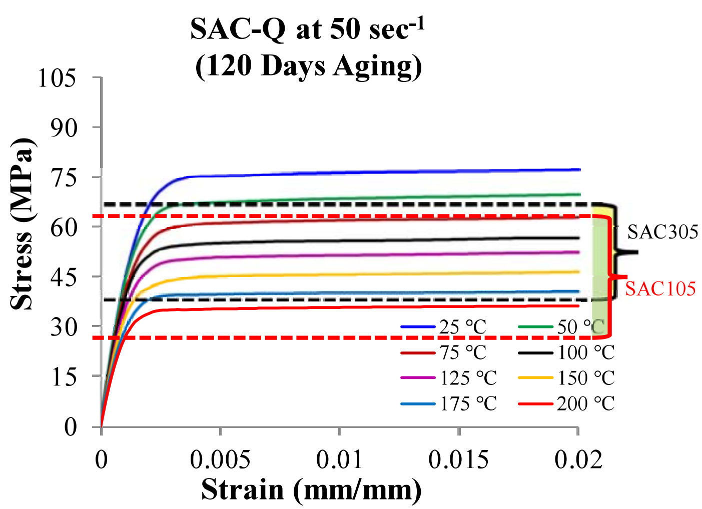

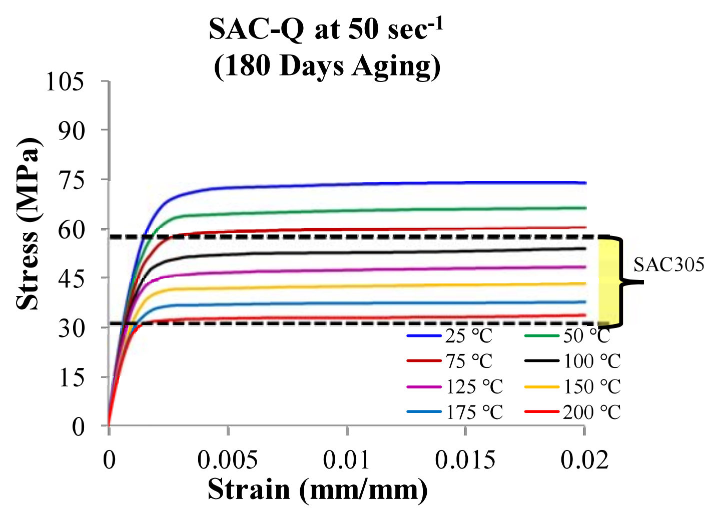

Stress-Strain Curve:

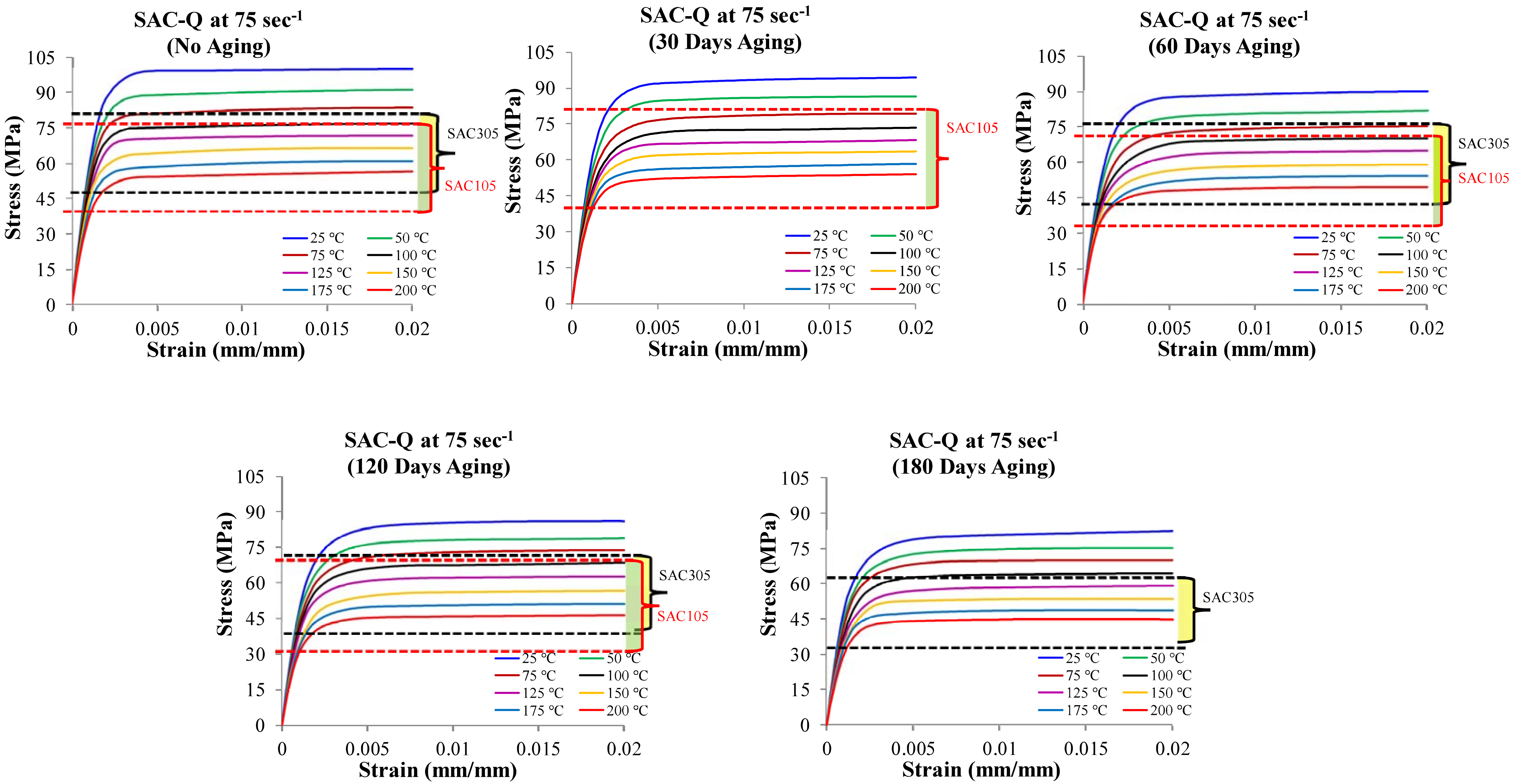

NSF Center for Advanced Vehicle and Extreme Environment Electronics

AUBURN UNIVERSITY

Ultimate Tensile Strength

Table: 10 per sec

Operating Temp. (°C)	0 Days	30 Days	60 Days	120 Days	180 Days
25	65.8	63.6	61.2	58.2	56.0
50	60.0	58.1	56.3	53.2	51.2
75	56.2	54.1	52.5	50.3	48.1
100	53.0	50.6	48.8	47.0	45.1
125	49.2	47.7	45.8	43.7	42.2
150	45.6	44.0	42.6	41.0	40.1
175	42.1	40.5	39.5	38.2	36.3
200	39.2	37.8	36.7	35.3	33.0

Table: 35 per sec

Operating Temp. (°C)	0 Days	30 Days	60 Days	120 Days	180 Days
25	78.8	75.4	72.6	69.7	67.4
50	70.8	68.1	65.5	63.7	61.0
75	64.4	62.4	60.3	58.4	56.3
100	59.9	58.0	55.5	53.8	52.1
125	55.9	53.5	51.6	49.7	47.7
150	51.4	48.4	47.4	46.3	44.2
175	47.2	44.6	42.4	41.3	39.8
200	43.1	40.9	40.1	38.2	36.0

Table: 50 per sec

Operating Temp. (°C)	0 Days	30 Days	60 Days	120 Days	180 Days
25	89.7	85.2	81.4	77.1	73.9
50	80.7	77.0	73.4	69.7	66.7
75	73.9	70.6	67.0	63.0	60.5
100	68.3	64.6	60.8	57.9	55.2
125	63.0	59.2	55.5	53.6	50.7
150	56.8	54.2	51.3	49.5	47.6
175	52.1	49.0	47.6	45.5	42.8
200	48.1	44.5	43.1	41.3	40.7

Table: 75 per sec

Operating Temp. (°C)	0 Days	30 Days	60 Days	120 Days	180 Days
25	100.0	94.3	89.9	86.0	82.4
50	91.2	86.5	82.2	79.0	75.0
75	83.6	79.5	75.5	73.8	70.0
100	77.0	73.2	70.3	68.4	64.5
125	71.6	68.3	64.8	62.4	59.1
150	66.5	63.5	59.0	56.6	53.8
175	61.1	58.1	54.2	51.3	48.8
200	56.4	54.0	49.6	46.6	44.6

Elastic Modulus

Table: 10 per sec

Operating Temp. (°C)	0 Days	30 Days	60 Days	120 Days	180 Days
25	41.3	39.9	38.7	37.4	36.3
50	39.8	38.9	37.3	36.3	35.3
75	38.1	37.1	35.9	34.9	33.5
100	37.4	36.7	34.8	33.6	32.3
125	35.4	34.3	33.6	32.5	30.9
150	33.8	32.5	31.7	30.3	28.8
175	31.9	30.4	28.8	27.5	26.4
200	30.2	29.1	27.9	26.5	25.1

Table: 35 per sec

Operating Temp. (°C)	0 Days	30 Days	60 Days	120 Days	180 Days
25	44.7	43.8	42.9	41.1	39.5
50	43.2	41.8	41	39.3	37.9
75	42.7	40.8	39.5	37.5	36.2
100	40.9	39.7	38.6	36.5	34.3
125	38.2	36.7	36.0	34.5	32.1
150	35.6	34.5	33.7	31.7	30.3
175	34.7	33.1	31.9	30.1	28.9
200	33.1	31.4	30.3	28.3	27.6

Table: 50 per sec

Operating Temp. (°C)	0 Days	30 Days	60 Days	120 Days	180 Days
25	47.7	45.8	45.3	43.0	41.8
50	46.4	44.8	44.2	42.0	40.5
75	44.9	43.4	42.5	40.3	38.4
100	43.4	41.5	40.9	38.6	37.2
125	41.5	39.7	39.1	37.0	35.1
150	39.8	38.1	37.4	35.1	33.4
175	38.4	36.8	36.1	33.4	32.1
200	36.8	35.2	34.2	31.7	30.3

Table: 75 per sec

Operating Temp. (°C)	0 Days	30 Days	60 Days	120 Days	180 Days
25	51.4	50.3	49.1	47.6	45.9
50	50.2	49.2	47.9	45.9	44.7
75	48.7	47.9	46.5	44.2	42.8
100	47.1	45.8	44.7	42.5	41.0
125	45.8	44.0	43.4	41.3	40.2
150	44.5	41.9	41.9	39.8	37.9
175	43.0	40.8	39.5	37.7	35.9
200	41.2	39.2	38.0	36.1	34.8

UTS vs Strain Rate

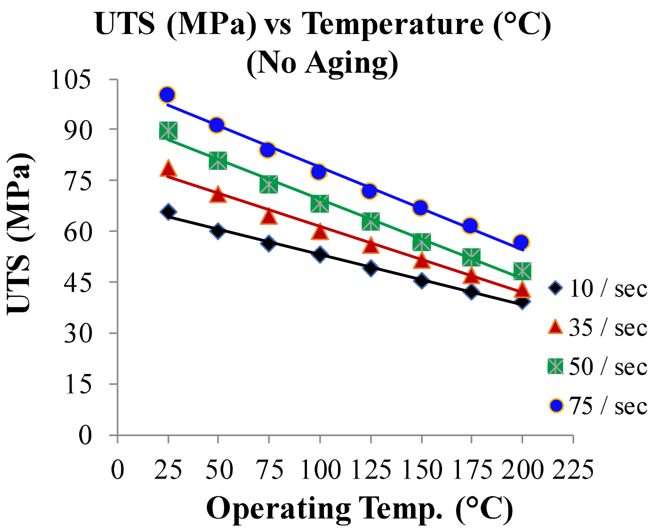

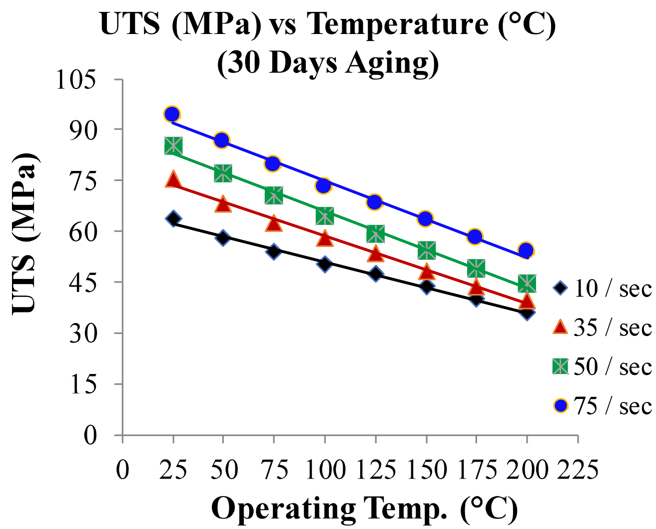

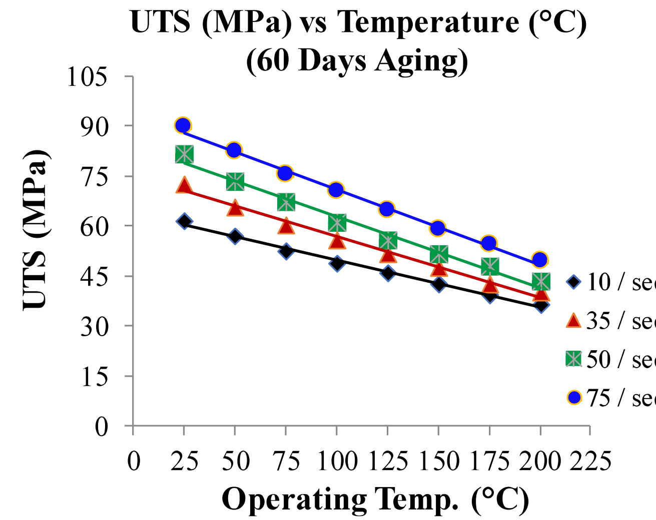

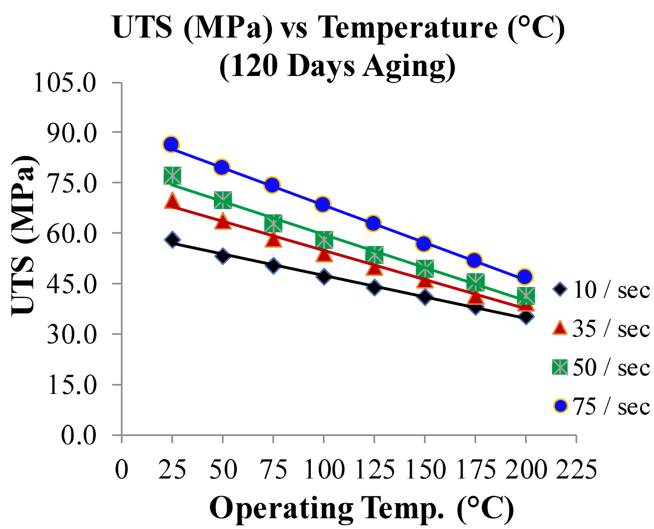

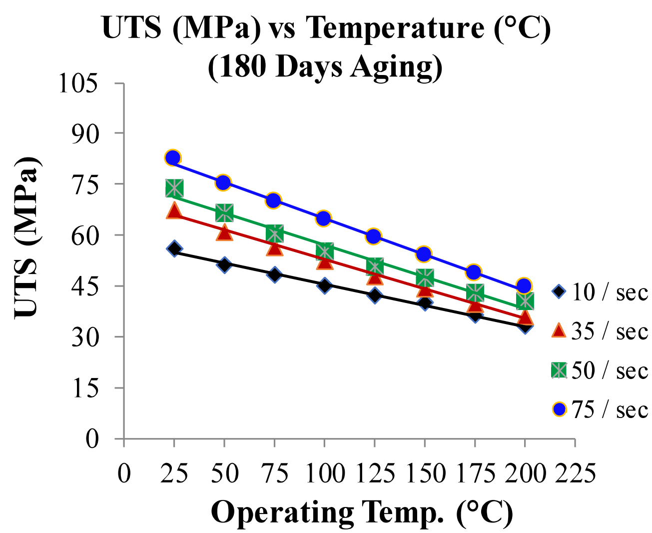

E vs Strain Rate

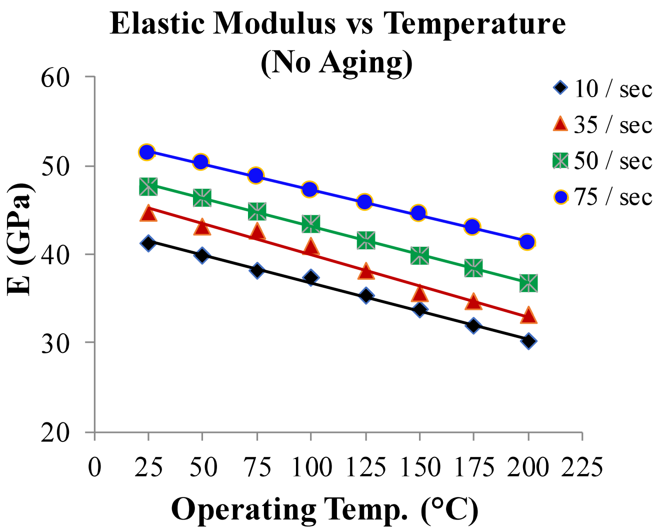

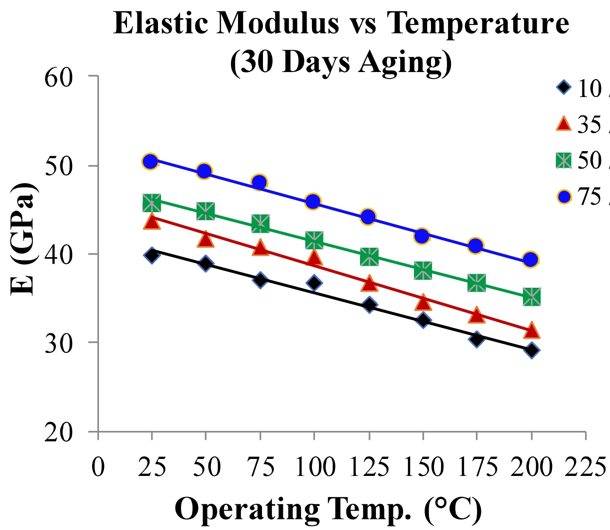

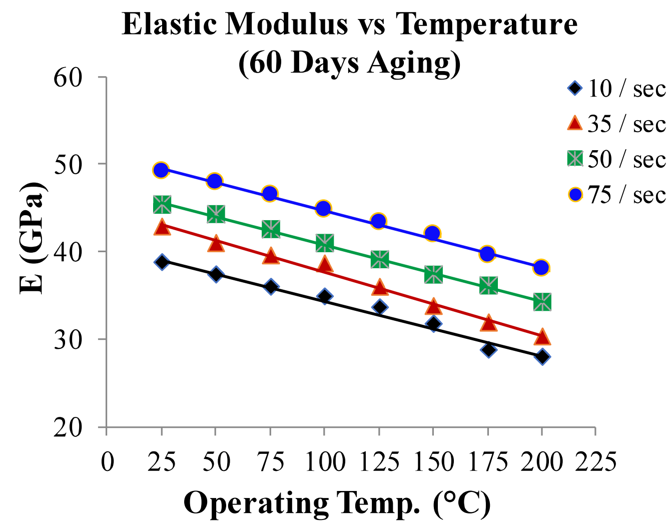

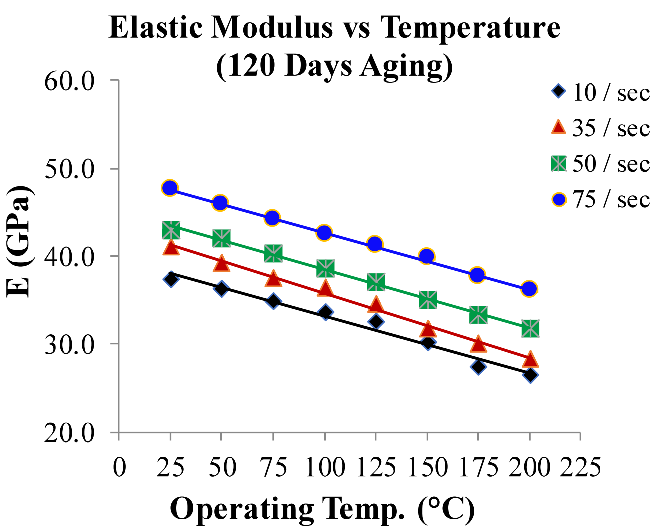

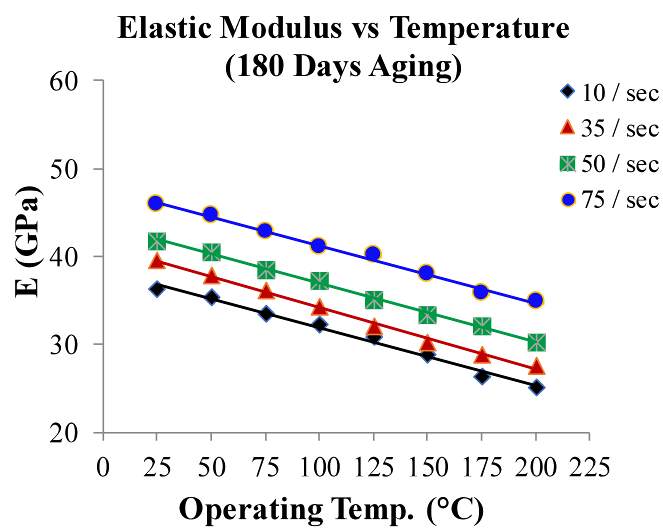

Effect of Aging on UTS

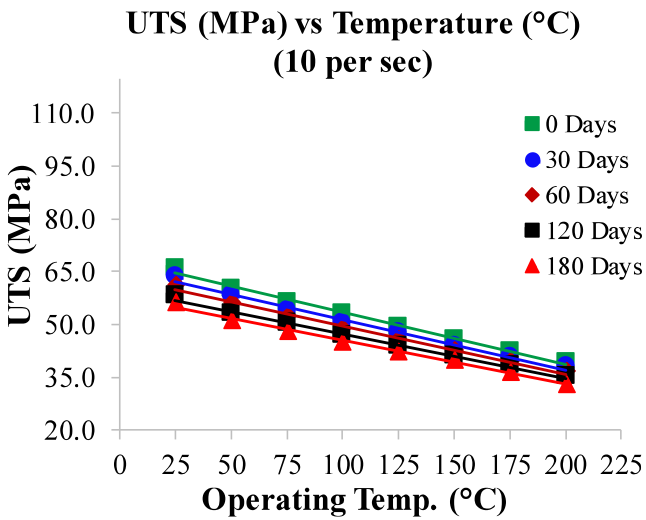

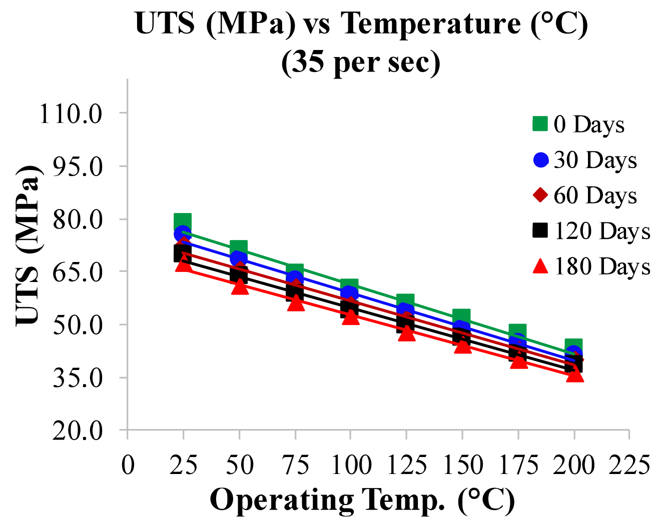

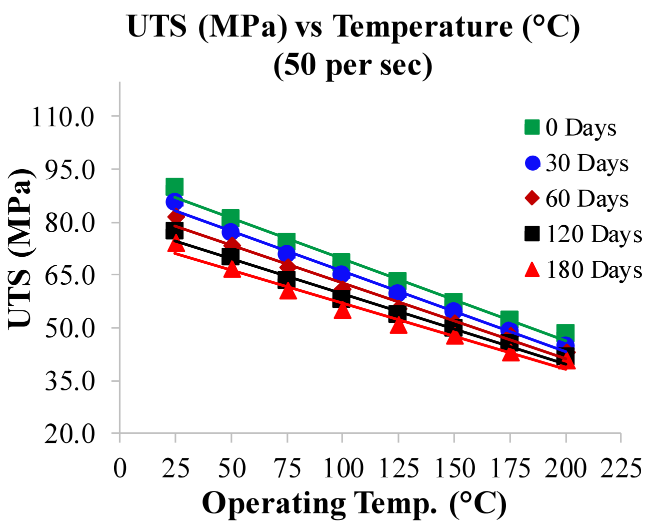

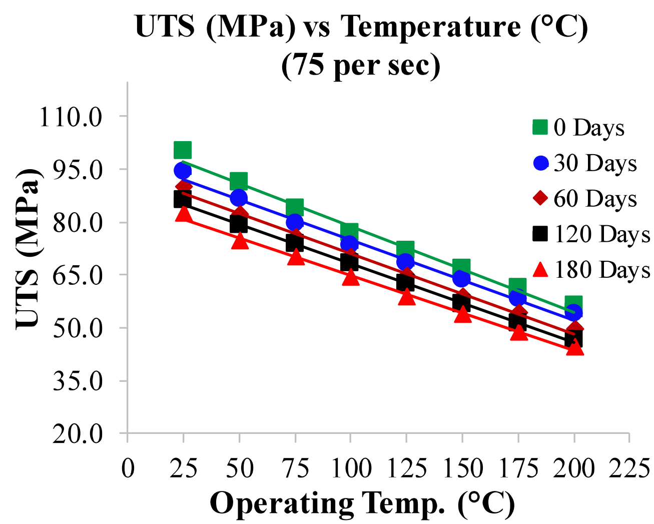

Effect of Aging on E

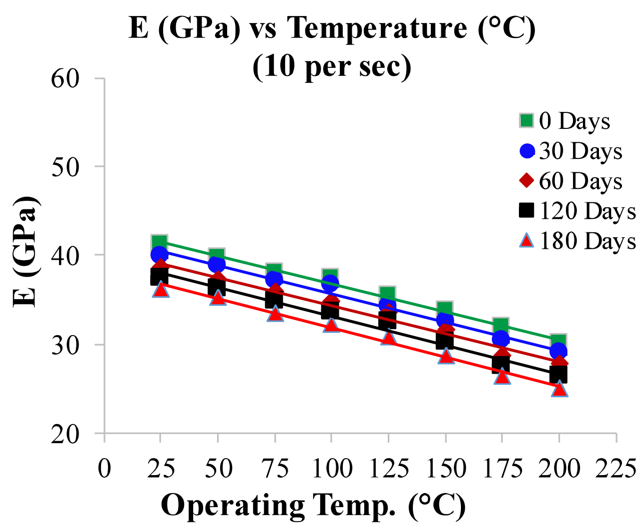

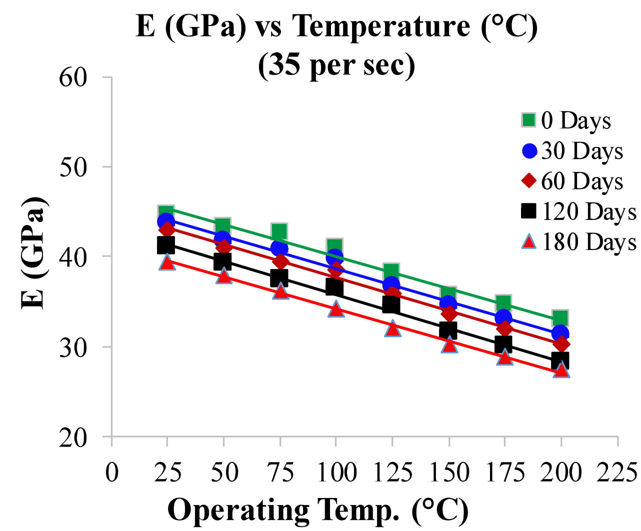

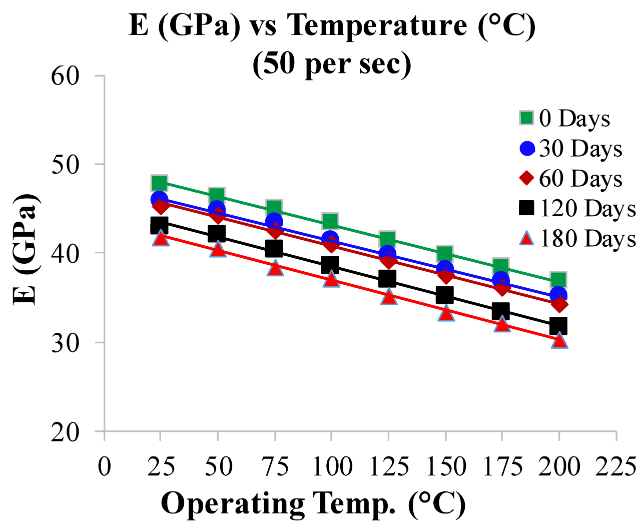

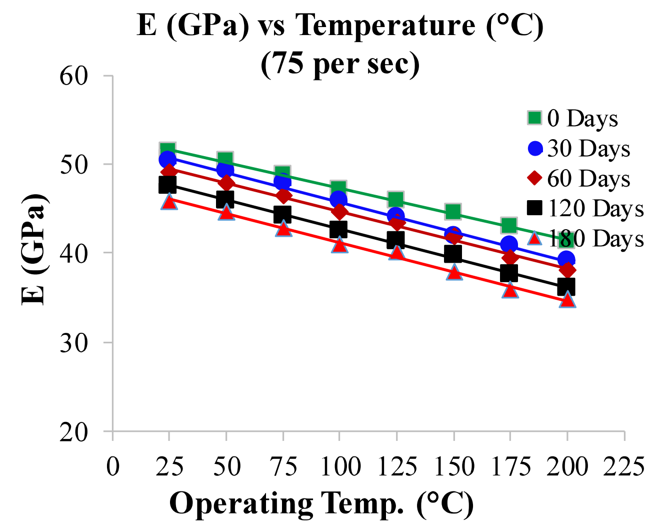

ANAND Model: Constitutive Equations

Stress Equation

$$\sigma = cs; c < 1$$

$$c = (\dot{\varepsilon}_{p,} T) = \frac{1}{\xi} \sinh^{-1}\{[\frac{\dot{\varepsilon}_p}{A} \exp(\frac{Q}{RT})]^m\}$$

Substitute (c) into σ

$$\sigma = \frac{s}{\xi} \sinh^{-1}\{[\frac{\dot{\varepsilon}_p}{A} \exp(\frac{Q}{RT})]^m\}$$

Solve stress equation for strain rate

Flow Equation

$$\dot{\varepsilon}_p = A \exp(-\frac{Q}{RT})[\sinh(\xi \frac{\sigma}{s})]^{1/m}$$

ANAND Model: Constitutive Equations

Evolution Equation

$$\dot{s} = [h_0(1-\frac{S}{S^*})^a \operatorname{sign}(1-\frac{S}{S^*})]\dot{\varepsilon}_p ; (a > 1)$$

Integrate the $\dot{s}$

$$s^* = \hat{s}[\frac{\dot{\varepsilon}_p}{A}\exp(\frac{Q}{RT})]n$$

$$s = s^* - \{(s^* - s_0)^{(1-a)} + (a-1)[h_0 (s^*)^{-a} \dot{\varepsilon}_p]\}^{1/1-a}$$

$$\sigma = \frac{s}{\xi}\sinh^{-1}\{[\frac{\dot{\varepsilon}_p}{A}\exp(\frac{Q}{RT})]^m\}$$

Final Version of Stress Equation

$$\sigma = \frac{1}{\xi}\sinh^{-1}\{[\frac{\dot{\varepsilon}_p}{A}\exp(\frac{Q}{RT})]^m\}\{\hat{s}[\frac{\dot{\varepsilon}_p}{A}\exp(\frac{Q}{RT})]^n - [(\hat{s}[\frac{\dot{\varepsilon}_p}{A}\exp(\frac{Q}{RT})]$$
$$- s_0)^{1-a} + (a-1)[h_0(\hat{s}[\frac{\dot{\varepsilon}_p}{A}\exp(\frac{Q}{RT})]^n)]^{-a}\varepsilon_p]]^{1/1-a}$$

Determine ANAND Constants

- Eq (1) should be employed to fit saturation Stress vs. Strain rate and Temperature data to determine the value of the parameters A, n ,Q/R, m, $\hat{s}$, and ξ.

$$\sigma^* = UTS = \sigma\Big|_{\varepsilon_p \to \infty} = \frac{\hat{s}}{\xi}[\frac{\dot{\varepsilon}_p}{A}\exp(\frac{Q}{RT})]^n \sinh^{-1}\{[\frac{\dot{\varepsilon}_p}{A}\exp(\frac{Q}{RT})]^m\} \quad (1)$$

- Eq (2) should be applied to fit Stress vs. Strain data at different strain rate and temperatures to determine the values of parameters a, h_0, s_0.

$$\sigma = \sigma^* - [(\sigma^* - cs_0)^{1-a} + (a-1)\{ch_0(\sigma^*)^{-a}\}\varepsilon_p]^{1/(1-a)} \quad (2)$$

ANAND's Constant

Anand Const.	0 Days	30 Days	60 Day	120 Day	180 Days
S_0	1.87	1.59	1.42	1.28	1.12
Q/R	8444	8444	8444	8444	8444
A	5577	6134	6572	6964	7337
ξ	4.28	4.28	4.28	4.28	4.28
m	0.55	0.51	0.46	0.43	0.39
h_0	87353	84101	81092	79153	76839
$\hat{s}$	36.67	32.23	29.32	27.53	24.12
n	.0071	.0054	.0045	.0034	.0027
a	1.28	1.34	1.40	1.47	1.55

Comparison of ANAND Model with Experimental Data

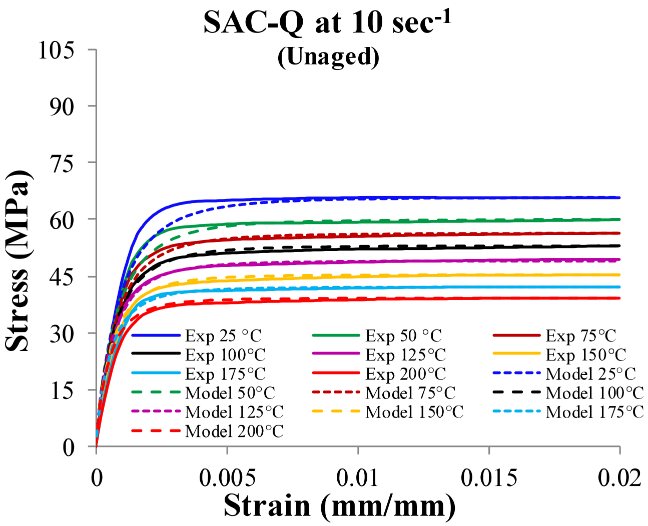

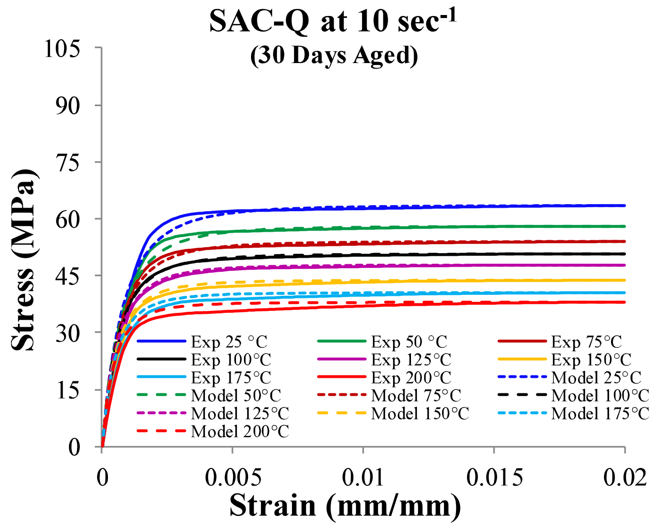

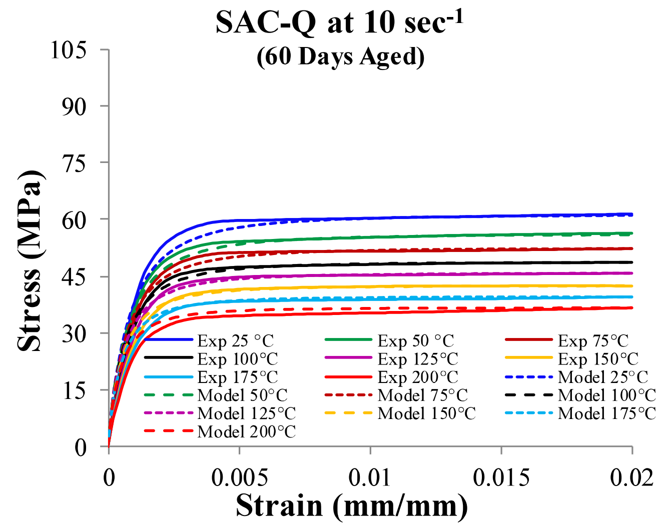

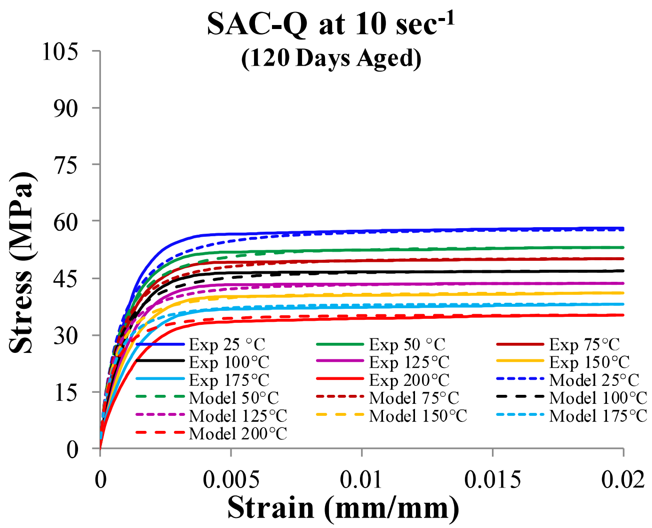

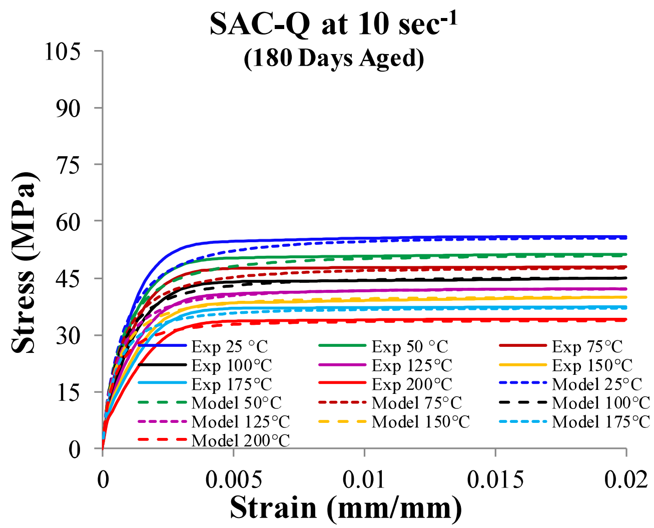

Comparison of ANAND Model with Experimental Data

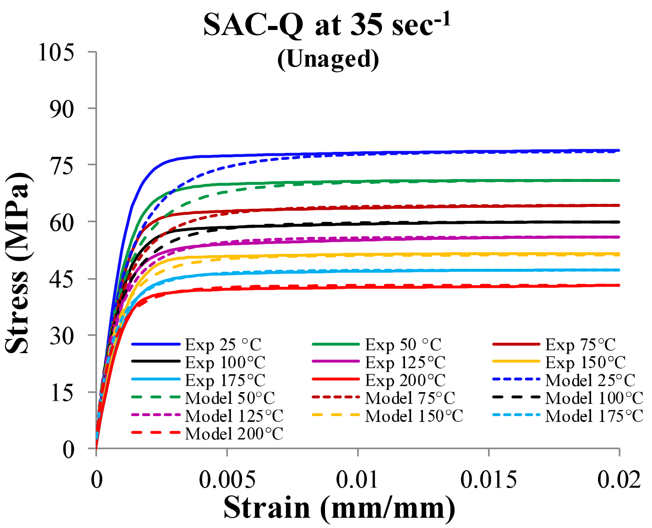

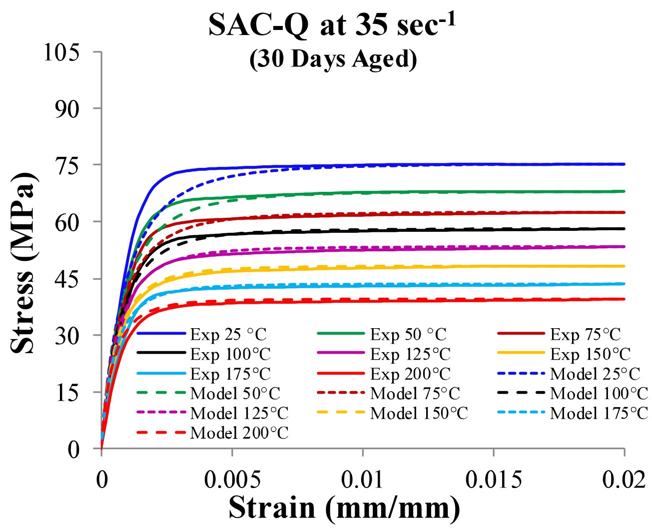

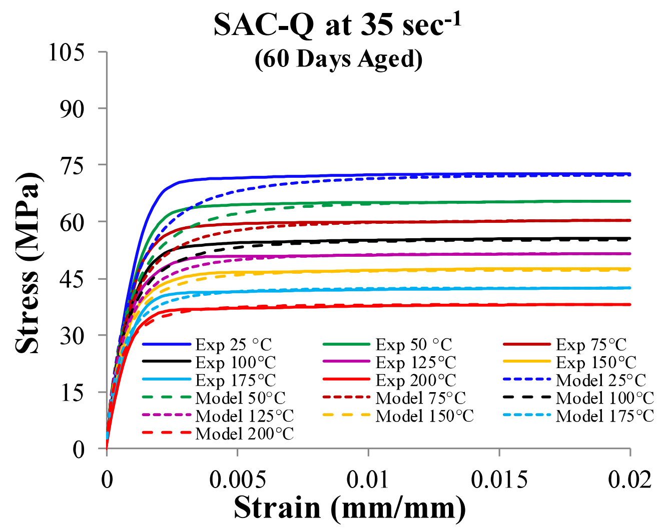

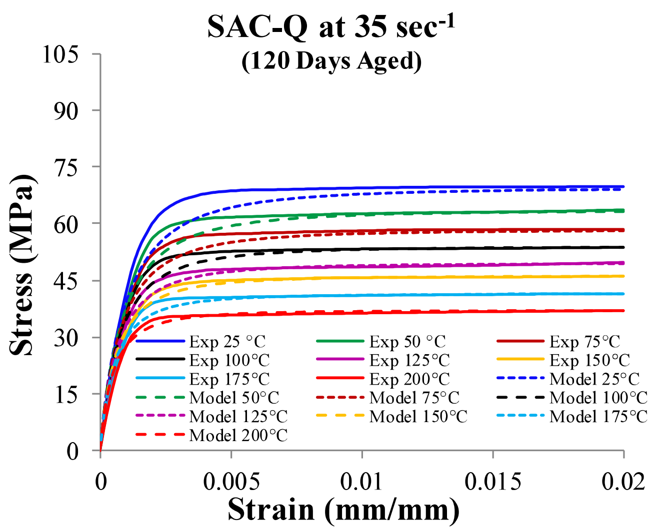

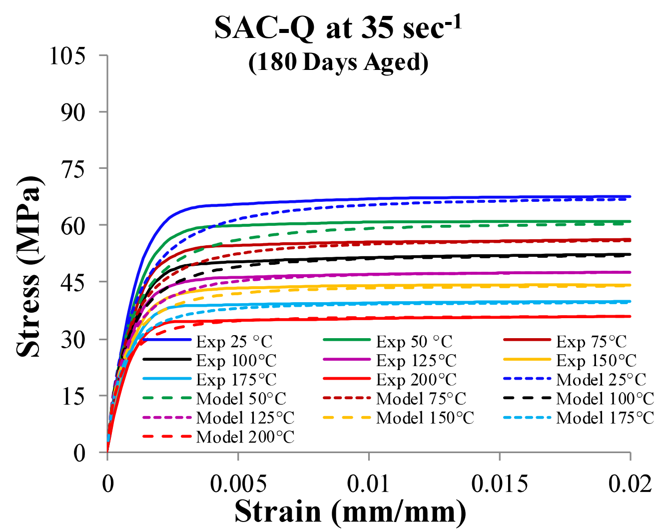

Comparison of ANAND Model with Experimental Data

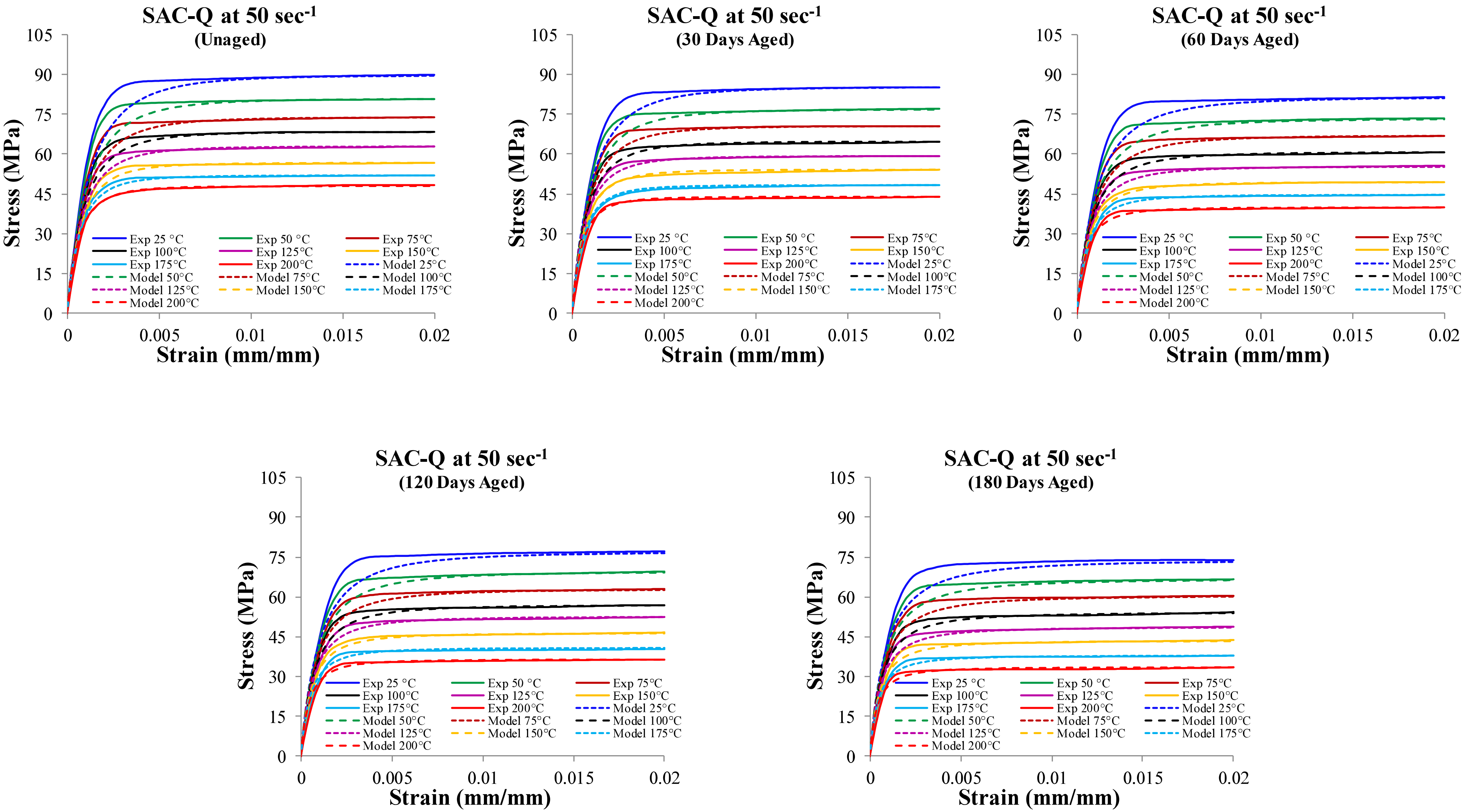

Comparison of ANAND Model with Experimental Data

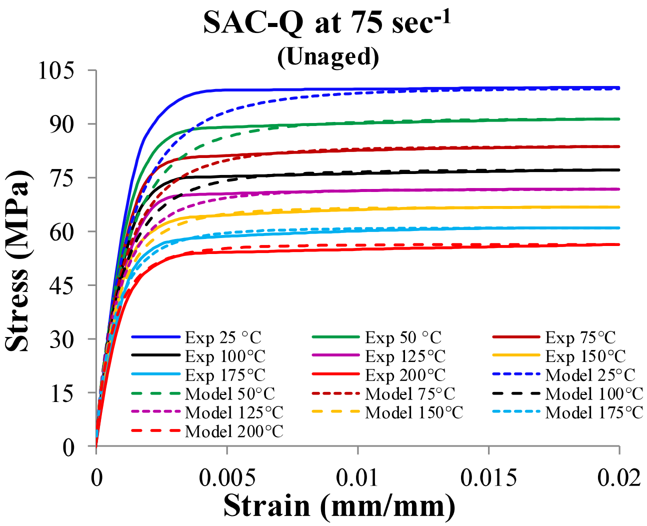

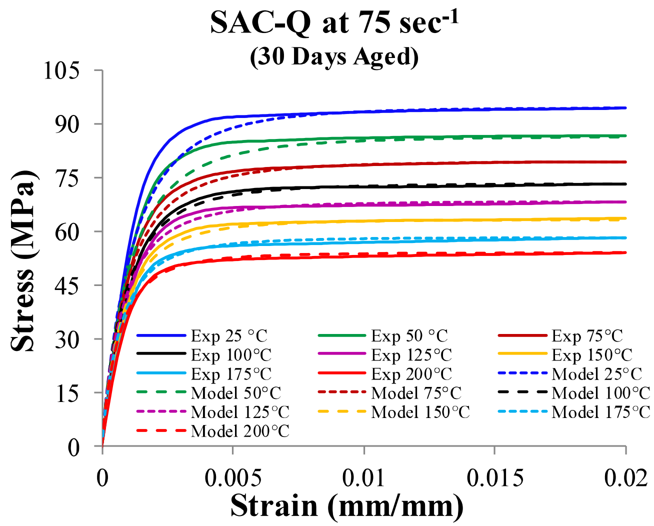

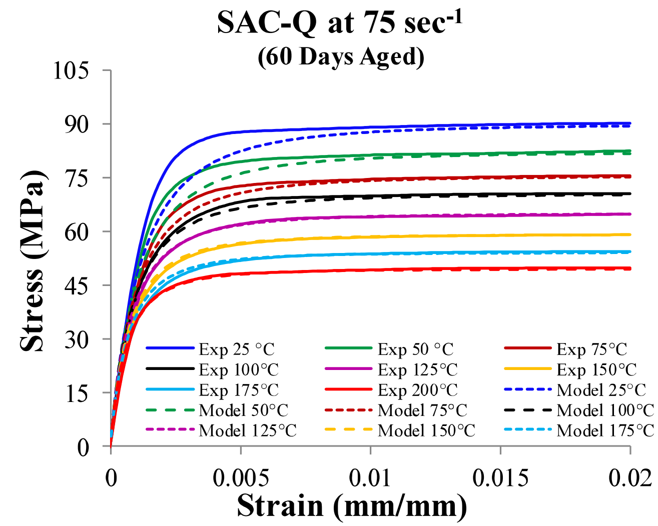

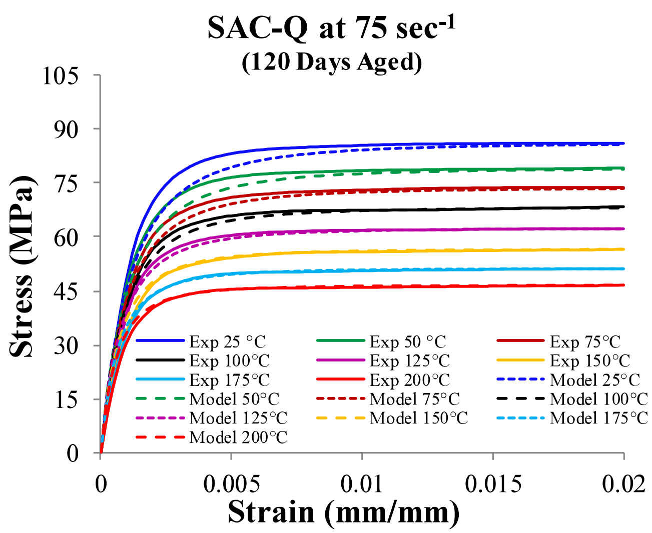

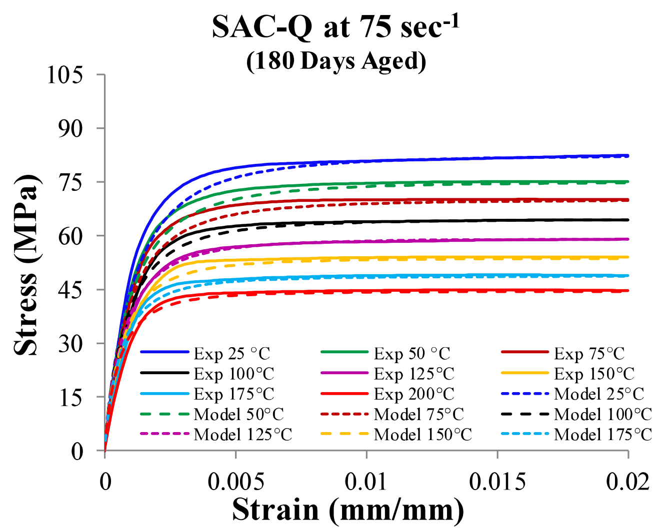

Summary and Conclusions

- Effect of 6-MONTH thermal aging on high strain rate mechanical behavior of SAC-Q Leadfree alloy at high operating temperature has been measured.
- Measured Ultimate Tensile Strength (UTS) and Young's Modulus (E) decreased as the operating temperature increased.
- Effect of high strain rates and high operating temperatures are much more pronounced on the ultimate tensile strength compared to the elastic modulus.
- The Anand model parameters for SAC-Q have been determined over a wide range of high strain rates and high operating temperatures for aged specimens.
- Accuracy of the predictive model with experimental data has been verified. Model predictions show good agreement with the experimental measurements.